

**NASA CONTRACTOR  
REPORT**



**NASA CR-2500**

**NASA CR-2500**

**CASE FILE  
COPY**

**FLIGHT CONTROL SYSTEMS  
PROPERTIES AND PROBLEMS**

**Volume I**

*Duane T. McRuer and Donald E. Johnston*

*Prepared by*  
**SYSTEMS TECHNOLOGY, INC.**  
Hawthorne, Calif. 90250  
*for Flight Research Center*



**NATIONAL AERONAUTICS AND SPACE ADMINISTRATION • WASHINGTON, D. C. • FEBRUARY 1975**



1. Report No. NASA CR-2500	2. Government Accession No.	3. Recipient's Catalog No.	
4. Title and Subtitle <b>FLIGHT CONTROL SYSTEMS PROPERTIES AND PROBLEMS Volume I</b>		5. Report Date February 1975	6. Performing Organization Code H-859
		8. Performing Organization Report No. TR-1018-1	10. Work Unit No.
7. Author(s) Duane T. McRuer and Donald E. Johnston	9. Performing Organization Name and Address Systems Technology, Inc. Hawthorne, California 90250		11. Contract or Grant No. NAS 4-1881
12. Sponsoring Agency Name and Address National Aeronautics and Space Administration Washington, D.C. 20546			13. Type of Report and Period Covered Contractor Report - Final
		14. Sponsoring Agency Code	
15. Supplementary Notes  NASA Technical Monitor: Herman A. Rediess, NASA Flight Research Center			
16. Abstract  This volume contains a delineation of fundamental and mechanization-specific flight control characteristics and problems gleaned from many sources and spanning a period of over two decades. It is not a complete exposition of systems past and present; however, everything described has actually occurred—often recurring with each new team of system or aircraft designers. It is organized to present and discuss first some fundamental, generic problems of closed-loop flight control systems involving numerator characteristics (quadratic dipoles, non-minimum phase roots, and intentionally introduced zeros). Next the principal elements of the largely mechanical primary flight control system are reviewed with particular emphasis on the influence of nonlinearities. The characteristics and problems of augmentation (damping, stability, and feel) system mechanizations are then dealt with. The particular idiosyncracies of automatic control actuation and command augmentation schemes are stressed, because they constitute the major interfaces with the primary flight control system and an often highly variable vehicle response. Specific emphasis is placed on high angle-of-attack and non-straight and level flight influences. Finally, various approaches to turn-coordination mechanization are covered.			
17. Key Words (Suggested by Author(s))  Aircraft control systems Systems design		18. Distribution Statement  Unclassified - Unlimited  Category: 08	
19. Security Classif. (of this report) Unclassified	20. Security Classif. (of this page) Unclassified	21. No. of Pages 171	22. Price* \$6.25

\*For sale by the National Technical Information Service, Springfield, Virginia 22151



## FOREWORD

The purpose of this program was to document and pass on past experiences to current and future generations of flight control system engineers, hopefully, to prevent costly rediscovery of past mistakes and to stimulate trade studies between possible competing mechanizational approaches.

This report is divided into two volumes. This volume contains the technical discussion while Volume II (NASA CR-2501) is a compendium of stability augmentation system and autopilot block diagrams and descriptive material for 48 different types of aircraft. These provide a broad representation of the many mechanizational approaches which have been employed in the past.



## TABLE OF CONTENTS

	<u>Page</u>
I. INTRODUCTION . . . . .	1
II. QUADRATIC DIPOLE PROBLEMS . . . . .	6
A. " $\omega_p/\omega_d$ Effect" in Bank Angle Control . . . . .	9
B. " $\omega_r/\omega_d$ Effect" in Dutch Roll Damping Augmentation . . . . .	17
C. Hydraulic and Electrohydraulic Actuation Systems . . . . .	20
III. SYSTEMS NUMERATOR PROBLEMS . . . . .	29
A. Non-Minimum Phase Zeros . . . . .	30
B. Intentionally Introduced Zeros . . . . .	46
IV. PROBLEMS ASSOCIATED WITH MECHANICAL FLIGHT CONTROL SYSTEM ELEMENTS . . . . .	53
A. Artificial Feel System Input/Output Characteristics . . . . .	53
B. Actuation Dynamics . . . . .	68
C. Bobweight Effects . . . . .	71
V. AUGMENTATION AND STABILIZATION SYSTEM PROBLEMS . . . . .	80
A. Command Insertion/Actuation Subsystem Combinations . . . . .	83
B. Electrical Command Preshaping or Filtering . . . . .	103
C. Feedback-Related Problems . . . . .	107
VI. TURN COORDINATION . . . . .	137
A. Directional Stiffening . . . . .	137
B. Control Crossfeeds to Rudder . . . . .	138
C. Roll Crossfeed to Rudder . . . . .	143
REFERENCES . . . . .	150
BIBLIOGRAPHY . . . . .	151
INDEX . . . . .	159

## LIST OF FIGURES

	<u>Page</u>
1. System Surveys for Quadratic Dipole . . . . .	7
2. Root Plot of Bank Angle/Aileron Transfer Function and Approximate Factors . . . . .	10
3. Closed-Loop Surveys for $r \rightarrow \delta_r$ Yaw Damper Systems . . . . .	18
4. Effect of Roll Damper on Yaw-Rate-to- Rudder Numerator . . . . .	19
5. A Fully-Powered Hydraulic Servo Surface Actuator. . . . .	20
6. Block Diagram of Actuator, Load, and Support . . . . .	21
7. Simplified Load Dynamics. . . . .	25
8. Rigid Support Structure, Compliant Load Coupling, Feedback Attached to $x_a$ . . . . .	28
9. Root-Locus Sketch of Altitude Control System . . . . .	31
10. System Survey of Pure Gain Pitch Attitude Control System . . . . .	34
11. Pure Gain Pitch Attitude Control System with Static-to-Short-Period Gain Ratio Less Than 1. . . . .	36
12. System Survey of Pitch Attitude Control System with Integrator. . . . .	37
13. Matrix for Coupled Equations with $\beta \neq 0$ . . . . .	40
14. Survey of $N_{\delta_e}^{\theta}$ Approximations for $\alpha = 18.8$ deg, $\beta = 6$ deg. . . . .	41
15. Pitch Attitude Closure Survey; $\alpha_0 = 19$ deg, $\beta_0 = 6$ deg. . . . .	44
16. Movement of 6 DOF $N_{\delta_e}^{\theta}$ Zeros for $0^{\circ} < \beta < 15^{\circ}$ . . . . .	45
17. Effect of $M_{\beta}$ on 6 DOF Poles and Zeros ( $\alpha_0 = 20$ deg, $\beta_0 = 1$ deg) . . . . .	47
18. Survey for Migration of Roots with SAS Loop Closure. . . . .	49
19. Comparison of Effective Vehicle Dynamics SAS On and Off . . . . .	51
20. Curve Fit of Equivalent Short Period Aircraft Dynamics . . . . .	52

	<u>Page</u>
21. Pilot-vehicle Control System . . . . .	54
22. Control System Schematic . . . . .	55
23. Detailed Characteristics of Typical Artificial Feel System . . . . .	56
24. Dynamic Characteristics, Feel System . . . . .	58
25. Survey of Feel System Poles with Change in Damping, $C_s$ . . . . .	60
26. Feel System Characteristics at Very Low Frequencies . . . . .	61
27. Waveforms in Artificial Feel System with Friction . . . . .	62
28. Mechanical Hysteresis Due to Coulomb Friction and Feel Spring . . . . .	63
29. Inverse Describing Function for Hysteresis, Friction and Preload, and Backlash . . . . .	65
30. Stick-to-Tail Gearing Versus Tail Deflection. . . . .	68
31. Block Diagram — Aircraft Control System with Valve Friction. . . . .	70
32. Negative Inverse Describing Function for a Control System with Valve Friction; $K_f = 1$ . . . . .	72
33. Block Diagram of Longitudinal Control System. . . . .	73
34. Root Survey for $N_s^B \frac{a}{z} = N_s^{a} \frac{cg}{z} - t_B N_s \ddot{\theta}$ . . . . .	75
35. Bobweight Loop Closure . . . . .	77
36. Effect of Increasing Control System Lags on Bobweight Loop Closure . . . . .	79
37. Generic Block Diagram for Command Augmentation Systems . . . . .	81
38. Full Authority Series Actuation . . . . .	85
39. Breakout Characteristics . . . . .	87
40. Pseudo Force Mechanization. . . . .	91
41. Control System Displacement Sensing. . . . .	93
42. Limited Authority Series Actuation with Automatic Trim. . . . .	95

	<u>Page</u>
43. Full Authority Parallel and Surface Actuators With Limited Authority Series Actuator and Trim . . . . .	97
44. Forward Loop Integration with Large Authority Series Servo . . . . .	100
45. Forward Loop Integration with Small Authority Series Servo and Series Trim . . . . .	101
46. Typical CAS with Automatic Series Trim. . . . .	102
47. Rolling Velocity Command Augmentation System. . . . .	103
48. Attitude Rate Command, Attitude Hold System . . . . .	115
49. Simplified Roll Rate CAS — Fixed-Wing Aircraft. . . . .	118
50. Simplified Roll Rate CAS — Swing-Wing Aircraft. . . . .	118
51. Typical $a_y \rightarrow \delta_r$ Bode Diagram. . . . .	124
52. Mid- and High-Frequency Portion of Bode Plot for $f(a_y) \rightarrow \delta_r$ Loop. . . . .	126
53. Roots of $(N^P_s/N^T_s) \tan (16 + \theta_T) = -1$ . . . . .	133
54. Yaw Rate Damper Effectiveness at $\alpha = 16$ deg . . . . .	135
55. Survey Sketch for Bank-Angle-to-Rudder . . . . .	145
56. Yaw Stability Augmentation System (SAS) . . . . .	146
57. Roll Stability Augmentation System (SAS) . . . . .	147
58. Survey Sketch of Bank-Angle-to-Aileron . . . . .	148

LIST OF TABLES

	<u>Page</u>
1. Two Decades of $\omega_p/\omega_d$ Problems . . . . .	3
2. Effects of Idealized Adjustments of $f(a_y) \rightarrow \delta_r$ Controller Parameters. . . . .	129
3. Summary of Configurations Utilized . . . . .	140



## SECTION I

### INTRODUCTION

From an overall systems viewpoint, the history of flight control system development can be considered in terms of stimulus and response. The stimuli have been flight control desires or troubles; these caused intermediate responses in the form of system configurations to satisfy the desires or to remedy the basic problems presumed to underlie the troubles; followed by final responses which were the most efficient system configurations which did indeed satisfy. In the course of such challenge-response evolutions, there have been two fundamentally independent types of competitions. The first is among imagined problem possibilities as the underlying causes for any observed troubles. This competition is decided primarily by analysis; it ends when the actual problem is defined in terms of pertinent vehicle and/or control system parameters and factors. The second competition is between system configurations, each capable in principle of satisfying the flight control desires or of correcting the fundamental flight control problems. Although all of the system configurations conceived may be possible, some are far more feasible and desirable than others. When practical mechanization possibilities, equalization requirements, sensor noise, sensitivity to system tolerances and controlled element uncertainties, responses to unwanted inputs, gain compensation, computational complexity, etc., are fully considered, many of the theoretically possible configurations are eliminated as practical possibilities. Historically, system configuration competitions have involved both sophisticated analyses and experimentation with actual equipment. In actuality, of course, few systems have been formally competitive, one with another. Rather the competition has been akin to historical evolution.

Each past flight control system design has had its share of advantages, limitations, and shortcomings. The advantages (real or potential) have quite often been extolled in various technical publications. Rarely, however, do the limitations and shortcomings achieve the same public (or even intracompany) notice. Yet these aspects really define the limitations on the state of the art, and there is much profit in learning from past

mistakes. Far too many shortcomings or mistakes are subtle, conceptual, recurring, and very costly. Table 1 presents an example of such recurrence for one of the fundamental problems discussed in Section II. This problem is known to have been encountered in the early 1950's. The principal causes and cures were identified and validated in the middle 1950's. These were promulgated on a widespread basis of technical reports and journal articles by the late 1950's. Yet it continues to pop-up.

Some shortcomings result in piling fix upon fix until an overly complex and unreliable design evolves. There is much to be gained from exposing past flight control system faults, over-design, and key limitations which have been very resistant to elimination. Particularly those characteristics which are basic in concept or which have been shown to have considerable carryover from one aircraft to another are high priority candidates.

The purpose of this program was the collection, unification, and dissemination of such information. This volume contains a delineation of both fundamental and mechanization specific problems gleaned from various sources. It is by no means a complete exposition of systems past and present; however, everything described has actually happened — often recurring with each new team of project or aircraft designers. The problems are both subtle and (in hindsight) obvious. Many are the consequence of compromises, resulting in some non-ideal rather than critically bad characteristics. Many were encountered and eliminated early in system development programs. Since mistakes are seldom advertised and many incidents are reported here as a result of verbal or inside information (e.g., items in Table 1), we do not have identifiable references on everything reported. Therefore, in the interest of even handed treatment, we have adopted a general policy of source anonymity.

The report is divided into two volumes. Volume I contains the technical discussions while Volume II is a compendium of system block diagrams. Volume I is organized to present and discuss first some fundamental, generic problems of closed loop flight control systems as generally as possible. This is done in Sections II and III. Section II delves into the family of flight control problems involving unfavorable quadratic dipole (pole-zero) effects. These include the  $\omega_p/\omega_d$  effect on closed loop roll control

TABLE 1  
TWO DECADES OF  $\omega_p/\omega_d$  PROBLEMS

YEAR	VEHICLE	REMARKS	SOURCE
Early 1950's	Snark Missile	Long range cruise missile. Two axis autopilot. Roll control unstable when push-over into terminal dive. Required changes in trajectory.	Undocumented Contractor Design Study
Mid-1950's	Q-2 Drone	Two axis autopilot. Essentially continuous dutch roll oscillation of significant amplitude with autopilot on.	Consulting activities
Late 1950's	KC-135A	Lateral-directional dutch roll oscillation in smooth air. Corrective aileron action by pilot amplifies oscillation. Use of rudder axis of autopilot stabilizes motion.	AFFTC TR-58-13
Late 1950's	F-101B	Lateral PIO at high dynamic pressure, subsonic conditions. Oscillation ceases when pilot releases stick.	AFFTC TR-58-11
1958	—	Identification of principal causes and cures.	WADC TR-58-82
1961	T-33VSA	In-flight simulation in variable stability T-33 validation of $\omega_p/\omega_d$ effects.	WADD TR-61-147
1961	X-15	Divergent lateral PIO with roll and yaw damper off at higher angles of attack due to negative dihedral effect of lower rudder.	NASA TND-1059
Early 1960's	B-58	Failure of yaw damper resulted in unstable roll damper and/or autopilot. Triple redundant yaw damper to be retrofitted.	Report of the A.S.D. Flight Control System Review Board
Late 1960's	B-70	Divergent lateral PIO with wing tips down and yaw augmentor off at high supersonic speeds. Aircraft could not be maneuvered in roll with SAS off.	NASA TM X-2933
Late 1960's	F-111	Large variation in $\omega_p/\omega_d$ partially due to swing-wing. Alleviated by triple redundant, fail-operational yaw damper.	Consulting activities and early contractor design studies
1970-71	M2-F2	Closed loop lateral instability (PIO) at low angle of attack in preflare maneuver. ARI aggravated.	NASA TND-6496

and roll PIO tendencies, the  $\omega_r/\omega_d$  effect which has determined the success or lack thereof of nearly all yaw damping mechanizations, and the quadratic dipole effect involved in electrohydraulic actuation systems. In each instance the causal factors are identified along with fundamental and direct means of countering the problems.

The influence, and problems, associated with unfavorable transfer function zeros, such as performance reversal in altitude control, are discussed in the first part of Section III. These are also known as "non-minimum phase" and/or "right half plane" zeros. Among the problems involving such zeros are speed divergence, longitudinal flight path divergence, and a newly identified lateral-longitudinal coupling which results in lateral "nose-slice" divergence. The second part of Section III presents some examples of problems encountered when zeros are intentionally introduced to attract closed loop poles of the basic vehicle response modes (e.g., longitudinal short period) to specified locations (frequency and damping). It is shown that while the specified results may be accomplished from an accounting standpoint, the equalization poles which inherently accompany the introduced zeros can negate the intended system benefits.

Section IV contains a discussion of the principal elements of the largely mechanical primary flight control system, from pilot stick input to control surface output. The interrelationship of the feel system, surface actuator, mechanical bobweight system, and series augmentation actuator is described. Particular attention is given to the influence of nonlinearities.

The characteristics and problems of various augmentation system mechanizations are dealt with in Section V. This first expands upon interfaces between the augmentation and primary flight control systems. Particular emphasis is placed upon command augmentation system considerations. These are generally high gain, large authority systems of inherently greater complexity than conventional stability augmentation systems. They can deliver more performance and, conversely, suffer greater problem potential. Problems associated with motion feedback sensing are also discussed with specific emphasis on the effects of high angle of attack and non-straight and level flight.

Section VI contains a discussion of three approaches to turn coordination mechanization. Some advantages and shortcomings of each are presented. A mathematical model of a theoretically ideal aileron-rudder interconnect (ARI) is developed which indicates the influence of various augmentation feedbacks, as well as airframe parameters, on the desired ARI characteristics.

As indicated previously, Volume II is a compendium of SAS and autopilot block diagrams and descriptive material for 48 different types of aircraft. These provide a broad representation of the many mechanizational approaches which have been employed in the past three decades. Collectively they also have exhibited many, if not all, of the problems discussed in this volume. A bibliography of source material is appended to Volume I.

## SECTION II

### QUADRATIC DIPOLE PROBLEMS

There are a remarkable number of flight control situations which are dominated by the dynamic properties of a lightly-damped quadratic dipole (quadratic pole-zero pair) in the crossover region of a feedback system. The essence of what can happen is indicated in Figs. 1a and 1b. This considers an open-loop system which can be approximated in the region of crossover by:

$$G(s) = \frac{K[s^2 + 2\zeta_N\omega_N s + \omega_N^2]}{s[s^2 + 2\zeta_D\omega_D s + \omega_D^2]} = \frac{K[\zeta_N, \omega_N]}{s[\zeta_D, \omega_D]} \quad (1)$$

In the idealized situations illustrated the closed-loop quadratic mode  $(\zeta_D', \omega_D')$  progresses as open-loop gain is increased from the open-loop pole  $(\zeta_D, \omega_D)$  to the open-loop zero  $(\zeta_N, \omega_N)$ , in a counterclockwise direction along a circular segment. Thus, when the pole is smaller than the zero, the closed-loop roots depart toward the right-half plane and suffer a damping decrease, whereas the reverse is true when the numerator,  $\omega_N$ , is smaller than the denominator,  $\omega_D$ . The maximum diminution or increase in damping is measured by the maximum phase deviation, due to the dipole, from the phase angle contributed by the rest of the system. This is given by:

$$\Delta\varphi(\omega_N, \omega_D)_{\max} = -\tan^{-1} \frac{2(\zeta_N + \zeta_D) \left( \sqrt{\frac{\omega_N}{\omega_D}} - \sqrt{\frac{\omega_D}{\omega_N}} \right)}{2 + 4\zeta_N\zeta_D \frac{\omega_N}{\omega_D} - \frac{\omega_D}{\omega_N}} \quad (2)$$

When  $\omega_N/\omega_D$  is near 1, this becomes approximately:

$$\Delta\varphi(\omega_N, \omega_D)_{\max} = -\tan^{-1} \frac{\zeta_N + \zeta_D}{2\zeta_N\zeta_D} \left( \frac{\omega_N}{\omega_D} - 1 \right) \quad (3)$$

7

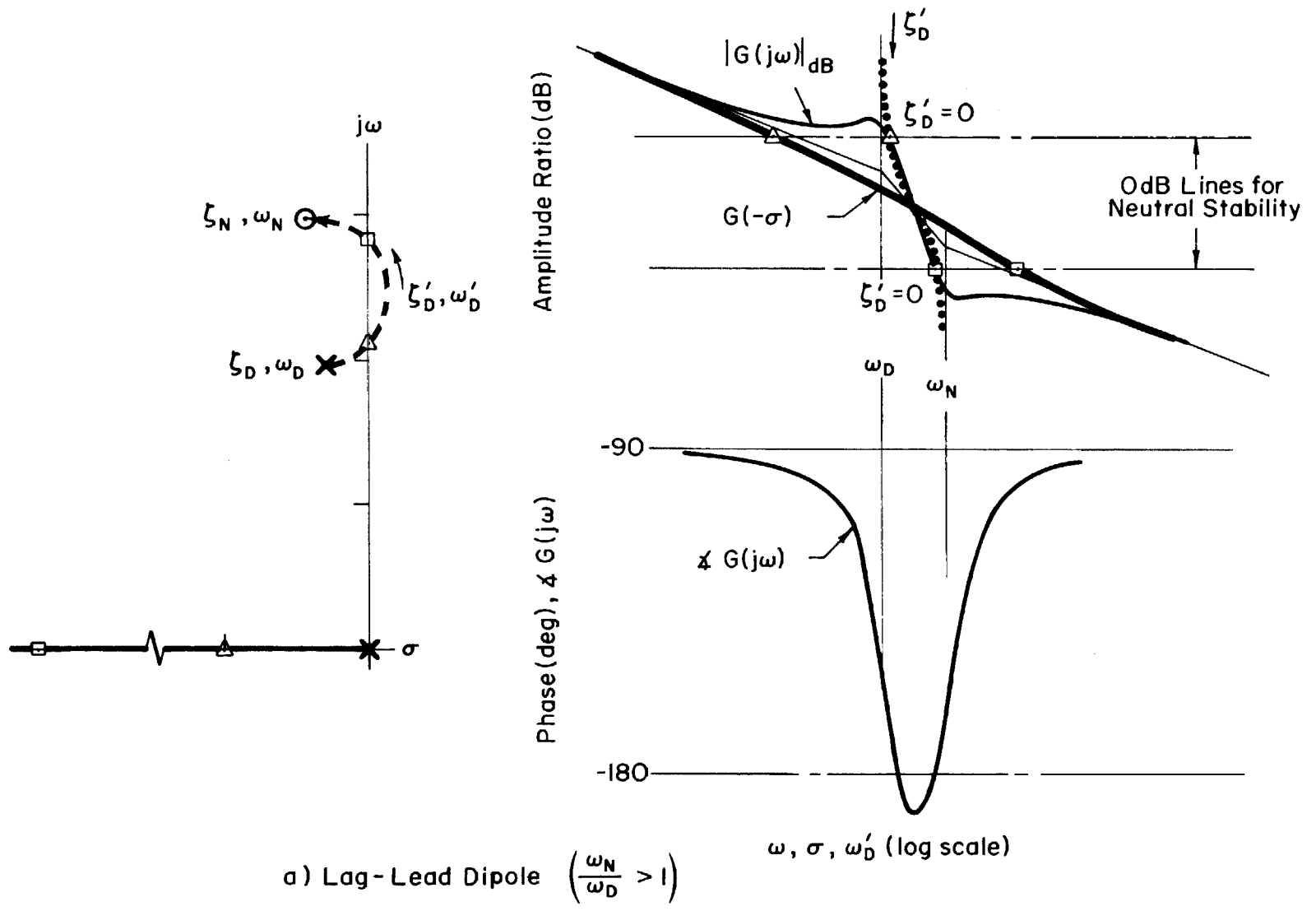
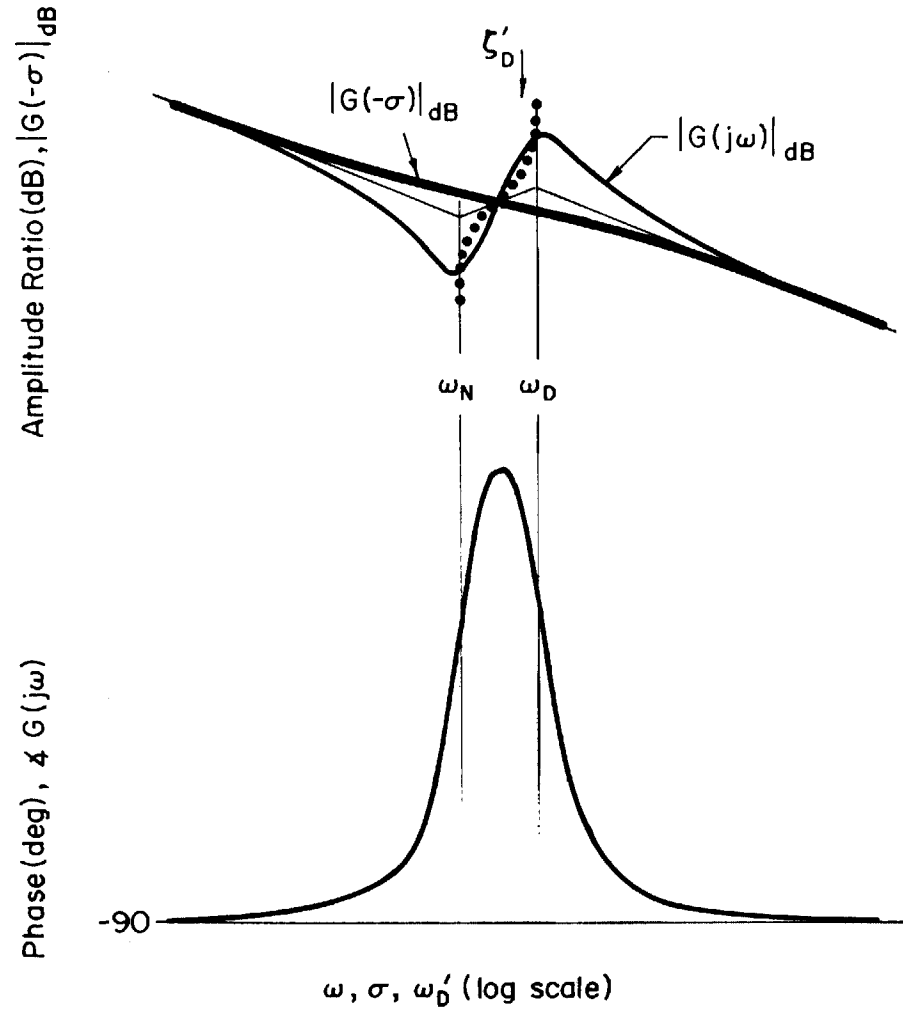
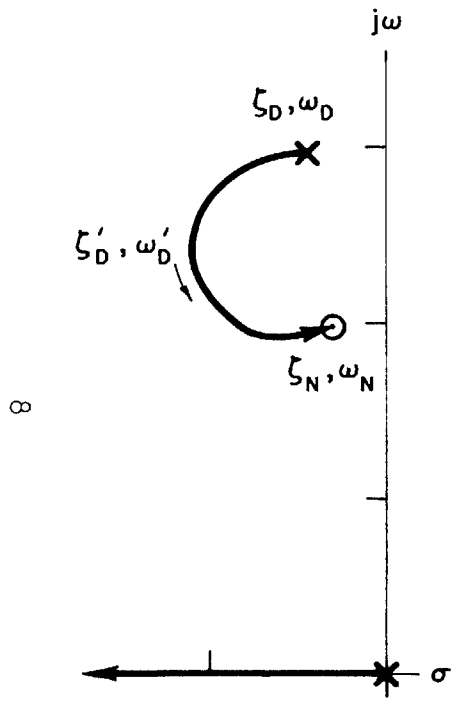


Figure 1. System Surveys for Quadratic Dipole



b) Lead-Lag Dipole ( $\frac{\omega_N}{\omega_D} < 1$ )

Figure 1. (Concluded)

When  $\omega_N/\omega_D > 1$ , the incremental phase is a dip resulting in a decreased phase margin (when crossover occurs in the dipole region) over that which would be present without the dipole. Conversely,  $\omega_N/\omega_D < 1$  implies a phase lead blip and an increased phase margin. The greater the blip, the larger the attainable closed-loop damping ratio,  $\zeta_D'$ .

All of the ramifications implicit in the idealized situations above are exhibited in practical control situations. When  $\omega_N/\omega_D > 1$  the presence of the dipole is a distinct nuisance, often causing instability or marginally stable operation. These are exemplified below by the " $\omega_\phi/\omega_d$  effect" encountered in roll control using ailerons and the oil-compressibility structural-compliance coupling associated with hydraulic surface actuators. On the other side of the coin, the presence of the dipole is advantageous in that  $\omega_N/\omega_D < 1$  situations permit the closed-loop damping to be increased over that available open loop. The classic case to be described below is the " $\omega_r/\omega_d$  effect" associated with yaw-rate-to-rudder feedback controls. Other examples, such as lateral-acceleration-to-rudder feedback ( $\omega_{ay}/\omega_d$ ) and longitudinal control systems containing dual bobweights ( $\omega_B/\omega_{SP}$ ), will be described in later sections.

#### A. " $\omega_\phi/\omega_d$ EFFECT" IN BANK ANGLE CONTROL

A root plot of the aircraft bank-angle/aileron transfer function is given in Fig. 2. Here, the quadratic dipole  $\omega_\phi/\omega_d$  ratio is greater than 1. In order to accomplish good roll control, stabilization, and regulation, a bank-angle-to-aileron controller would contain equalization which would make the total open-loop system transfer function, less the dipole, appear like a K/s in the crossover region. To the extent that this is accomplished, the bank angle controller approaches the  $\omega_N/\omega_D > 1$  situation idealized above. Accordingly, by analogy with Fig. 1, the closed-loop dutch roll damping will be less for low and moderate gains than the open loop and will then turn about and approach a damping ratio  $\zeta_\phi$  and damping  $\zeta_\phi\omega_\phi$  as the gain becomes very large. Thus, the dutch roll undamped natural frequency is increased and the damping and damping ratio (at other than high gains) is decreased by virtue

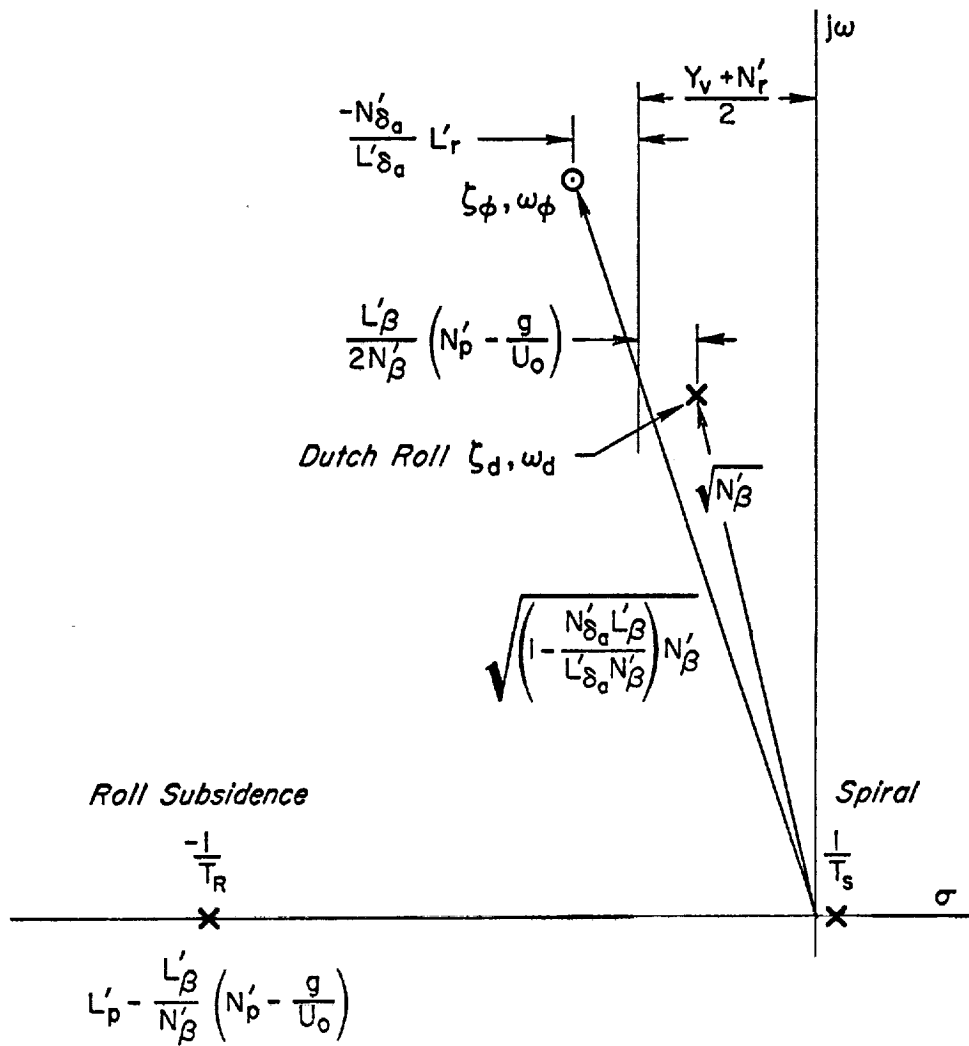


Figure 2. Root Plot of Bank Angle/Aileron Transfer Function and Approximate Factors

of the bank angle controller. (When the feedback control equalization does not approximate that needed to make good the K/s-like property, the  $\omega_\phi/\omega_d$  effects are somewhat the same in general but differ significantly in detail. See Chap. 8 of Ref. 1.)

Marginal dutch roll damping problems arising from the  $\omega_\phi/\omega_d$  effect can cause longitudinal problems as well. For instance, to help maintain altitude in turns bank angle is crossfed to the pitch axis to provide up-elevator bias, i.e.:

$$\Delta\delta_e = \phi \frac{(1 - \cos \phi)}{\cos \phi} \quad (4)$$

With an unfavorable  $\omega_\phi/\omega_d$ , and with the relatively large  $|\phi/\beta|_d$  characteristic of most high performance craft, the lateral dynamics of an aileron-only controlled aircraft will exhibit an almost continuous large amplitude roll oscillation when disturbed by turbulence or turning maneuvers. Thus, in both level flight and in turns the dutch roll oscillation is coupled into pitch excursions. At steep bank angles large load factor oscillations result [for  $\beta = \dot{h} = 0$ ,  $n_z = (1 - \cos \phi)/\cos \phi$ ].

In general, if only aileron is available for feedback control purposes, it is desirable that  $\omega_\phi/\omega_d$  approximately equal 1 so that the dutch roll poles are nearly cancelled by the aileron bank angle numerator zeros. This has the benefit of permitting excellent closed-loop bank angle control and regulation with little excitation of the dutch roll mode by aileron inputs. The dutch roll is then essentially decoupled from rolling motions; with exact cancellation of the dipole pair, the mode is not "observable" in terms of the state variable,  $\phi$ , nor "controllable" by the control variable,  $\delta_a$ .

As separation between the pair increases, the aileron excitation of the dutch roll mode also increases. When  $\omega_\phi/\omega_d > 1$ , the closed-loop stability is degraded; whereas when  $\omega_\phi/\omega_d < 1$ , the ailerons are effective in damping the dutch roll. As described above, the degree of damping degradation or improvement is determined primarily by the phase dip or blip, which in turn depend predominantly on the separation of the dipole pair ( $\omega_N/\omega_D - 1$ ) and the effective dipole composite damping ratio,  $\xi_\phi \xi_D / (\xi_\phi + \xi_D)$ , as indicated by Eq. 3. As shown in Fig. 2, the separation of the dipole pair is

largely determined by the stability derivative,  $N_{\delta_a}'$ , which accounts for the aileron-induced yawing acceleration. The general level of damping,  $\zeta_{\phi\omega_{\phi}}$  and  $\zeta_{d\omega_d}$ , on the other hand, is primarily dependent on  $N_r'$ , the yawing acceleration due to yawing velocity stability derivative, while the predominant distinction between numerator and denominator damping is a more complex function of yawing acceleration due to rolling velocity,  $N_p'$ , and the lateral-directional sideslip coupling,  $L_{\beta}'/N_{\beta}'$ .

Because dutch roll is a nuisance mode in roll attitude control, it is highly desirable that  $\omega_{\phi}/\omega_d$  approximately equal 1 and/or that the dutch roll is well damped at all flight conditions. For high performance manned aircraft, both conditions are desired, although the first may be sufficient for many missile situations and for minimum complexity flight control systems. The conventional means to correct non-ideal  $\omega_{\phi}/\omega_d$  is to incorporate an aileron-to-rudder interconnect which serves to reduce the effective adverse yawing components,  $N_{\delta_a}'$  and sometimes  $N_p'$ , and/or to rely on a yaw damper to provide sufficient dutch roll damping so that no stability problem occurs.

#### 1. Adjustment of $\omega_{\phi}/\omega_d$

The value of  $\omega_{\phi}/\omega_d$  is most simply adjusted to an "optimum" value near 1 by modifying the effective yawing moment due to aileron deflection,  $N_{\delta_a}'$ , so as to reduce the amount of dutch roll excitation due to aileron. This is commonly accomplished using a mechanical aileron-to-rudder interconnect (e.g., A-5, A-7, B-58, F-4, F-8, F-14, F-102, F-106, etc.). Because the  $\omega_{\phi}/\omega_d$  problem exists throughout a range of flight conditions, it is common to schedule the interconnect gain with elevator position (A-7, F-8) or dynamic pressure (F-102, F-106).

When  $\omega_{\phi} \equiv \omega_d$  the dutch roll excitation via aileron is minimized except for the pole-zero damping difference,  $\zeta_{\phi\omega_{\phi}} - \zeta_{d\omega_d}$ . This difference can be reduced substantially by either equalization in the interconnect or by roll-rate-to-rudder feedback. This can simply be illustrated by noting that, with  $L_{\delta_r}' \doteq 0$ , the rudder required to offset aileron and rolling velocity induced yawing terms is:

$$\begin{aligned}\delta_r &= K_{\delta_a}^{\delta_r} \delta_a + K_p^{\delta_r} p \\ &= -\frac{N_{\delta_a}'}{N_{\delta_r}'} \delta_a - \frac{\left(N_p' - \frac{g}{U_0}\right)}{N_{\delta_r}'} p\end{aligned}\tag{5}$$

When this combined crossfeed and feedback signal is sent to the rudder, the effective  $N_{\delta_a}'$  and  $N_p'$  are made very small, thereby reducing both the separation in frequency and damping between the dipole quadratics. If the rolling velocity is approximated by:

$$p \doteq \frac{L_{\delta_a}' \left(\frac{\omega_d}{\omega_d}\right)^2}{T_R s + 1} \delta_a\tag{6}$$

then the elimination of the undesired yawing components due to both aileron and rolling velocity can be accomplished with the equalized crossfeed given by:

$$\delta_r = -\frac{N_{\delta_a}' + \left(N_p' - \frac{g}{U_0}\right) L_{\delta_a}' \left(\frac{\omega_\phi}{\omega_d}\right)^2}{N_{\delta_r}'} \left[ \frac{\frac{T_R}{s+1}}{1 + \left(N_p' - \frac{g}{U_0}\right) \frac{L_{\delta_a}' \omega_\phi^2}{N_{\delta_a}' \omega_d^2}} \right] \delta_a\tag{7}$$

This crossfeed can be either a lead-lag or a lag-lead depending on the sign of  $N_p'/N_{\delta_a}'$ .

An alternative viewpoint to the  $\omega_\phi/\omega_d$  effect is obtained by recognizing that the undesired excitation of the dutch roll mode arises through roll-control-induced sideslip. Then, the total elimination via crossfeed of dutch roll excitation requires that:

$$\left(N_{\delta_a}^\beta\right)_{\text{effective}} + Y_{CF} \left(N_{\delta_r}^\beta\right)_{\text{effective}} = 0\tag{8}$$

where  $Y_{CF}$  is a dynamically shaped roll-control-to-rudder crossfeed and the effective numerators reflect appropriate ratioing of aileron and spoiler contributions, appropriate augmentation (SAS or CAS) closures, etc. For example, the ideal crossfeed for an aileron-controlled aircraft with a yaw damper,  $\delta_r = G_r r$ , is:

$$Y_{CF} = \frac{-(N_{\delta_a}^\beta)_{\text{effective}}}{(N_{\delta_r}^\beta)_{\text{effective}}} = \frac{-(N_{\delta_a}^\beta + G_r N_{\delta_a}^\beta r_g)}{N_{\delta_r}^\beta} \quad (9)$$

where  $N_{\delta_a \delta_r}^{\beta r_g}$  is the airplane coupling numerator which accounts for the effect of yaw damper action on the aileron-induced yaw rate. When  $G_r$  is representative of a simple washed-out yaw damper, i.e.:

$$G_r = \frac{K_r s}{s + 1/T_{wo}} \quad (10)$$

the crossfeed will be:

$$Y_{CF_1} = - \frac{\left[ -N_{\delta_a}^i \left( s + \frac{1}{T_{\beta_1}} \right) \left( s + \frac{1}{T_{\beta_2}} \right) + \frac{K_r s}{(s + 1/T_{wo})} \times -N_{\delta_a}^i Y_{\delta_r}^* \left( s + \frac{1}{T_{\beta r_1}} \right) \left( s + \frac{1}{T_{\beta r_2}} \right) \right]}{N_{\delta_r}^i \left( s + \frac{1}{T_{\beta r_1}} \right) \left( s + \frac{1}{T_{\beta r_2}} \right)} \quad (11)$$

$$= \frac{N_{\delta_a}^i}{N_{\delta_r}^i} \frac{\left[ \left( s + \frac{1}{T_{\beta_1}} \right) \left( s + \frac{1}{T_{\beta_2}} \right) \left( s + \frac{1}{T_{wo}} \right) + K_r Y_{\delta_r}^* s \left( s + \frac{1}{T_{\beta r_1}} \right) \left( s + \frac{1}{T_{\beta r_2}} \right) \right]}{\left( s + \frac{1}{T_{wo}} \right) \left( s + \frac{1}{T_{\beta r_1}} \right) \left( s + \frac{1}{T_{\beta r_2}} \right)}$$

This complicated looking shaping can usually be approximated by a simple first-order lag-lead operating on  $p$  as a feedback to rudder plus a constant for aileron crossfeed. In a fashion similar to that used in conjunction with Eq. 5 the rudder needed to offset the aileron, rolling velocity, and yaw-damper induced sideslip will be approximately (Ref. 2):

$$\begin{aligned}
\delta_r &\doteq -\frac{N'_{\delta a}}{N'_{\delta r}} \delta_a - \left[ \frac{\left(N'_p - \frac{g}{U_0}\right)}{N'_{\delta r}} - \frac{K_r \left(\alpha_g s + \frac{g}{U_0}\right)}{s + \frac{1}{T_{wo}}} \right] p \\
&= -\frac{N'_{\delta a}}{N'_{\delta r}} \delta_a - \left\{ \frac{\left(N'_p - \frac{g}{U_0} - K_r N'_{\delta r} \alpha_g\right) s + \left[\left(N'_p - \frac{g}{U_0}\right) \frac{1}{T_{wo}} - \frac{g}{U_0} K_r N'_{\delta r}\right]}{N'_{\delta r} (s + 1/T_{wo})} \right\} p
\end{aligned} \tag{12}$$

In this equation the natural damping  $N'_r$  is neglected, the yawing acceleration  $\dot{r}$  is approximated by  $(g/U_0)p$ , and the yaw rate gyro inclination relative to the stability axes is  $\alpha_g$ . If only an aileron crossfeed is desired the rolling velocity approximation of Eq. 6 can be used. Then the relationship between rudder and aileron will be:

$$\delta_r \doteq -\frac{1}{N'_{\delta r}} \left\{ \frac{\left\{ T_R N'_{\delta a} s^2 + \left[ N'_{\delta a} \left( \frac{T_R}{T_{wo}} + 1 \right) + L'_{\delta a} \left( \frac{\omega_p}{\omega_d} \right)^2 \left( N'_p - \frac{g}{U_0} - K_r N'_{\delta r} \alpha_g \right) \right] s + \frac{N'_{\delta a}}{T_{wo}} + L'_{\delta a} \left( \frac{\omega_p}{\omega_d} \right)^2 \left[ \left( N'_p - \frac{g}{U_0} \right) \frac{1}{T_{wo}} - \frac{g}{U_0} K_r N'_{\delta r} \right] \right\}}{(s + 1/T_{wo})(T_R s + 1)} \right\} \delta_a \tag{13}$$

Often the second-order crossfeed shaping indicated by Eq. 13 is adequately approximated by a lag-lead. The important aspect, however, is to note that the desired crossfeed can be strongly influenced by the yaw damper gain and shaping. Furthermore, the yaw damper always opposes aileron-commanded maneuvers to some extent and therefore actually augments adverse aileron yaw.

If the aircraft also includes a lateral-acceleration-to rudder loop, the ideal crossfeed is obtained from:

$$Y_{CF2} = -\frac{\left( N_{\delta a}^{\beta} + G_r N_{\delta a}^{\beta} \frac{r}{\delta r} + G_{ay} N_{\delta a}^{\beta} \frac{ay}{\delta r} \right)}{N_{\delta r}^{\beta}} \tag{14}$$

Addition of a roll rate damper results in

$$Y_{CF3} = -\frac{\left( N_{\delta a}^{\beta} + G_r N_{\delta a}^{\beta} \frac{r}{\delta r} + G_{ay} N_{\delta a}^{\beta} \frac{ay}{\delta r} \right)}{\left( N_{\delta r}^{\beta} + G_p N_{\delta r}^{\beta} \frac{p}{\delta a} \right)} \tag{15}$$

Additional considerations can include such things as the contribution of any lateral stick-to-surface shaping (e.g., resulting from forward path filtering in a roll rate CAS), etc.

In all of these cases, incorporation of the ideal  $Y_{CF}$  can make  $\omega_{\phi}/\omega_d \equiv 1$ ; although the theoretical shaping can become quite complex. This corresponds to the ideal decoupling case, and is seldom of practical importance. Instead, as noted previously, the shaping is usually approximated. More often than not this can be accomplished by a simple lag-lead or, sometimes, even a straight gain.

## 2. Influence of the Yaw Damper on $\omega_{\phi}/\omega_d$

The fundamental purpose of a yaw damper is to increase the dutch roll damping without greatly detracting from the aircraft's ability to fly coordinated turns. As indicated by the root plot of Fig. 2, the dutch roll damping of the aircraft alone is predominantly dependent on  $Y_v$  and  $N_r'$ . If a stability derivative  $N_{\dot{\beta}}$  were also explicitly carried in the aircraft equations of motion, it would add directly to these two. Thus, to augment the dutch roll damping implies augmentation of one of these three derivatives in the region of the dutch roll frequency. The most common techniques are to use a washed-out signal from a rate gyro measuring yawing velocity or a lead-equalize signal from a lateral accelerometer (properly located to deliver an approximation to  $\dot{\beta}$ ). The influence of these types of yaw damper on the damping terms in the dipole may be seen from the following approximate factors.

$$2(\zeta_d^{\omega_d})_{aug} \doteq -(Y_v + N_{r'aug}' + N_{\dot{\beta}aug}') - \frac{L_{\dot{\beta}}'}{N_{\dot{\beta}}'} \left( N_p' - \frac{g}{U_0} \right) \quad (16)$$

$$2\zeta_{\phi}^{\omega_{\phi}} \doteq -(Y_v + N_{r'aug}' + N_{\dot{\beta}aug}') + \frac{N_{\dot{\beta}a}'}{L_{\dot{\beta}a}'} L_r'$$

The contribution of the yaw damper in augmenting  $N_r'$  or  $N_{\dot{\beta}}$  is such that the pole-zero pair "track." Thus, an effective yaw damper will increase the damping of both terms and reduce the significance of the dipole in affecting the closed-loop roll axis dynamics. On the other hand, an ineffective

yaw damper or one that has failed will result in both terms moving toward the  $j\omega$  axis where  $\omega_\phi > \omega_d$  can have the serious consequences already noted.

This then leads to the second quadratic dipole problem,  $\omega_r/\omega_d$ .

### B. " $\omega_r/\omega_d$ EFFECT" IN DUTCH ROLL DAMPING AUGMENTATION

The effectiveness of yaw rate feedback to rudder as a means to damp the dutch roll often depends on the location of the quadratic zero of the yaw-rate-to-rudder numerator,  $\omega_r$ . Assuming the sensor measures stability axis yawing velocity,  $r$ , the  $r/\delta_r$  numerator approximate factors most often encountered in practice are\*:

$$\omega_r^2 \doteq \frac{g}{U_o} \frac{L_\beta}{L_p} \quad ; \quad 2\zeta_r \omega_r \doteq - \left( Y_v - \frac{N_\beta}{N_{\delta_r}} Y_{\delta_r}^* - \frac{g}{U_o} \frac{L_\beta}{L_p^2} \right) \quad (17)$$

$$\frac{1}{T_r} \doteq L_p$$

Normally,  $\omega_r$  is considerably less than  $\omega_d$ . However, at low speeds, at high angles of attack, or for conditions of low  $L_p$  and/or high  $L_\beta$ ,  $\omega_r$  can approach  $\omega_d$ . In these cases, yaw-rate-to-rudder feedback is relatively ineffective in damping dutch roll. Sketches of system surveys are given in Fig. 3 (not to scale). Clearly, the damping potential for yaw rate to rudder is much greater when  $\omega_r \ll \omega_d$ . Furthermore, the full benefits of a washout circuit, which reduces the low-frequency adverse yaw due to yawing velocity, with  $1/T_{w_o} \doteq \omega_r$  (the usual case) can be obtained when  $\omega_r/\omega_d \leq 0.3$ , but as  $1/T_{w_o} = \omega_r \rightarrow \omega_d$  the washout actually mitigates against an increase in the dutch roll damping. The latter situation is commonly encountered in landing approach where angle of attack is large or in maneuvering flight where high angle of attack and increased load factor combine.

To improve situations where  $\omega_r$  is not sufficiently small, it can be decreased by augmenting roll damping ( $L_p$ ) via roll rate feedback to aileron.

---

\* $N_{\delta_r}^r$  is of third degree. All possible combinations of minimum and non-minimum phase first- and second-degree terms have occurred in practice. These particular approximate factors are, therefore, only one of several. Others are provided in Refs. 1 and 3.

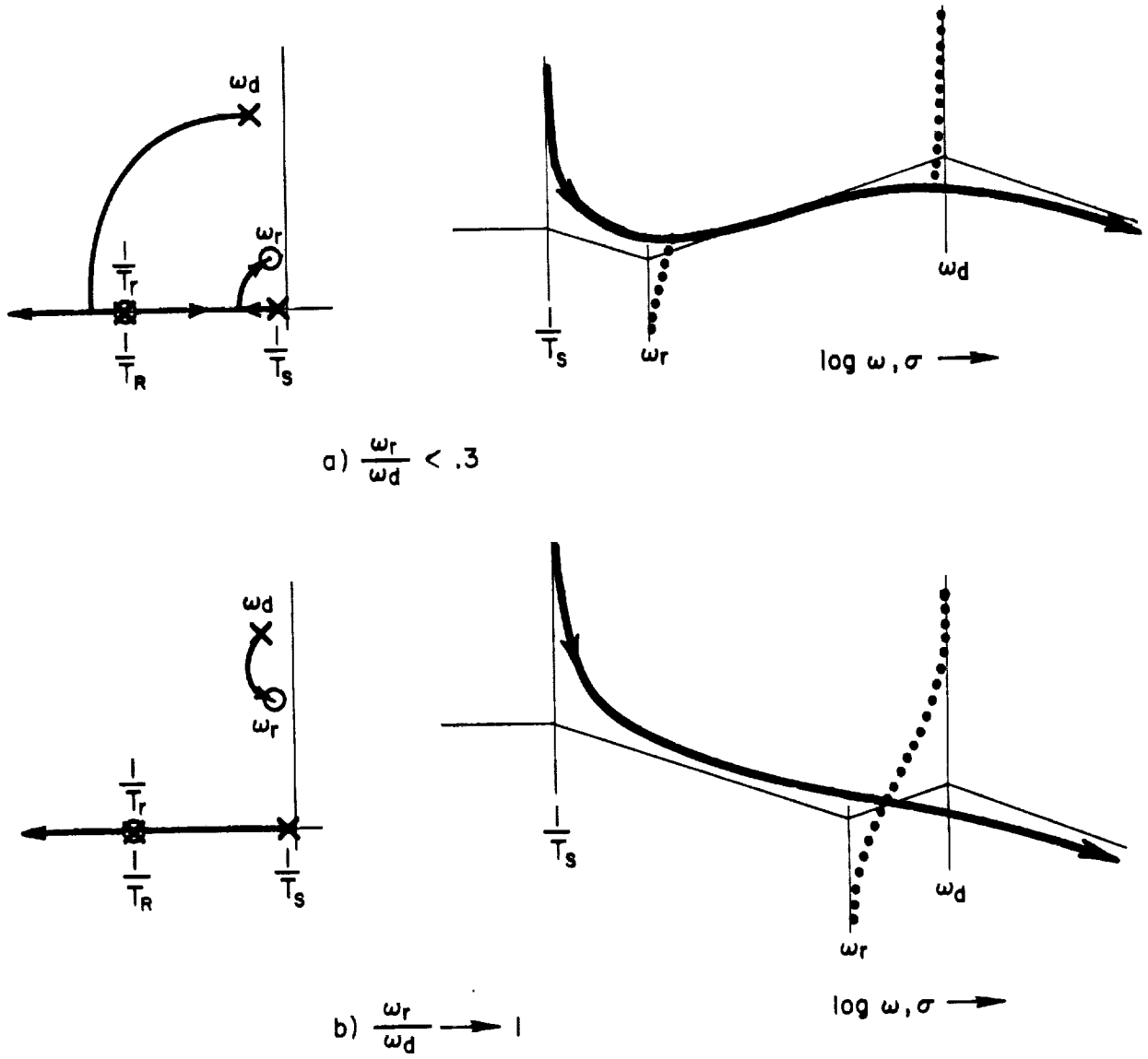


Figure 3. Closed-Loop Surveys for  $r \rightarrow \delta_r$  Yaw Damper Systems

The consequences of this procedure are revealed by considering the  $r/\delta_r$  numerator with the roll damper loop closed, i.e.:

$$N_{\delta_r}^r \Big|_{p+\delta_a} = N_{\delta_r}^r + K_p N_{\delta_a}^p N_{\delta_r}^r \quad (18)$$

The roots of the roll rate augmented numerator are obtained by treating this equation as a feedback problem, i.e., from the expression:

$$\frac{K_p N_{\delta_a}^p N_{\delta_r}^r}{N_{\delta_r}^r} = \frac{K_p L_{\delta_a}^i N_{\delta_r}^i s \left( s + \frac{1}{T_{p,r}} \right)}{N_{\delta_r}^i \left( s + \frac{1}{T_r} \right) \left[ s^2 + 2 \zeta_r \omega_r s + \omega_r^2 \right]} = -1 \quad (19)$$

The ratio of coupling numerator to the  $N_{\delta_r}^r$  numerator is typically of the form shown in Fig. 4. Since  $L_{\delta_a}^i$  is usually quite large, the complex root  $\omega_r'$  rapidly moves toward the origin with increasing roll damper gain,  $K_p$ . This may be observed by comparing the relative motions of the closed-loop roots  $\omega_r'$  and  $1/T_r'$ . Note that  $\omega_r'$  moves toward the origin at a rate just slightly less than that of the root  $1/T_r'$  moving to higher frequency. The

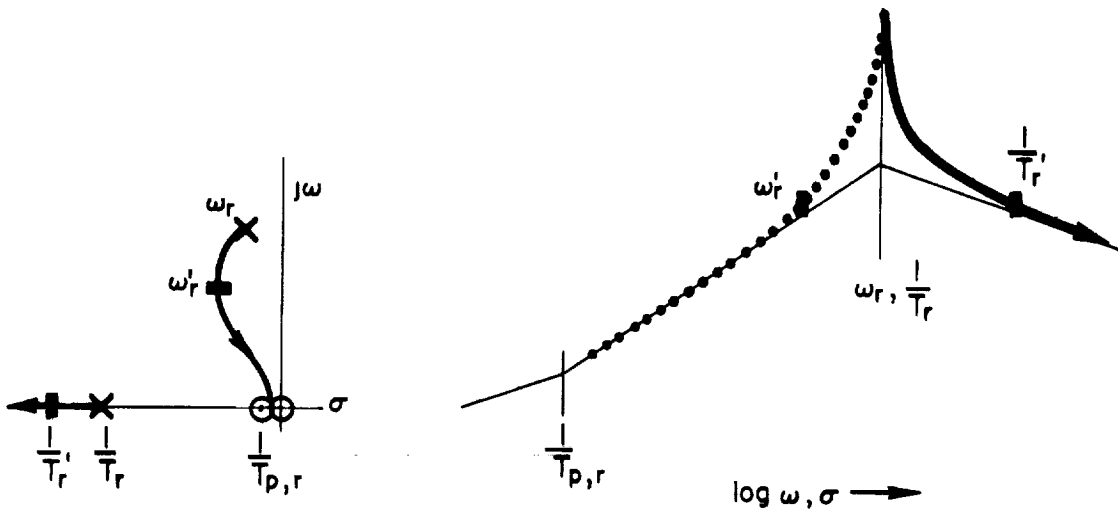


Figure 4. Effect of Roll Damper on Yaw-Rate-to-Rudder Numerator

latter movement is almost identical to that of the roll rate damper augmented roll subsidence mode ( $1/T_R' \doteq L_p' + K_p L_{\delta_a}'$ ) which is the usual reason for incorporating this feedback. Thus, the usual near cancellation of  $1/T_R$  and  $1/T_R'$  in the yaw-rate/rudder transfer function is enhanced along with the reduction of  $\omega_r$ .

### C. HYDRAULIC AND ELECTROHYDRAULIC ACTUATION SYSTEMS

A typical fully-powered hydraulic surface positional actuator as used for flight control purposes is illustrated in Fig. 5. A block diagram emphasizing the installation is shown in Fig. 6. This block diagram applies to either the surface actuator of Fig. 5 or to an electrohydraulic autopilot or SAS servo. For the fully-powered mechanical input surface-actuating systems, the load dynamics comprise hinge moment, surface inertia, elasticity between actuator output and surface, etc., while the support dynamics are ordinarily very rigid. In the case of a stability augmentor connected in

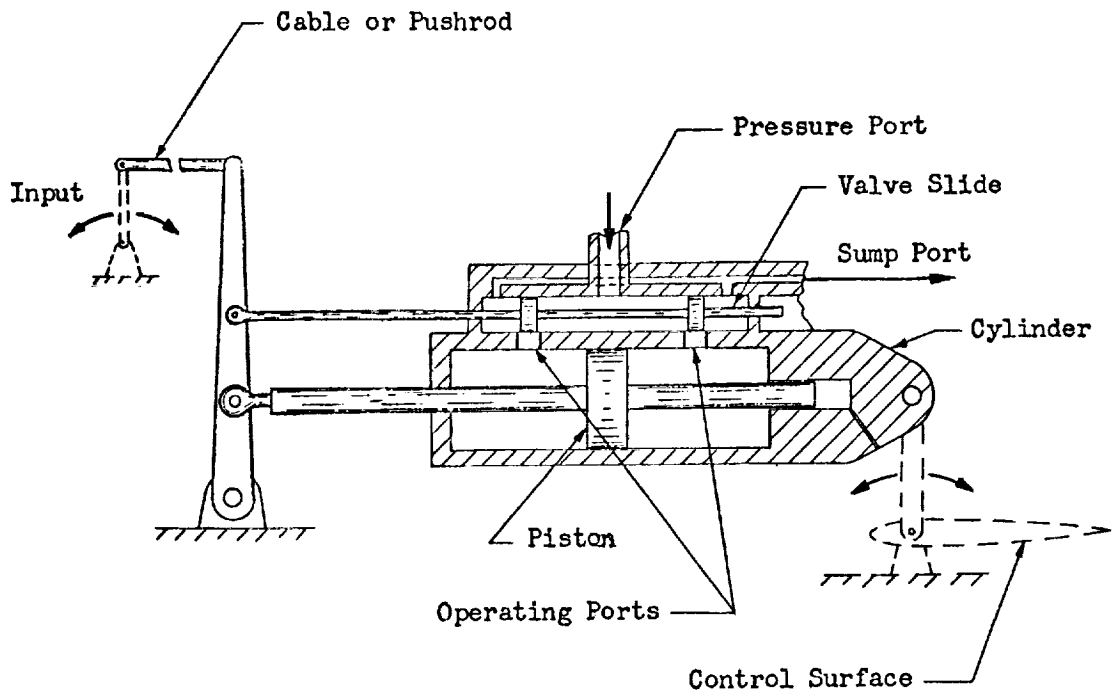


Figure 5. A Fully-Powered Hydraulic Servo Surface Actuator

H-859

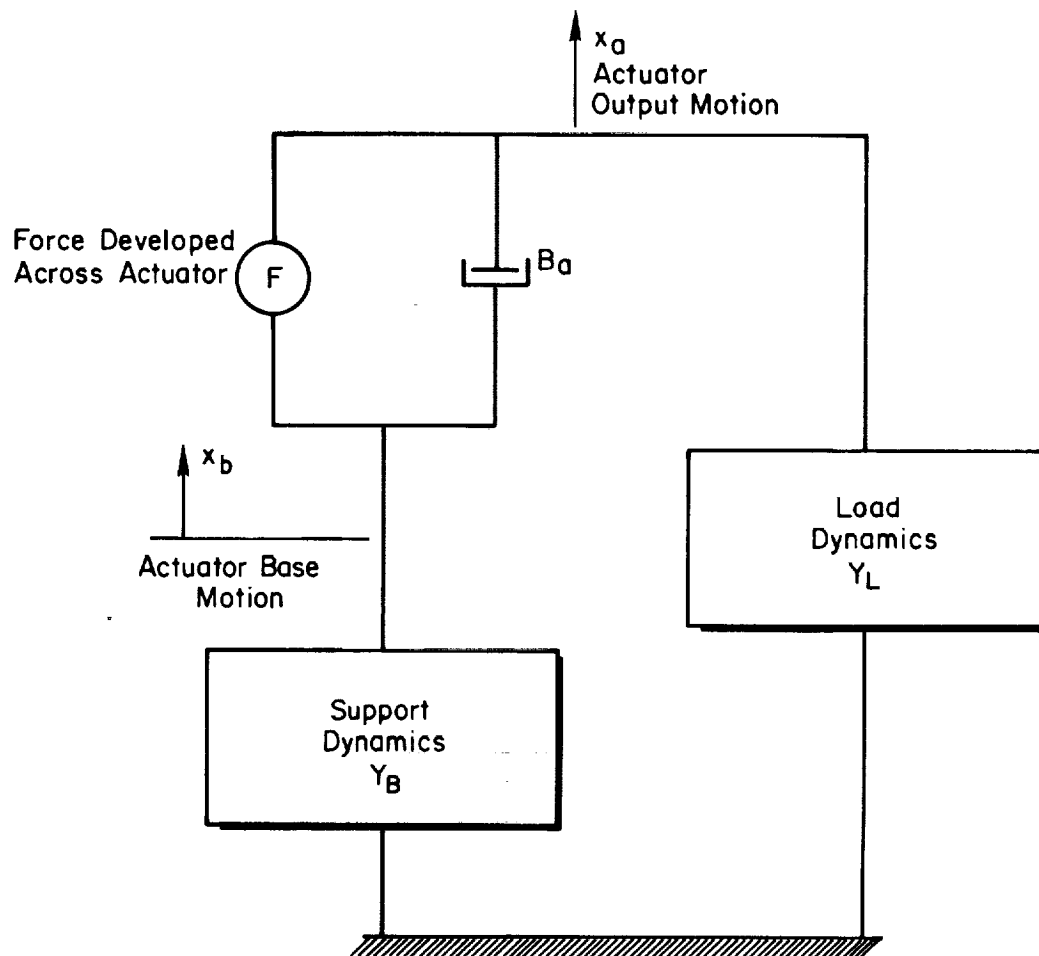


Figure 6. Block Diagram of Actuator, Load, and Support

series within the manual control system, the support dynamics consist primarily of detents, friction, and preload, while the load dynamics may be dominated by valve friction and artificial feel system forces.

The force,  $F$ , in Fig. 6 is developed across the piston of the actuator by the metering activities of the valve. The viscous friction term,  $B_a$ , represents a frictional force proportional to the velocity across the piston. In most actuators, this is very small, although viscous dampers or extra leakage flow can make it very large. From a performance standpoint,  $B_a$  is kept as small as possible.

The equations governing the load dynamics for the general case are given by:

$$\begin{bmatrix} (Y_L + B_a s) & -B_a s \\ Y_L & Y_B \end{bmatrix} \begin{bmatrix} x_a \\ x_b \end{bmatrix} = \begin{bmatrix} F \\ 0 \end{bmatrix} \quad (20)$$

Thus, the transfer function relating the actuator displacement,  $x_a$ , and force across the piston is:

$$\frac{x_a}{F} = \frac{1}{Y_L + B_a s \left( 1 + \frac{Y_L}{Y_B} \right)} \quad (21)$$

Ideally, the purpose of the actuator is to move the load dynamics rather than support structure, so  $x_a$  is hopefully much larger than  $x_b$ . Because  $x_a/x_b = -Y_B/Y_L$ , this is accomplished by making  $Y_B$  much greater than  $Y_L$  for the varieties and kinds of piston forces developed. Making good this inequality for series SAS servos is sometimes difficult without compromising other elements in the manual control system such as stick breakout forces or trim systems. Nonetheless, it is only when this inequality approaches ideal values that a series installation will operate effectively. Similarly, the surface actuator should operate with very little backup structure deformation (although some installations use so-called structural feedback to circumvent stability problems). Consequently, for both types of actuators operating in near-ideal circumstances, Eq. 21 will reduce to:

$$\frac{x_a}{F} \doteq \frac{1}{Y_L + B_a s} \quad , \quad \frac{Y_L}{Y_B} \ll 1 \quad (22)$$

A general equation defining the behavior of an electrohydraulic or hydraulic actuator is given by (Ref. 4):

$$As(x_a - x_b) = C_i i - \left( \frac{A^2 s}{k_o} + C_p \right) p_C \quad (23)$$

where

- A = Piston area
- $k_o = \text{Actuator oil "spring"} = A^2 N / V_e$
- N is effective bulk modulus of the oil-air-structural combination
- $V_e$  is the equivalent volume of the actuator cylinder
- $p_C = \text{Load-induced pressure differential across the piston}$
- $C_p = \text{Slope of servovalve flow versus load pressure}$
- $C_i = \text{Slope of servovalve flow versus valve command}$

This equation states that the flow into the cylinder,  $As(x_a - x_b)$ , is equal to a flow due to the valve command,  $i$ , as diminished by a "regulation" flow due to load pressure variation,  $C_p p_C$ , plus a flow due to compressibility,  $(A^2 s / k_o) p_C$ . For the surface actuator, the general valve input,  $i$ , would be valve error,  $\epsilon$ ; whereas for an electrohydraulic actuator the input,  $i$ , could be the current in the electrohydraulic valve assuming that various high-frequency lags between coil current and valve motion are negligible.

Consider now the simple case where the support structure is rigid ( $x_b = 0$ ) and the effects of compressibility and pressure variation are negligible and where, further, the valve input,  $i$ , is taken to be the valve error,  $\epsilon$ . Then Eq. 23 becomes:

$$Asx_a = C_i \epsilon \quad (24)$$

Assume now for simplicity that the valve error,  $\epsilon$ , is simply the difference between an actuator input command,  $x_i$ , and the output,  $x_a$ ; then the open-loop transfer function will be:

$$\begin{aligned} \frac{x_a}{\epsilon} &= \frac{C_i}{As} \\ &= \frac{\omega_c}{s} = \frac{1}{Ts} \end{aligned} \quad (25)$$

This is the pure-integrator open-loop form of an idealized hydraulic actuator. The crossover frequency and closed-loop bandwidth,  $\omega_c$ , is  $C_i/A$ , which is also the inverse time constant of the closed-loop system.

In line with the principal thesis in this section of quadratic dipole problems, it is the departure of the physical actuator dynamics from these ideal characteristics which is of primary interest here. This will be worst for the most difficult stability situation which will occur when the actuator is holding little or no steady-state hinge moment. Accordingly, the flow due to pressure variation,  $C_p P_C$ , can be ignored since  $C_p k_o/A^2 \ll \omega_c$  except near actuator stall. The force developed across the piston will then be:

$$A p_C = F = \frac{C_i k_o}{A s} \epsilon - k_o (x_a - x_b) \quad (26)$$

From Eqs. 20 and 26 one can derive the open-loop transfer function relating the actuator output,  $x_a$ , and the valve error,  $\epsilon$ . This is:

$$\frac{x_a}{\epsilon} = \frac{K_i/s}{Y_L + (B_a s + k_o) \left(1 + \frac{Y_L}{Y_B}\right)} \quad (27)$$

where  $K_i = C_i k_o/A$

Consider now a completely rigid support structure and a set of simplified load dynamics such as shown in Fig. 7. The coupling compliance,  $K_C$ , is the only spring involved in this simplified situation. More generally, a spring in parallel with the load mass,  $M_\ell$ , would appear representing the hinge moment gradient. This spring, however, will always be much less than typical coupling compliance, so its effect on stability is relatively minor. The load admittance is:

$$Y_L = \frac{F}{x_a} = \frac{M_a s^2 \left[ s^2 + \frac{K_C}{M_\ell} \left(1 + \frac{M_\ell}{M_a}\right) \right]}{s^2 + \frac{K_C}{M_\ell}} \quad (28)$$

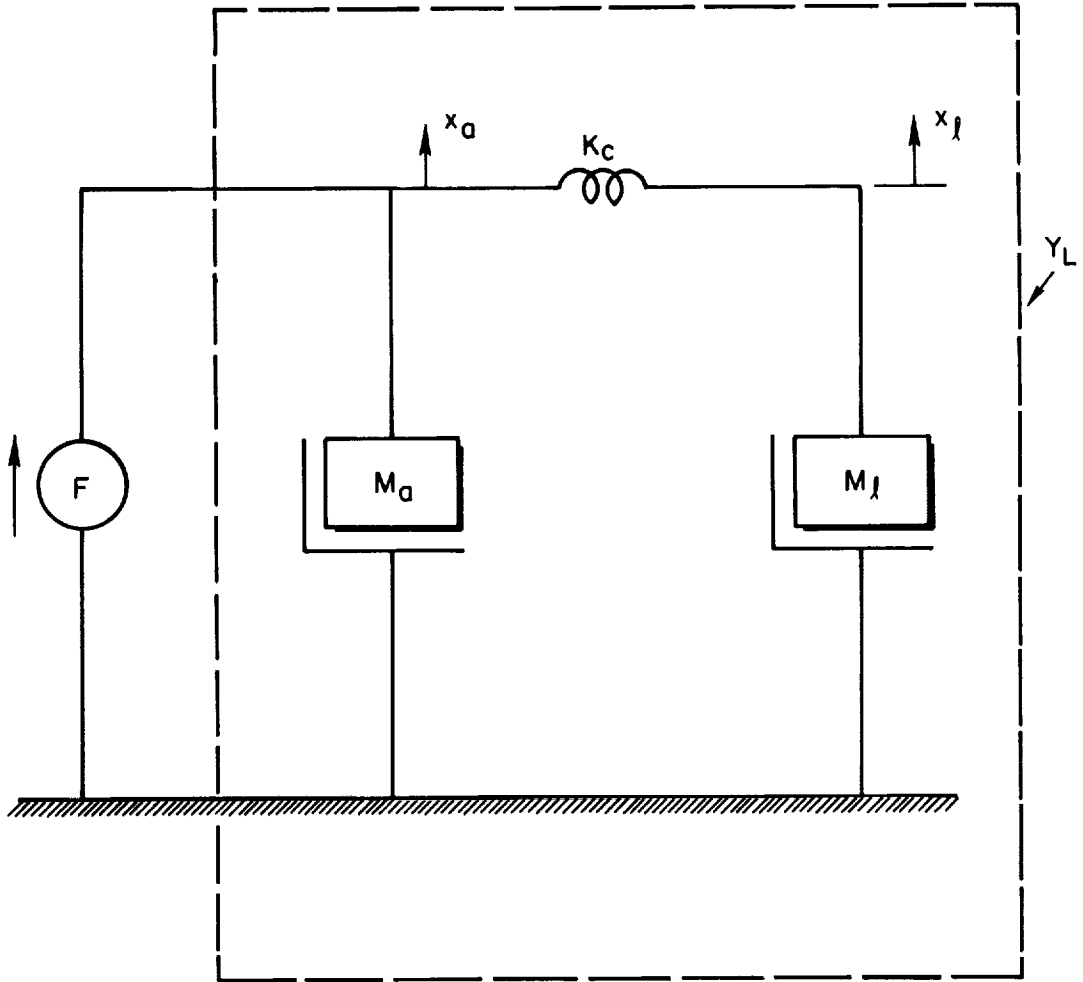


Figure 7. Simplified Load Dynamics

Ordinarily, for a surface actuator the actuator mass will be much less than the load mass, i.e.,  $M_a/M_l \ll 1$ . The lower-frequency characteristics of the load admittance then become approximately:

$$Y_L \doteq \frac{K_c s^2}{s^2 + \frac{K_c}{M}} \quad (29)$$

and the open-loop transfer function becomes:

$$\begin{aligned} \frac{x_a}{\epsilon} &\doteq \frac{K_i \left( s^2 + \frac{K_c}{M_l} \right)}{s B_a \left( s + \frac{K_c + k_o}{B_a} \right) \left[ s^2 + \frac{B_a}{M_l} \left( \frac{K_c}{K_c + k_o} \right) s + \frac{K_c}{M_l} \left( \frac{k_o}{K_c + k_o} \right) \right]} \\ &\doteq \frac{K_i}{(K_c + k_o) s} \frac{\left( s^2 + \frac{K_c}{M_l} \right)}{\left[ s^2 + \frac{B_a}{M_l} \frac{(K_c/k_o)}{(1 + K_c/k_o)} s + \frac{K_c}{M_l (1 + K_c/k_o)} \right]} \\ &\doteq \frac{\omega_c}{s} \frac{\left[ \left( \frac{s}{\omega_2} \right)^2 + 1 \right]}{\left[ \left( \frac{s}{\omega_1} \right)^2 + \frac{2\zeta_1 s}{\omega_1} + 1 \right]} \end{aligned} \quad (30)$$

where

$$\omega_c = K_i/k_o = C_i/A$$

$$\omega_1 = \omega_2 \sqrt{1/(1 + K_c/k_o)}$$

$$\omega_2 = \sqrt{K_c/M_l}$$

Thus, the quadratic pair atop an  $\omega_c/s$  characteristic again appears. The numerator and denominator are very close together and essentially cancel when the compressibility spring,  $k_o$ , becomes infinite, thereby reducing to the idealized case already discussed. The open- and closed-loop transfer

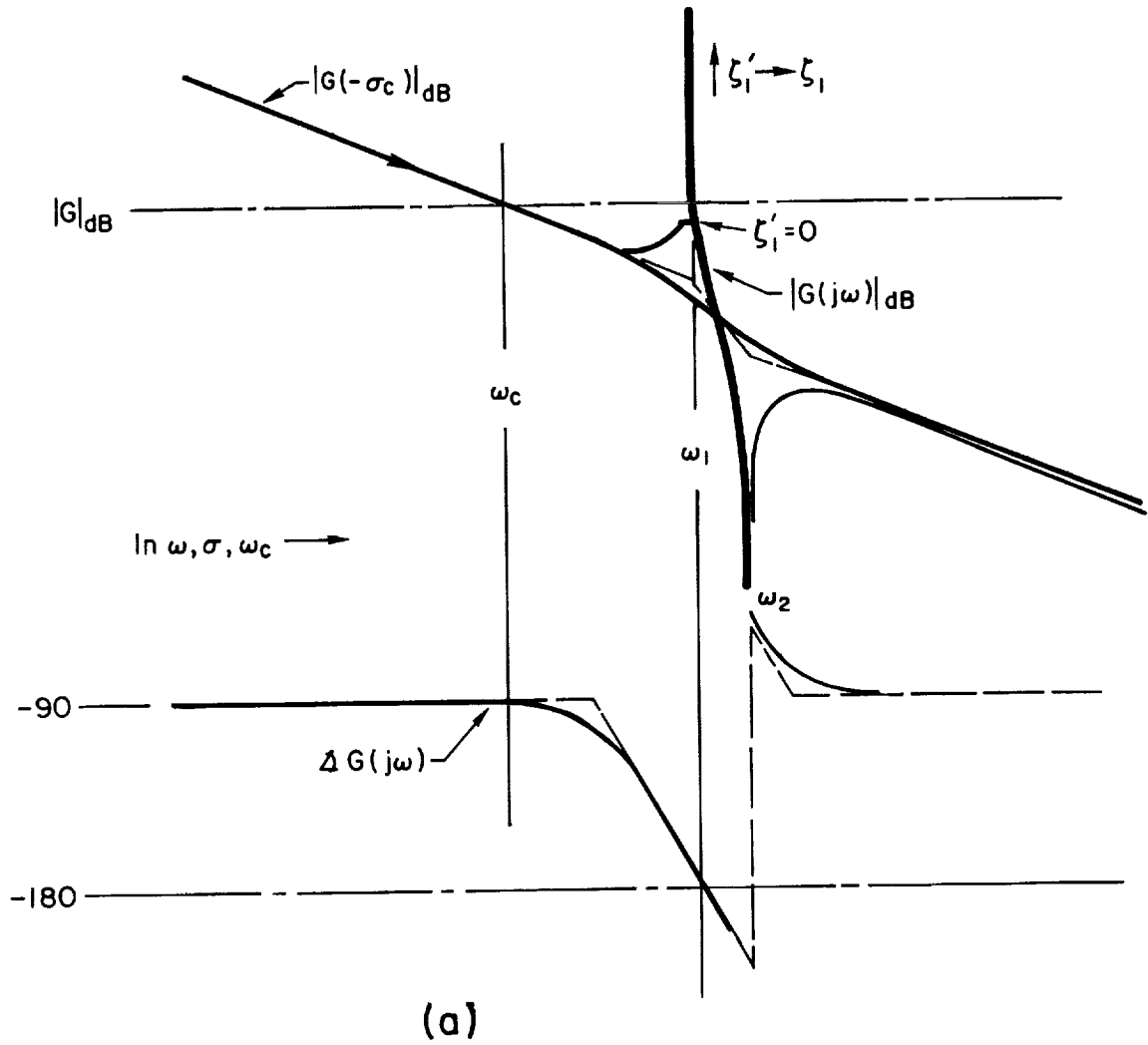
function characteristics are portrayed in conventional and Bode root locus form in the system survey of Fig. 8. The available bandwidth is limited to a value which will permit a finite gain margin. The gain margin in this case is given approximately by the negative of the gain of the peak of the Bode plot of  $G(j\omega)$  near the frequency  $\omega_1$ .

In principle, since there is ordinarily some damping in the load, one can never get an  $s^2 + K_c/M_\ell$  numerator without some slight damping. Under such conditions, it is theoretically possible to increase the bandwidth by increasing the system gain to the extent that the denominator roots are driven back into the stable left half plane toward the numerator zeros. This cannot ordinarily be accomplished without exciting higher-frequency structural modes or encountering limiting in the hydraulic actuator. Limiting, of course, effectively decreases the gain and forces the roots back into the region of instability.

The limitation of bandwidth due to the dipole emphasizes the need for stiff actuator-to-surface compliance and effective oil spring. For many systems these steps are sufficient. When they are not, the gain margin can be increased by modifying the effective damping of the  $\omega_1$  mode. This can be accomplished in a large number of ways, the simplest being to permit more leakage, and hence a larger  $B_a$ , at the cost of increased drain on the power system. Relatively complicated hydraulic-mechanical equalization or, in the case of electrohydraulic valves, electrical equalization can be used to alleviate the deleterious effects of the dipole. Closing the actuator loop using a specially contrived structural link can also serve the same purpose.\*

---

\*An exhaustive treatment of these and other appropriate techniques is provided in Ref. 4.



$$G = \frac{x_a}{\epsilon} = \frac{\omega_c \left[ \left( \frac{s}{\omega_2} \right)^2 + 1 \right]}{s \left[ \left( \frac{s}{\omega_1} \right)^2 + \frac{2\zeta_1 s}{\omega_1} + 1 \right]}$$

$$\omega_c = \frac{C_i}{k_o}$$

$$\omega_2 = \sqrt{\frac{K_a}{M_I}}$$

$$\omega_1 = \omega_2 \sqrt{\frac{1}{1 + K_c/k_o}} \quad (b)$$

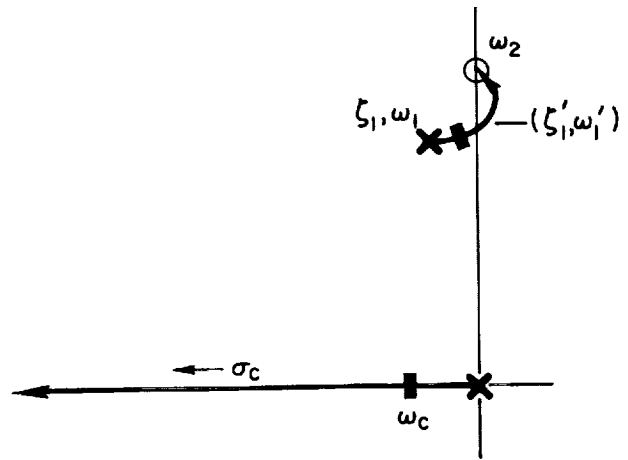


Figure 8. Rigid Support Structure, Compliant Load Coupling, Feedback Attached to  $x_a$

### SECTION III

#### SYSTEMS NUMERATOR PROBLEMS

A fundamental feature of feedback control systems is the property that some system poles progress toward open-loop zeros as loop gains are increased. Thus, any open-loop zeros which are present in a frequency regime associated with high amplitude ratio of some feedback loop are close approximations to a closed-loop mode. Ordinarily, this property is a highly desirable attribute of feedback, for it simply indicates that a closed-loop mode is essentially canceled by an open-loop zero — thereby providing a more direct correspondence between a specified system command input and its associated output. This feature may not be so desirable, on the other hand, if the zero being approached is in the right half plane; then an unstable mode can be introduced into the closed-loop system. This unstable mode will be hardly apparent in the motion being commanded because of the near pole-zero cancellation in that particular closed-loop transfer function. But the instability is there and inevitably will be a dominant feature in some other degree of freedom where this nice near-cancellation is not present. There are a number of interesting cases in flight control where this phenomenon occurs. These will be exemplified in the first section following. The most common non-minimum phase zero occurring in flight control is probably the "performance reversal" associated with control of altitude or rate of climb. Closely connected with the same root causes is a less common, but nonetheless important, divergence associated with a negative pitch attitude control zero. This is particularly insidious when it does occur, because attitude control is an omnipresent requirement for almost any aircraft maneuver or steady-state situation. A third example of the non-minimum phase zero is also associated with longitudinal control although its effect is felt predominately in a lateral divergence. This interesting condition occurs in some so-called "nose slice" departures occurring in high-angle-of-attack flight.

Another circumstance in which zeros play a key role occurs when they are intentionally introduced as desirably located "sinks" in the root plane to be approached by root loci originating at undesirably located

open-loop airframe poles. This technique offers an often beneficial, and always simple, design technique to place the poles in a desirable location. But this may lead to very little benefit when the overall system dynamics are viewed, because poles accompany the intentionally introduced zeros as an offshoot of the mechanization. These additional poles also influence the system dynamic characteristics and can negate the intended improvement associated with the zeros. An example is given in Subsection B.

## A. NON-MINIMUM PHASE ZEROS

### 1. Altitude Control

Altitude and rate of climb are very important quantities which must often be controlled accurately. This is accomplished by direct feedback of the controlled variable since both altitude and rate of climb are both very low-frequency path quantities. Any control exerted to affect them is outer loop in nature; thus the essential features can be considered with a simplified airframe description. An appropriate version is the three degree-of-freedom phugoid equations of motion of Ref. 1. These are:

$$\begin{bmatrix} (s - X_u) & -X_w & g \\ -Z_u & (s - Z_w) & -U_0 s \\ -M_u & -M_w & 0 \end{bmatrix} \begin{bmatrix} u \\ w \\ \theta \end{bmatrix} = \begin{bmatrix} X_{\delta_e} \\ Z_{\delta_e} \\ M_{\delta_e} \end{bmatrix} \delta_e \quad (31)$$

With  $X_{\delta_e}$  neglected the altitude-to-elevator transfer function is given by:

$$\frac{h}{\delta_e} = \frac{[(Z_{\alpha}/M_{\alpha})M_{\delta} - Z_{\delta}][s + (1/T_{h1})]}{s[s^2 + 2(\zeta\omega)_p s + \omega_p^2]} \quad (32)$$

where

$$2(\zeta\omega)_p = -X_u + \frac{M_u(X_{\alpha} - g)}{M_{\alpha}} ; \omega_p^2 = -\frac{g}{U_0} [Z_u - (M_u/M_w)Z_w]$$

and the zero,  $1/T_{h1}$  is

$$1/T_{h1} = -X_u + \frac{(X_\alpha - g)(Z_{\delta_e} M_u - M_{\delta_e} Z_u)}{(Z_{\delta_e} M_\alpha - M_{\delta_e} Z_\alpha)} \quad (33)$$

It is apparent from the root locus sketch of Fig. 9 that the feedback of altitude alone increases the phugoid undamped natural frequency and decreases its damping ratio. In the usual circumstance where  $1/T_{h1}$  is positive the phugoid roots are in fact driven into the right half plane at very low values of gain. Consequently, some form of equalization is required to improve the phugoid characteristics. By far the most common means to accomplish this is an inner pitch attitude loop. The details of how this inner loop changes the phugoid are illustrated in the next article. But, for now, we will simply state that it directly increases the phugoid damping so that the phugoid characteristics are no longer of concern in our present discussion.

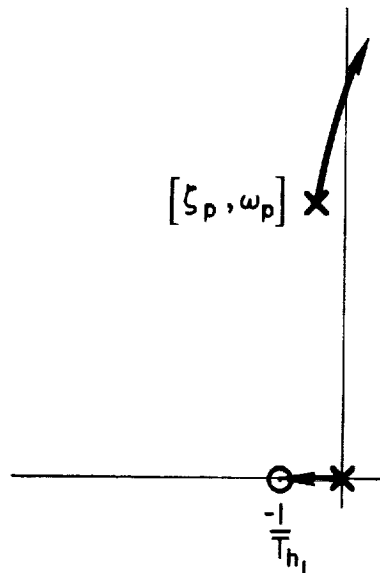


Figure 9. Root-Locus Sketch of Altitude Control System

The major problem with altitude control once the phugoid is attended to is encountered for situations where  $1/T_{h1}$  becomes negative. In this event closure of an altitude loop will drive the pole at the origin into

the right half plane toward  $1/T_{h1}$ . The result is a divergent instability at any value of closed-loop gain. For the typical values of altitude control gain used conventionally, the pole at the origin is driven quite close to  $1/T_{h1}$ . Therefore, while the divergence is theoretically present it is effectively canceled by the  $1/T_{h1}$  zero in the closed-loop altitude transfer function as far as any altitude command inputs are concerned. Thus a divergence in altitude is the last thing seen in a typical negative  $1/T_{h1}$  situation. It is present but again only marginally indicated in the pitch response, because the pitch attitude is tightly held to control phugoid. The divergence appears full blown in the speed, because this transfer function does not contain the  $-1/T_{h1}$  zero. Eventually, of course, airspeed will slow to a point where the available lift is inadequate for control of the flight path. In other words, the altitude (path) control gain cannot be maintained so the divergence will become more apparent. In fact when carried to its ultimate limit, the airplane will stall and all closed-loop control is lost.

The key to this situation is  $1/T_{h1}$ . As shown in Ref. 1, this can be approximated by:

$$\frac{1}{T_{h1}} \doteq \frac{1}{m} \left( \frac{dD}{dU} - \frac{\partial T}{\partial U} \right) \quad (34)$$

It follows that  $1/T_{h1}$  will reverse sign at that flight condition corresponding to maximum excess thrust; or, if thrust variations with speed are unimportant, at the minimum drag condition ( $dD/dU = 0$ ). Or, in other words, the zero will change sign whenever the airplane goes from the front side to the back side of the thrust required versus speed curve. This is a common situation on very low speed approaches, particularly on carrier approaches. It is also encountered in steep climbs near the vehicle's absolute ceiling, and at other situations where flight at near-minimum drag is desirable. Since the condition coincides with one version for maximum rate of climb, it also has implications for rate of climb systems set up to give maximum climb rates.

To correct the performance reversal, the zero must be made positive, thereby essentially providing for front side operation. Several possible means of accomplishing this are revealed from the literal expression for  $1/T_{h1}$  in Eq. 33. This shows that modifying either  $X_u$  or  $X_a$  can eliminate the divergence. This is conventionally accomplished by throttle. It should be recalled that in any case a zero cannot be modified without actuation of an additional control (other than the elevator, in this case).

The maximum rate of climb difficulties associated with the performance reversal are most usually alleviated by the use of airspeed-like feedbacks to control either indicated airspeed or Mach number to values which approximate those for best climb. Feedbacks of these quantities do not suffer from performance reversal problems. Further, they usually do not require command scheduling as a function of altitude to come quite close to best climb performance. Consequently this type of system, which sidesteps the performance reversal, often offers a simple and adequate solution.

## 2. Pitch Attitude Control Reversal

The control and regulation of the airplane's pitch attitude is perhaps the most ubiquitous longitudinal control function. It is present in almost all automatic flight control systems and is furthermore the most common function provided by the pilot in non-automatic circumstances. It is also a constituent of most more complex systems such as the attitude control and regulation system discussed above. Figure 10 shows a block diagram of a typical  $\theta \rightarrow \delta_e$  feedback control system with a pure gain controller. In this system the short period is assumed to be well enough damped, either inherently or via a pitch damper, to permit a pure gain closure to be adequate. The figure also contains a "system survey" using Bode and conventional root loci which show the migration of the closed-loop roots in their progression from the open-loop poles to the open-loop zeros and the high-gain asymptotes. From the system survey it can be appreciated that the closed-loop phugoid roots are driven into close proximity to the  $1/T_{\theta 1}$  and  $1/T_{\theta 2}$  zeros. The phugoid is in fact overdamped, and the pitch attitude in this entire frequency range is very well controlled. This is evidenced by the closed-loop asymptotic amplitude Bode plot constructed for the example 0 dB line. Its nearly flat properties in the

34

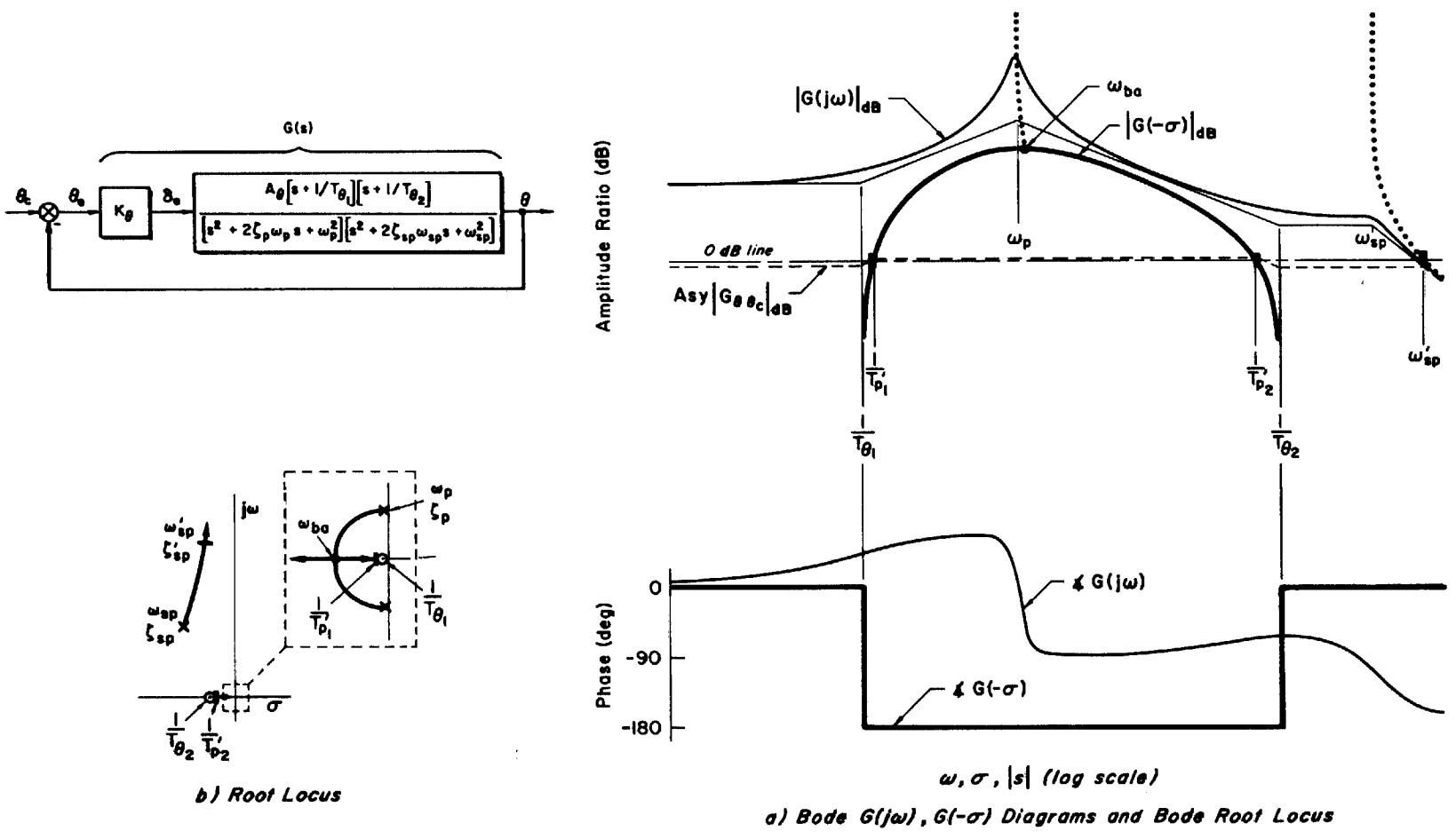


Figure 10. System Survey of Pure Gain Pitch Attitude Control System

vicinity of the modified phugoid roots due to the essential cancellation of the overdamped phugoid poles by the open-loop zeros,  $1/T_{\theta 1}$  and  $1/T_{\theta 2}$ , indicate that the closed-loop mode will be suppressed almost completely in the pitch attitude response to  $\theta_c$  commands.

In the system as shown, the open-loop gain does not become infinite at zero frequency, and therefore the closed-loop frequency response has an amplitude ratio slightly less than 1 at low frequencies. This is not serious for the situation depicted in Fig. 10. However, at conditions when  $1/T_{h1}$  is near zero the static-to-short-period gain ratio,  $1/\omega_p^2 T_{\theta 1} T_{\theta 2}$ , is small and the system may appear as shown in Fig. 11. When this occurs the long-term response of the closed-loop system to commands is very poor. As indicated graphically by the closed-loop asymptotes, there will be a very low-frequency lead/lag and a dc gain less than unity. In the response of  $\theta$  to a step  $\theta_c$ , these would correspond to a very long time constant mode and to a steady-state position error.

For automatic pilot systems which are intended to follow commands, such as systems with attitude-hold features, this sort of deficiency in low-frequency gain can be made up using integral control. A pitch integrator is added in parallel to the straight-through gain of the controller, leading to the configuration shown in Fig. 12. The transfer function of the controller is now  $K_{\theta} + K_{\theta}^i/s$  and an integration and a lead,  $(K_{\theta}/s)(s + K_{\theta}^i/K_{\theta})$ , are cascaded with the open-loop function representing the dynamics of the airplane. As shown in the amplitude ratio asymptotes for the compensated system, the lead time constant is shown so that its breakpoint,  $K_{\theta}^i/K_{\theta}$ , is greater than the phugoid undamped natural frequency, thus making the low-frequency amplitude ratio in the region of the phugoid as large as feasible. This effectively eliminates the droop and other characteristics shown in Fig. 11. With the aid of the integral control we are thus returned to a closed-loop situation similar to that shown in Fig. 10. In the sense of our current emphasis, in both cases a closed-loop root is present near  $1/T_{\theta 1}$ .

Let us now define more precisely the aircraft characteristics which govern the static-to-short period gain ratio,  $1/\omega_p^2 T_{\theta 1} T_{\theta 2}$ . This can be expressed in terms of the approximate factors of Ref. 1 as:

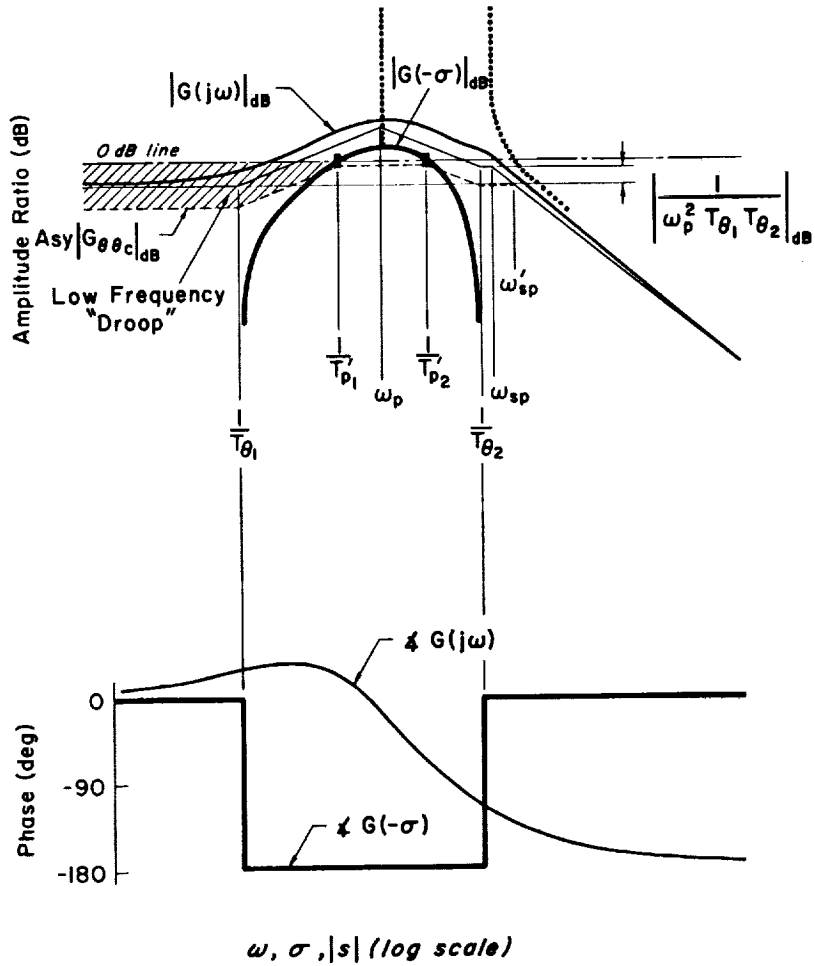
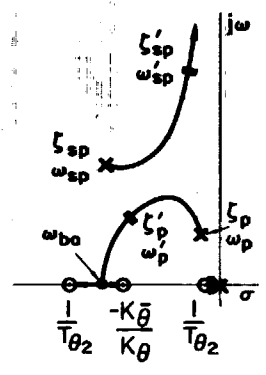
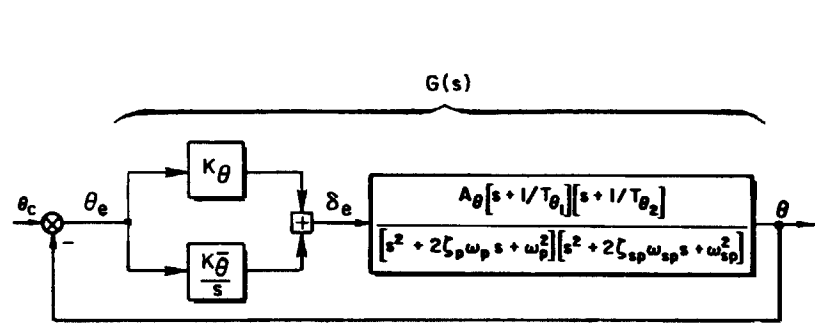
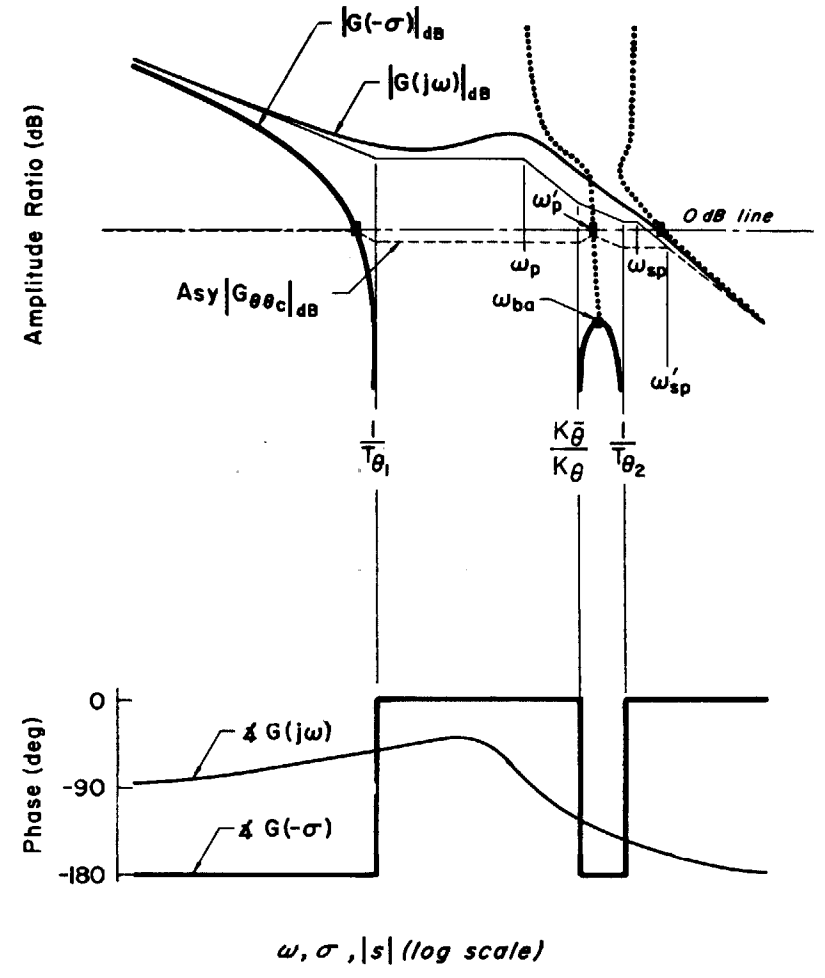


Figure 11. Pure Gain Pitch Attitude Control System with Static-to-Short-Period Gain Ratio Less Than 1



b) Root Locus



a) Bode  $G(j\omega)$ ,  $G(-\sigma)$  Diagrams and Bode Root Locus

Figure 12. System Survey of Pitch Attitude Control System with Integrator

$$\frac{1}{\omega_p^2 T_{\theta_1} T_{\theta_2}} \doteq \frac{[1 - (Z_w M_q / M_\alpha)] [Z_w X_u - X_w Z_u + (Z_{\delta_e} / M_{\delta_e})(X_w M_u - X_u M_w)]}{-(g/U_o)[Z_u - (M_u Z_w / M_w)]} \quad (35)$$

For the simplified, but not unusual, conditions where  $|Z_w M_q / M_\alpha| \ll 1$  and  $|Z_{\delta_e} M_w / Z_w M_{\delta_e}| \ll 1$  and the  $M_u$  terms negligible, the static-to-short-period gain ratio will become:

$$\frac{1}{\omega_p^2 T_{\theta_1} T_{\theta_2}} \doteq 1 + \frac{U_o Z_w}{g Z_u} \left( \frac{1}{T_{h_1}} \right) \quad (36)$$

Thus, the magnitude of  $1/\omega_p^2 T_{\theta_1} T_{\theta_2}$  will be unity when  $1/T_{h_1} = 0$  and less than unity when  $1/T_{h_1}$  decreases to negative values. Consequently the static-to-short-period gain of 1 occurs approximately at performance reversal. Because near-minimum drag flight is often desirable from a performance standpoint, flight conditions near the performance reversal are not uncommon and, as described in the above discussion, good attitude control is still possible under these conditions. There is, however, a lurking specter analogous to the  $1/T_{h_1}$  performance reversal situation in altitude control. This is the possibility that  $1/T_{\theta_1}$  will become negative and thereby draw a closed-loop root into the right half plane. If Eq. 36 is solved for  $1/T_{\theta_2}$  it is approximately:

$$\begin{aligned} \frac{1}{T_{\theta_1}} &\doteq \frac{1}{T_{h_1}} - \frac{g}{U_o} Z_u T_{\theta_2} \\ &\doteq \frac{1}{T_{h_1}} + 2 \left( \frac{g}{U_o} \right)^2 T_{\theta_2} \end{aligned} \quad (37)$$

$T_{\theta_2}$  is always positive in unstalled flight. Therefore, while  $1/T_{\theta_1}$  can become negative if  $1/T_{h_1}$  is sufficiently large and negative, the change in sign in the pitch characteristic will not occur until the airplane is well on the back side. The performance regime for good pitch attitude control with elevator is therefore wider than that for path control with elevator alone, but a divergence can nonetheless appear when the backsidedness

exceeds the safety margin given by  $2(g/U_0)^2 T_{\theta 2}$ . While a pitch attitude divergence caused by a negative  $1/T_{\theta 1}$  is less likely than the associated performance reversal due to  $1/T_{h1}$ , it is in many ways more embarrassing because of the ever-present nature of attitude control loops.

### 3. Coupled Lateral-Longitudinal (Non-Minimum Phase Zeros) Dynamic Effects

For high performance military aircraft at high angles of attack, it is common for sideslip to exist either intentionally (e.g., rudder maneuvering) or unintentionally (e.g., adverse aileron yaw, mistrim, etc.). The longitudinal-lateral coupling resulting from unsymmetrical flight can create non-minimum phase zeros in the pitch attitude numerator. These can occur at angles of attack considerably below that for stall and at relatively small sideslip angles. Conventional feedback of pitch attitude or rate to elevator (either automatic or manual) then produces a coupled longitudinal-lateral divergence known as nose slice.

As an example (Ref. 5), Fig. 13 presents a nine by nine matrix (three body axis moments, three flight path displacements, and three Euler angle transformation equations) for coupled, non-symmetric flight. The elements of the matrix are obtained from the small perturbation expansion of the complete nonlinear (inertial and aerodynamic) equations of motion in which aerodynamic coefficients are a function of  $\alpha$  and  $\beta$ . Only the most significant off-diagonal terms are identified. Example numerical values are given for a current operational aircraft at 19 deg  $\alpha$  and 6 deg  $\beta$ .

The major coupling associated with nose slice is provided by the terms within the heavy borderlines. Two of these,  $L_\alpha$  and  $N_\alpha$ , are aerodynamic and two,  $\beta_0 \cos \alpha_0 \equiv Z_p$  and  $\beta_0 \sin \alpha_0 \equiv Z_r$ , are nonlinear kinematic terms. The effect of the off-diagonal terms on pitch attitude transfer function pole-zero locations is demonstrated in Fig. 14. Figure 14a shows a completely uncoupled six-degree-of-freedom case for reference. Here the two lateral-directional modes ( $\omega_d$  and  $\omega_{SR}$ ) have cancelling pole-zero dipoles as would be expected. Figure 14d presents the pole-zero locations for the completely coupled 6 DOF case which shows the poles to be little affected by coupling, whereas a major shift occurs in zero locations. The most significant movement is the real zero which moves into the right half plane.

OF

$(s - X_u)$ [s + .0634]	$-X_w U_0$ [22.68]		$-X_\beta$ [5.766]			$-g \frac{\cos \theta}{\sin \beta}$ [-3.187]	$g \cos \beta_0$ [32.024]		u	$X_{\delta_e}$ [-.1025]	$X_{\delta_r}$ [.698]	$\delta_e$
$\frac{-Z_u}{U_0}$ [.00087]	$(s - Z_w)$ [s + .323]	-1		$\beta_0 \cos \alpha_0$ [.0995]	$\beta_0 \sin \alpha_0$ [.0338]				$\alpha - \alpha_0$	$Z_{\delta_e}$ [-.057]		$\delta_a$
	$-M_\alpha$ $-M_w Z_\alpha$ [3.577]	$s - M_q$ $-M_\alpha$ [s + .386]		$r_0( )$ $+p_0( )$ [.00818]	$-r_0( )$ $+p_0( )$ [-.0025]				q	$M_{\delta_e}$ [-2.92]		$\delta_r$
	$-Y_\alpha$ [-.0122]		$(s - Y_v)$ [s + .1062]	$-\sin \alpha_0$ [-.3216]	$\cos \alpha_0$ [.9469]	$\frac{-g}{U_0} \cos \alpha_0$ [-.1166]	$\frac{-g}{U_0} \sin \beta$ [-.0129]		$\beta - \beta_0$	$Y_{\delta_e}$ [-.0037]	$Y_{\delta_r}$ [.0255]	
	$-L'_\alpha$ [-3.09]		$-L'_\beta$ [4.45]	$(s - L'_p)$ [s + .849]	$-L'_r$ [-.3323]				p	$L'_{\delta_e}$ [-.292]	$L'_{\delta_a}$ [.431]	$L'_{\delta_r}$ [1.4]
	$-N'_\alpha$ [1.486]		$-N'_\beta$ [.1885]	$-N'_p$ [-.0193]	$(s - N'_r)$ [s + .1276]				r	$N'_{\delta_e}$ [.1095]	$N'_{\delta_a}$ [.031]	$N'_{\delta_r}$ [-.998]
				-1	$-\tan \epsilon_0$ [-.3396]	s	$\frac{-r_0}{\cos^2 \theta_0}$ [.0116]		$\psi - \psi_0$			
		-1				$r_0 \cos \theta_0$ [-.0104]	s		$\theta - \theta_0$			
					$\frac{-1}{\cos \theta_0}$ [-1.056]		$\frac{-r_0 \sin \theta}{\cos^2 \theta_0}$ [.0037]	s	$\psi - \psi_0$			

Figure 13. Matrix for Coupled Equations with  $\beta \neq 0$

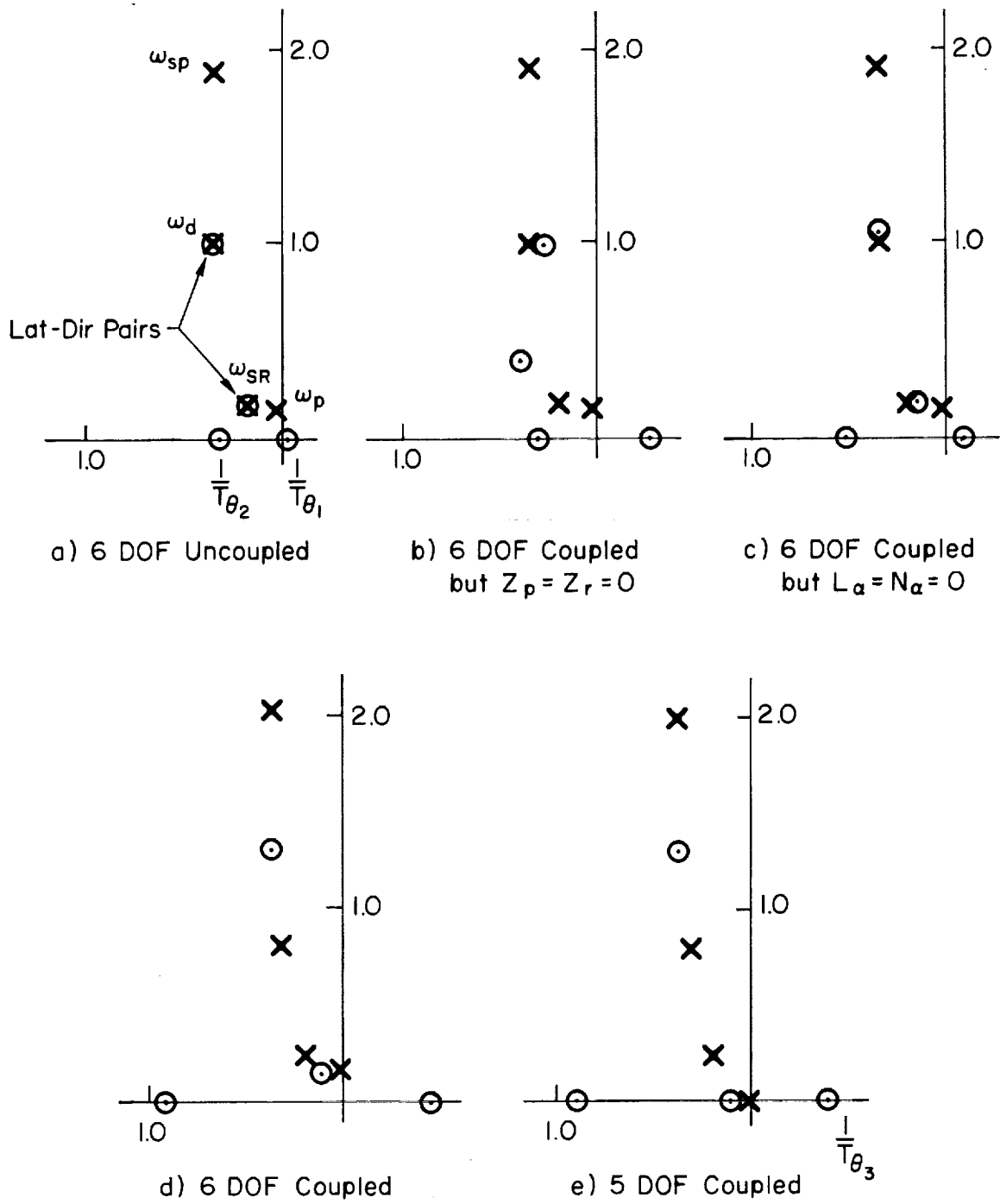


Figure 14. Survey of  $N_{\delta e}^{\theta}$  Approximations for  $\alpha = 18.8$  deg,  $\beta = 6$  deg

The influence of the individual pair of coupling terms is identified in Figs. 14b and 14c. In Fig. 14b the Z equation off-diagonal terms are set to zero; in Fig. 14c the L and N equation off-diagonal terms are removed. Both result in similar influences on the various zeros and indicate these "effective" derivatives must occur in combined or multiplicative form in the transfer function numerator. This can be demonstrated in a simplified model by deleting the X equation from the matrix of Fig. 13, expanding the remaining five body equations in literal terms and obtaining the polynomial coefficients. Approximations containing only the most significant terms are presented in Eq. 38.

$$N_{\delta_e}^{\theta} = M_{\delta_e} [As^5 + Bs^4 + Cs^3 + Ds^2 + Es + F] \quad (38)$$

where

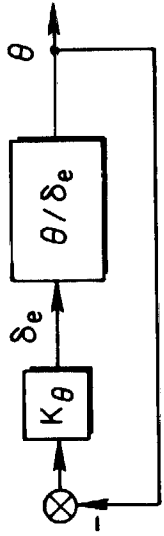
$$\begin{aligned} A &= 1 \\ B &\doteq Z_w + L_p + (N_r + Y_v) \\ C &\doteq L_p(Z_w + N_r) - L_{\beta} \sin \alpha - \underline{L_{\alpha} Z_p} \\ D &\doteq -L_{\beta} [(g/U_0) \cos \theta - (Z_w + N_r) \sin \alpha] - N_{\beta} (Z_w + L_p) \cos \alpha \\ E &\doteq L_{\beta} (g/U_0) \cos \theta [(Z_w + N_r) - (Z_{\delta_e}/M_{\delta_e}) M_w] + \underline{Z_p (L_{\beta} N_{\alpha} - N_{\beta} L_{\alpha})} \\ F &= -L_{\beta} (g/U_0) \cos \theta [N_r Z_w] \end{aligned}$$

It may be observed that the off-diagonal terms are multiplicative and primarily influence the C and E coefficients.

As an aid in identification of the modes reflected by the poles and zeros of Fig. 14c, the five degrees-of-freedom model is shown in Fig. 14e. Deletion of the X equation should eliminate the  $1/T_{\theta_1}$  zero and convert the complex phugoid pole into a first-order pole at the origin. However, Fig. 14e shows the same first order zeros as shown in Fig. 14d, i.e., the real axis zeros for five degrees-of-freedom remain unchanged from the six-degrees-of-freedom case. The complex zero previously identified as  $\omega_{SR}$  becomes, for five degrees-of-freedom, a first-order zero near the origin; and the phugoid mode is transformed into a first-order pole at the origin. Because the pole-zero configuration of Fig. 14e reflects coupled lateral-longitudinal modes (compare with Fig. 14d), the real zero in the right half plane will be identified as  $1/T_{\theta_3}$  since this is a new coupled lateral-longitudinal mode.

A single-loop system-survey for elevator control of pitch attitude with the six-degrees-of-freedom coupled airframe in non-symmetrical flight is shown in Fig. 15. The transfer function is shown in the upper left. The root locus in the top right of the figure reflects root migrations for a pure gain closure. Note that the roots starting at  $\omega_{SR}$  rapidly move to the real axis and then split into two real roots; one of which moves towards  $1/T_{\theta 2}$ , the other moves towards  $1/T_{\theta 3}$ . The rapidity of the movement of these closed-loop poles towards the zeros is demonstrated by the siggy-Bode plot in the bottom half of Fig. 15. The heavy solid and dashed lines of the Bode correspond to the path of the closed-loop roots along the real ( $\sigma$ ) axis in the root locus above. As the loop gain is increased, the complex poles emanating from  $\omega_{SR}$  meet the real axis at the apex of the solid curve in the Bode-siggy plot. Further increase in gain moves one closed-loop root to a lower frequency or towards the origin while the other root moves to higher frequency and, at very high gain, asymptotically approaches the  $1/T_{\theta 2}$  zero at 0.866 rad/sec. The root that goes toward the origin passes into the right half plane as shown in the root locus. This is represented in the Bode-siggy by the dashed line which reflects the mirror image of the closed-loop pole asymptotically approaching the  $1/T_{\theta 3}$  zero at -0.3 rad. If an autopilot or pilot is to achieve effective control of pitch attitude, the loop must be closed so that the gain line lies below the low-frequency asymptote of the Bode plot. It is obvious that this then results in a closed-loop pole in the right half plane. If the gain "crossover" is achieved in the region of 1-3 rad/sec, which covers the range of usual "loose" to "tight" piloted pitch attitude control, it may be seen that the closed-loop poles will lie very close to the open-loop zeros. For example, a unity dc gain provides a crossover between 1.5 and 2.5 rad/sec and closed-loop roots at -0.28 and +0.66 rad/sec. The resulting first-order divergence has a time constant of about 3.6 sec.

The sensitivity of the pitch non-minimum phase zero — and hence nose slice — to sideslip can be observed in Fig. 16 which indicates the zero migrations for  $\alpha \doteq 19$  deg and  $0^\circ < \beta < 15^\circ$ . The table insert also shows the values of the key derivatives. It is evident from Figs. 14 and 16 that the pitch numerator is quite sensitive to the coupling derivatives and, therefore, to sideslip.



$$\frac{\theta}{\delta_e} = \frac{-2.9(-.3)(.866)[.28, .185][.27, .14]}{[.163, .167][.71, .29][.36, .88][.185, 2.1]}$$

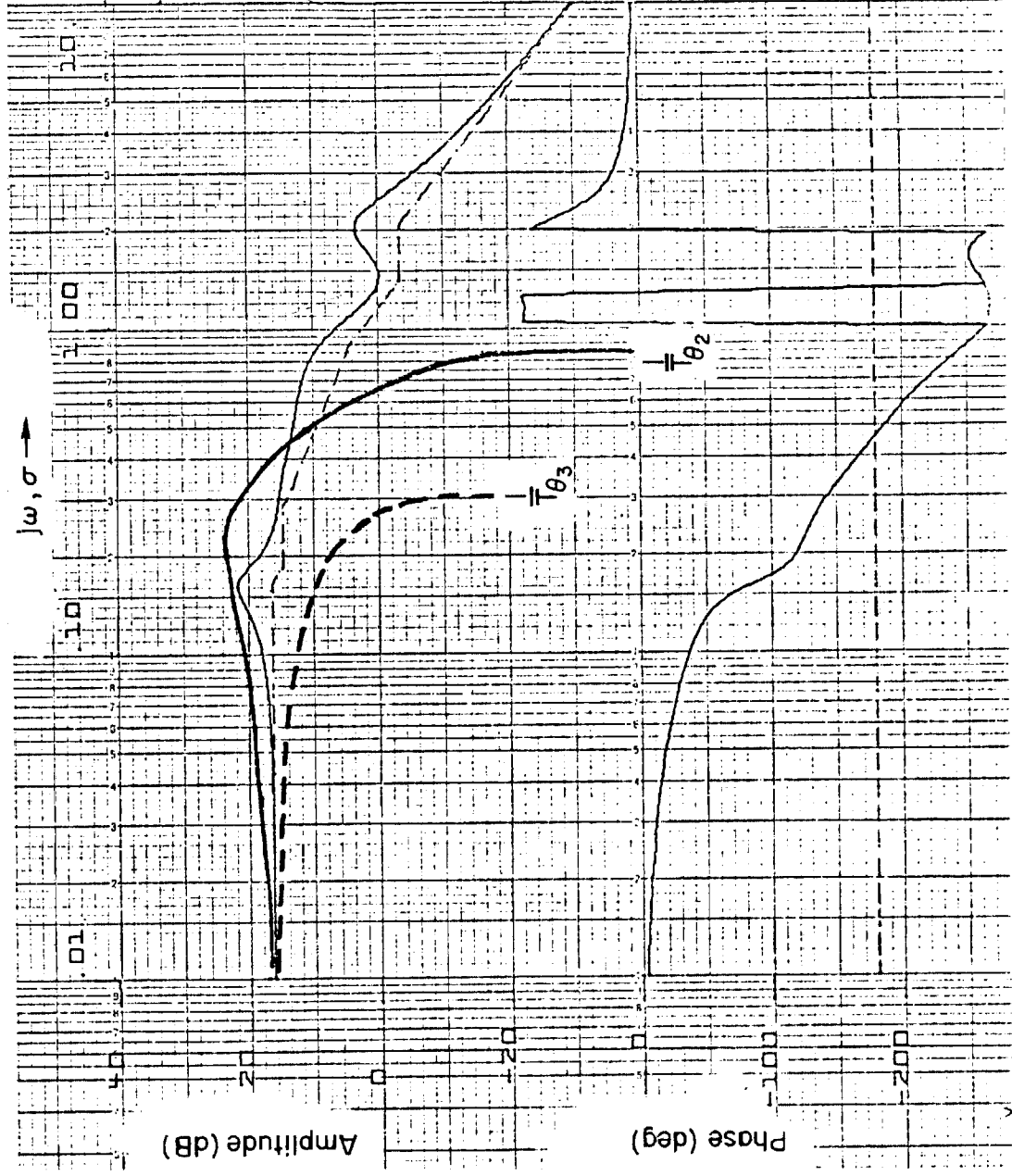
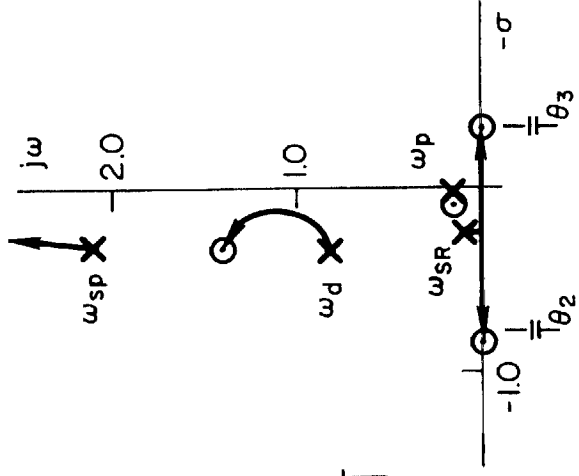


Figure 15. Pitch Attitude Closure Survey;  $\alpha_0 = 19$  deg,  $f_0 = 6$  deg

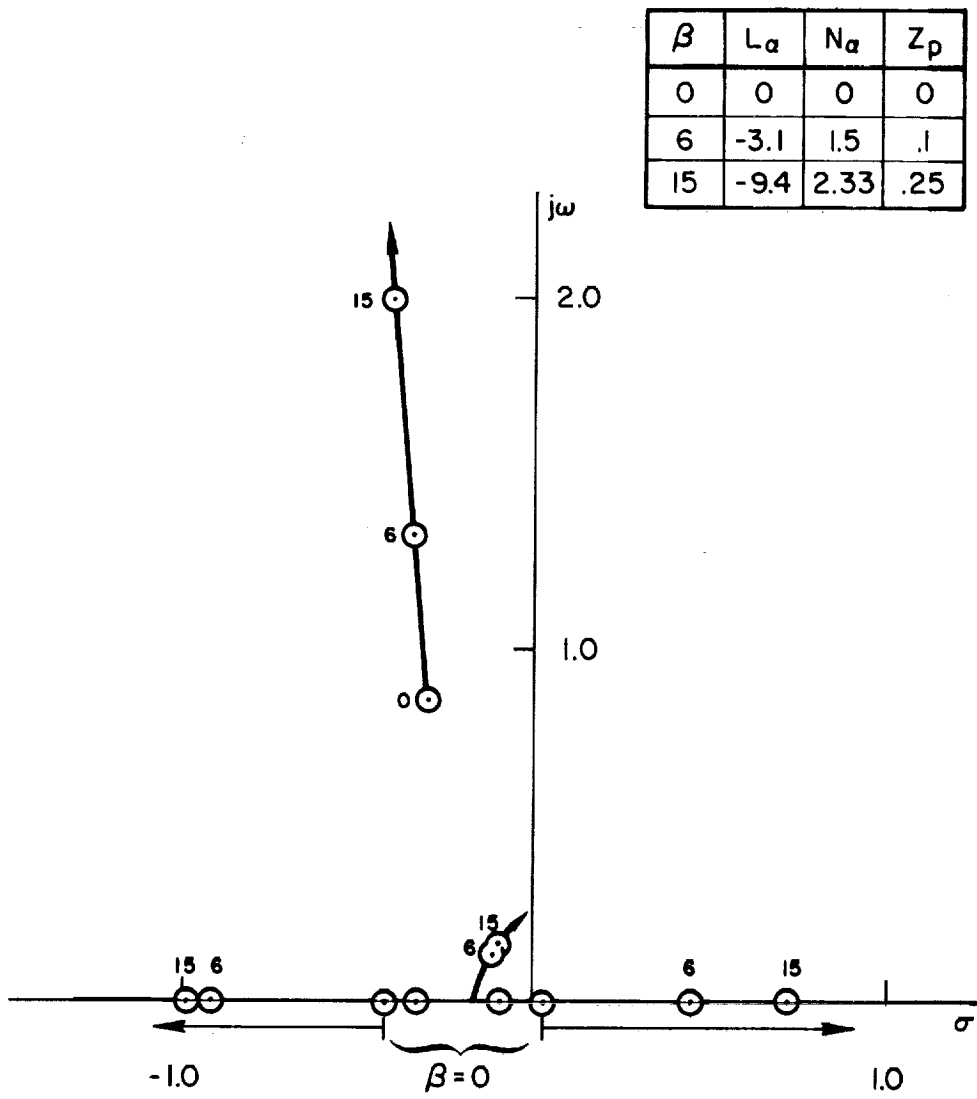


Figure 16. Movement of 6 DOF  $N_{\delta_e}^{\theta}$  Zeros for  $0^\circ < \beta < 15^\circ$

One other significant coupling derivative for some aircraft configurations is  $M_{\beta}$  (see Fig. 13). This derivative principally influences the open-loop lateral and longitudinal short period damping and the lateral-directional numerator zeros. There is evidence that it contributes to one version of the phenomenon known as wing rock. As an example, Fig. 17 presents 6 DOF pole-zero locations for another high performance jet fighter at  $\alpha = 20$  deg and  $\beta = 1$  deg. The nominal value of  $M_{\beta}$  for this flight condition is  $-1.63$ . Note that this not only destabilizes the open-loop dutch roll mode but also moves the zeros  $\omega_p$  and  $\omega_r$  toward  $\omega_q$  and the right half plane.

These examples are much more complicated than the simple performance reversals described at the beginning of this section, yet they exhibit entirely similar phenomena. That is, the basic motion being controlled, in these latter cases pitch attitude, is responsible for but does not reflect the divergent characteristic. Instead, this appears in another degree of freedom, such as airspeed in the  $1/T_{h_1}$  associated performance reversal. One of the fascinating aspects of the nose slice and wing rock examples is that in these instances the causative right half plane zero is longitudinal whereas the resulting motions are in the lateral degrees of freedom!

As a final comment, we should note that although these examples use zeros inherent in the aircraft characteristics, similar features can be introduced by sensor orientation. When rolling velocity as sensed by a roll rate gyro is used as a feedback, for instance, the roll rate numerator has a small real root whenever the rate gyro's sensitive axis departs from a straight, level, and horizontal stability axis. This zero is often negative. When it is, a high-gain roll rate command system would exhibit a spiral mode determined not by the usual spiral characteristics but instead by the value of the rolling velocity zero.

## B. INTENTIONALLY INTRODUCED ZEROS

There have been several instances of military aircraft in which difficulty has been experienced in meeting short period frequency and damping requirements dictated by handling quality specifications. The designers' solution often has been to incorporate an "inverse model"

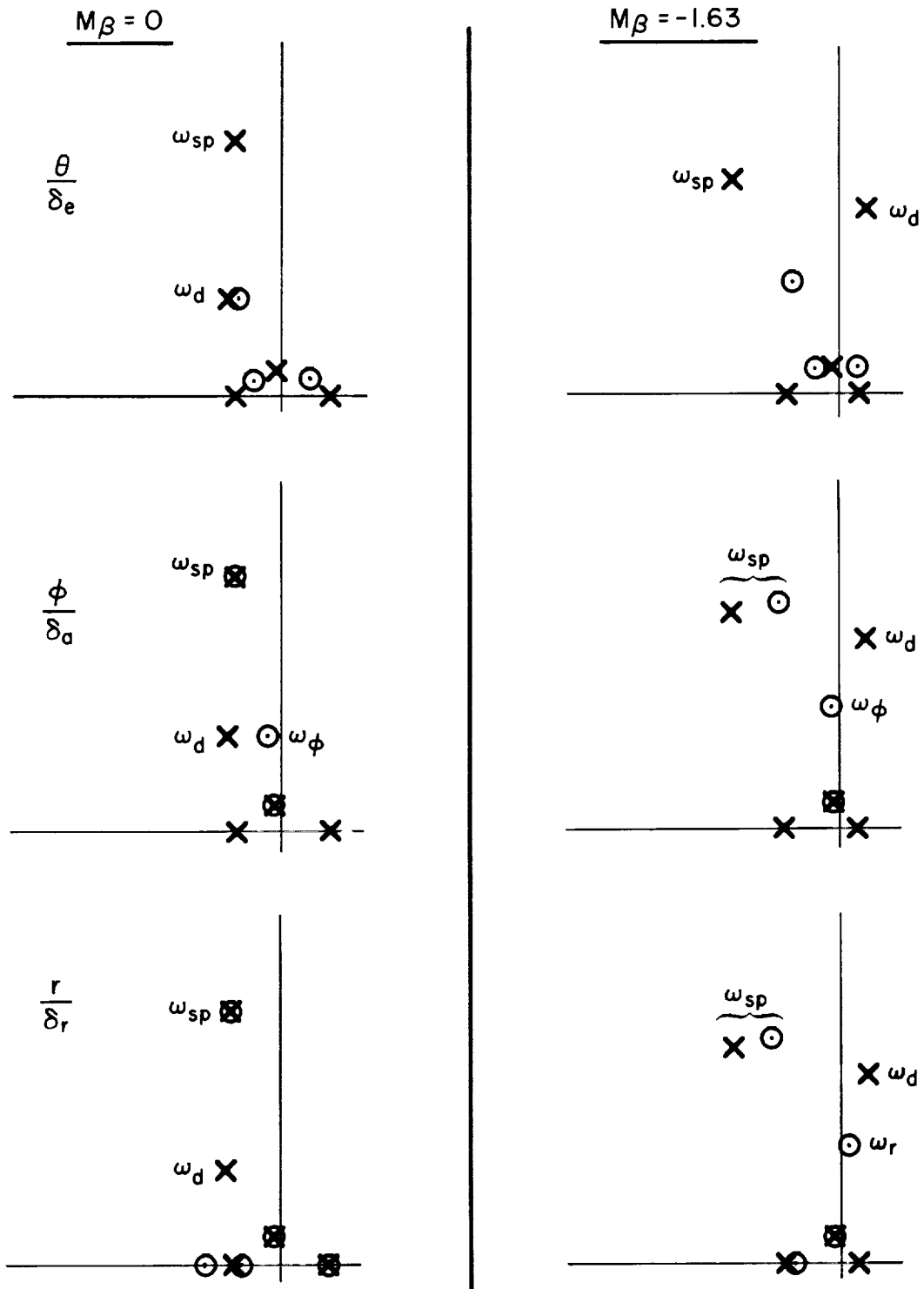


Figure 17. Effect of  $M_\beta$  on 6 DOF Poles and Zeros  
 ( $\alpha_0 = 20$  deg,  $\beta_0 = 1$  deg)

in the stability augmentor feedback and then to employ high gain which drives the short period roots into or near the zeros of the inverse model. The short period mode thus is forced to meet the specification requirement.

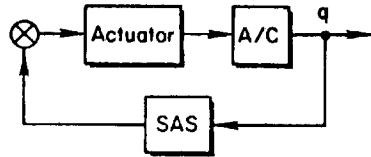
Unfortunately, when multiple zeros are introduced to modify one mode it is usually necessary to introduce accompanying poles, either to prevent undesirable influence on modes at higher frequency than the zeros or as an offshoot of the mechanization. The additional poles also influence system dynamic characteristics and, from a total or equivalent system standpoint, can negate the intended improvement in system handling qualities.

A specific example is presented here for illustration. The aircraft had a short period of considerably less than 1 rad/sec in some flight conditions and it was desired to increase it to greater than 1 rad/sec. Additional considerations, including provision of relatively constant short period characteristics throughout the aircraft performance envelope and the use of a fixed gain pitch rate feedback, led to SAS shaping of the form

$$Y_{SAS} = \frac{K_q s}{(s + 0.5)} \frac{(s + 5)^2}{(s + 1.89)(s + 14)} \quad (39)$$

WASHOUT
SHORT PERIOD CONTROL

A survey plot for the system open and closed-loop characteristics is presented in Fig. 18. The two zeros at 5 rad/sec introduced to attract the short period perform as advertised. The Bode-root locus indicates the migration of system closed loop roots as the pitch rate gain is varied. The specific roots for a gain of  $K_q = 0.42$  deg/deg/sec are indicated as (■). The root migrations of major interest are those emanating from the short period and the SAS pole  $1/T_{s1}$ . Notice that as  $\omega_{sp}$  moves to the desired higher frequency ( $> 1$  rad/sec) the SAS-introduced root rapidly moves toward  $1/T_{\theta 2}$ . The net result is a trade in system low frequency lag between the two modes. Comparing the SAS off-on characteristics in the short period region



$$\text{SAS} = \frac{422(5)(5)(0)}{(14)(1.89)(5)} \quad \text{Actuator} = \frac{20}{(20)}$$

$$\text{A/C} = \frac{q}{\delta_H} = \frac{1.582(0)(.099)(.511)}{(697,775)(.048,177)}$$

Closed Loop Roots are:

$$\underbrace{(464)(589)(15.8)(17.9)}_{\text{SAS}} \underbrace{(-.011, .104)}_{\text{Act}} \underbrace{(.889, 1.546)}_{\text{Phugoid}} \underbrace{.889, 1.546}_{\text{Short Period}}$$

64

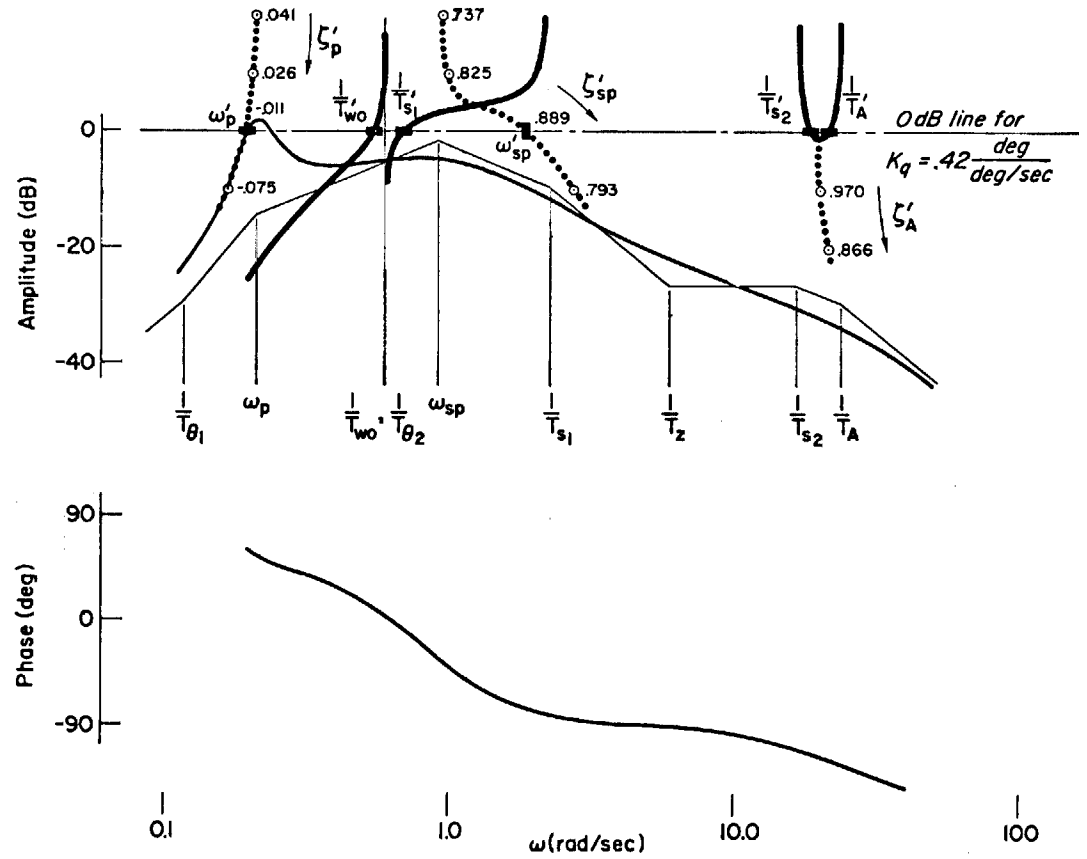
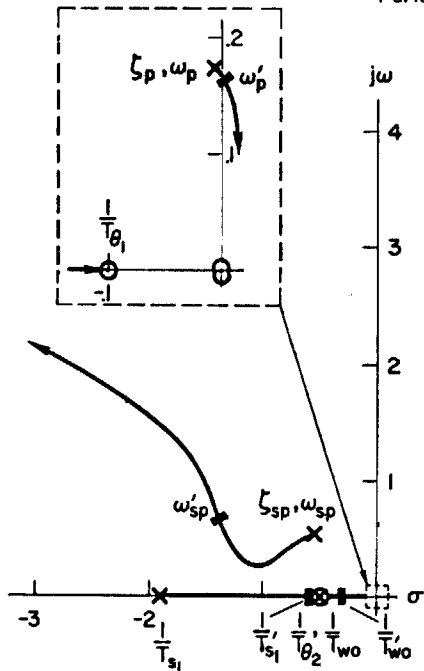


Figure 18. Survey for Migration of Roots with SAS Loop Closure

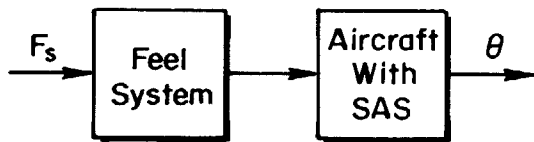
$$\text{SAS OFF } \frac{\theta}{\delta_H} = \frac{1.58(0.51)}{(0)[0.70, 0.78]}$$

$$\text{SAS ON } \frac{\theta'}{\delta_H} = \frac{1.58(0.51) (1.89)(0.50)}{(0)[0.89, 1.55](0.59)(0.46)}$$

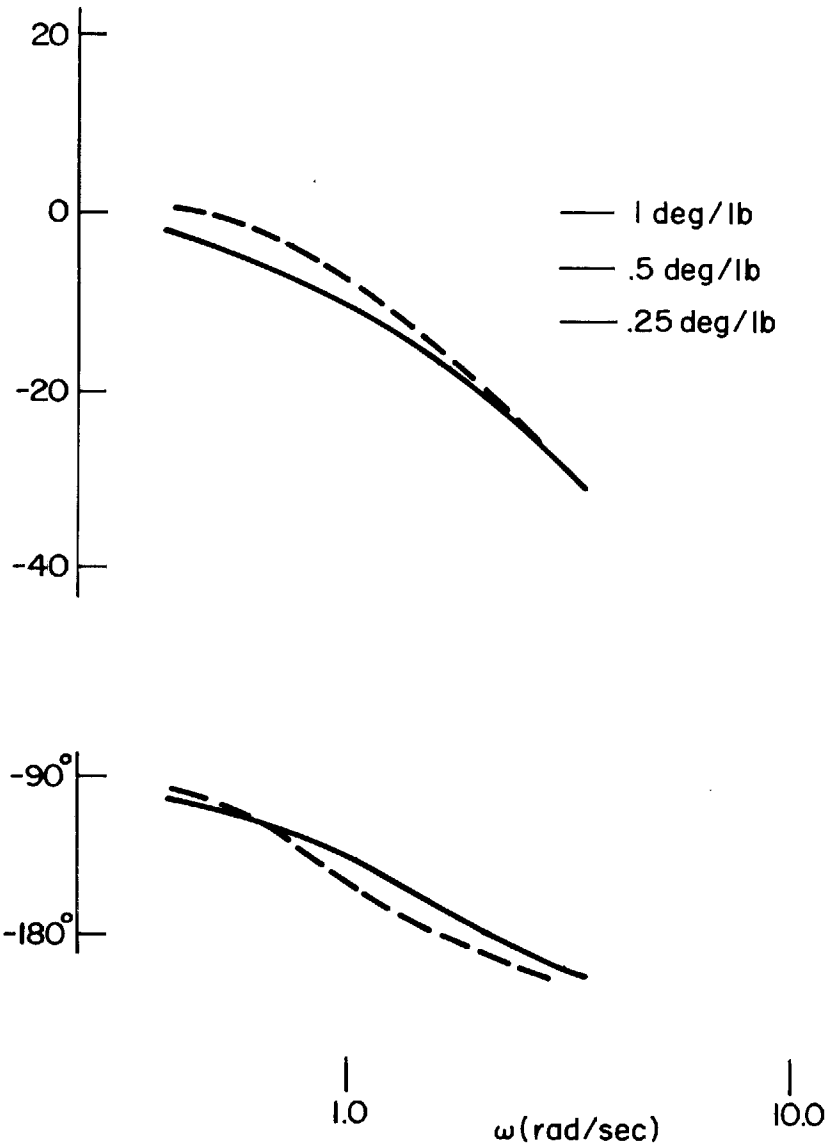
The washout contribution essentially cancels but the SAS lag-lead contribution is now very significant. The factor of three lag-lead separation (0.6 to 1.9) introduces 30 deg of phase lag at a frequency midway between the pole and zero.

The effect of this SAS on vehicle short period characteristics as seen by the pilot is shown in Fig. 19. This Bode diagram indicates attitude response for stick force input versus frequency. (The feel system contributes an additional pole at 4 rad/sec and, because it contains a bobweight loop, slightly alters the closed loop aircraft and SAS roots as may be noted by comparing the SAS-on roots identified in Figs. 18 and 19.) The important aspect of Fig. 19 is that there is little difference between the SAS on and off short period handling characteristics even though the SAS has increased the short period mode (per se) from 0.78 to 1.55 rad/sec. This may be further demonstrated by curve fitting the SAS-on Bode amplitude and phase shown in Fig. 19 with a third-order short period model for the effective airframe model. This is shown in Fig. 20. The equivalent airframe will appear to the pilot as a nearly critically damped short period at 0.9 rad/sec.

Thus the effective contribution of the rather involved SAS feedback shaping has been to increase short period damping from 0.64 to 0.92 with only a slight modification in frequency (from 0.78 to 0.9 rad/sec). The basic reason the desired improvement does not materialize may be traced back to the migration of the root  $1/T_{S_1}'$  in Fig. 18.



$$\left| \frac{\theta}{F_s} \right|$$



51

<u>SAS on</u>	1.76 (.511)	<del>(.5)(1.89)</del>
	(0)(.907, 1.404)	(4.81)(.712)(4.008)
<u>SAS off</u>	1.76 (.511)	
	(0)(.638, .8)	(4.013)

Figure 19. Comparison of Effective Vehicle Dynamics SAS On and Off

52

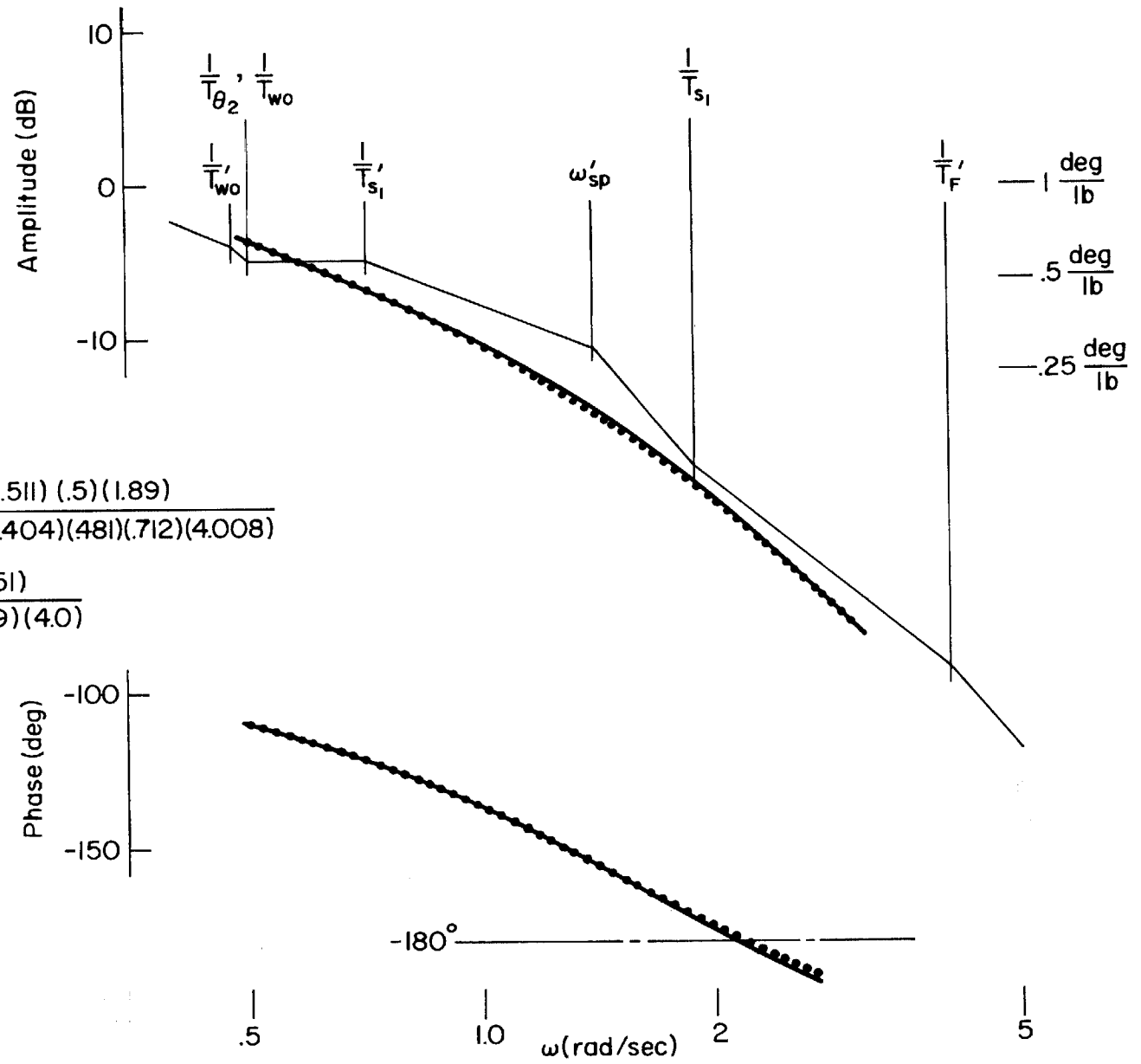


Figure 20. Curve Fit of Equivalent Short Period Aircraft Dynamics

## SECTION IV

### PROBLEMS ASSOCIATED WITH MECHANICAL FLIGHT CONTROL SYSTEM ELEMENTS

Some situation-specific problems are not easily sorted into such convenient bins as "quadratic dipoles". These can sometimes be conveniently classified into categories which emphasize their causes. In this section, we shall be concerned with mechanical flight control elements. These mainly involve the primary controls actuated by the pilot and certain interfaces between the mechanical primary system and stability augmentation. In a general framework, they are the mechanical elements of the components enclosed within dashed lines on Fig. 21 except that very limited consideration is given to the stability augmentation actuator. This and the force feedforward are more integral with the augmentation system, per se, and are elaborated on in the next section. To be more concrete, the major mechanical elements to be described here are shown in the control system schematic of Fig. 22. This layout is representative of a general longitudinal control system containing bobweights as force stability augmentors and series actuators as extensible links between the force feel package and the surface actuator. It is also applicable to lateral, and even directional, control as an overall generalization; for while bobweights may not be intentionally present in these systems, there is often some mass unbalance which can amount to the same thing. Thus, by treating longitudinal control, the other axes are covered by analogy.

In the following articles, dynamic models for each segment in the schematic diagram of Fig. 22 are developed and discussed as to their past or potential problem areas or points deserving of special attention by the designer.

#### A. ARTIFICIAL FEEL SYSTEM INPUT/OUTPUT CHARACTERISTICS

The stick input/output properties of the artificial feel system are derived from the combination of spring, mass, damper, friction, etc., elements in the control system. Figure 23 shows both linear and nonlinear models of these. For the stick force/displacement characteristics considered here, the bobweights and other massive elements contribute to a net inertia,  $I_T$ ; the effects of the bobweights as a force stability augmentor are the subject of a later

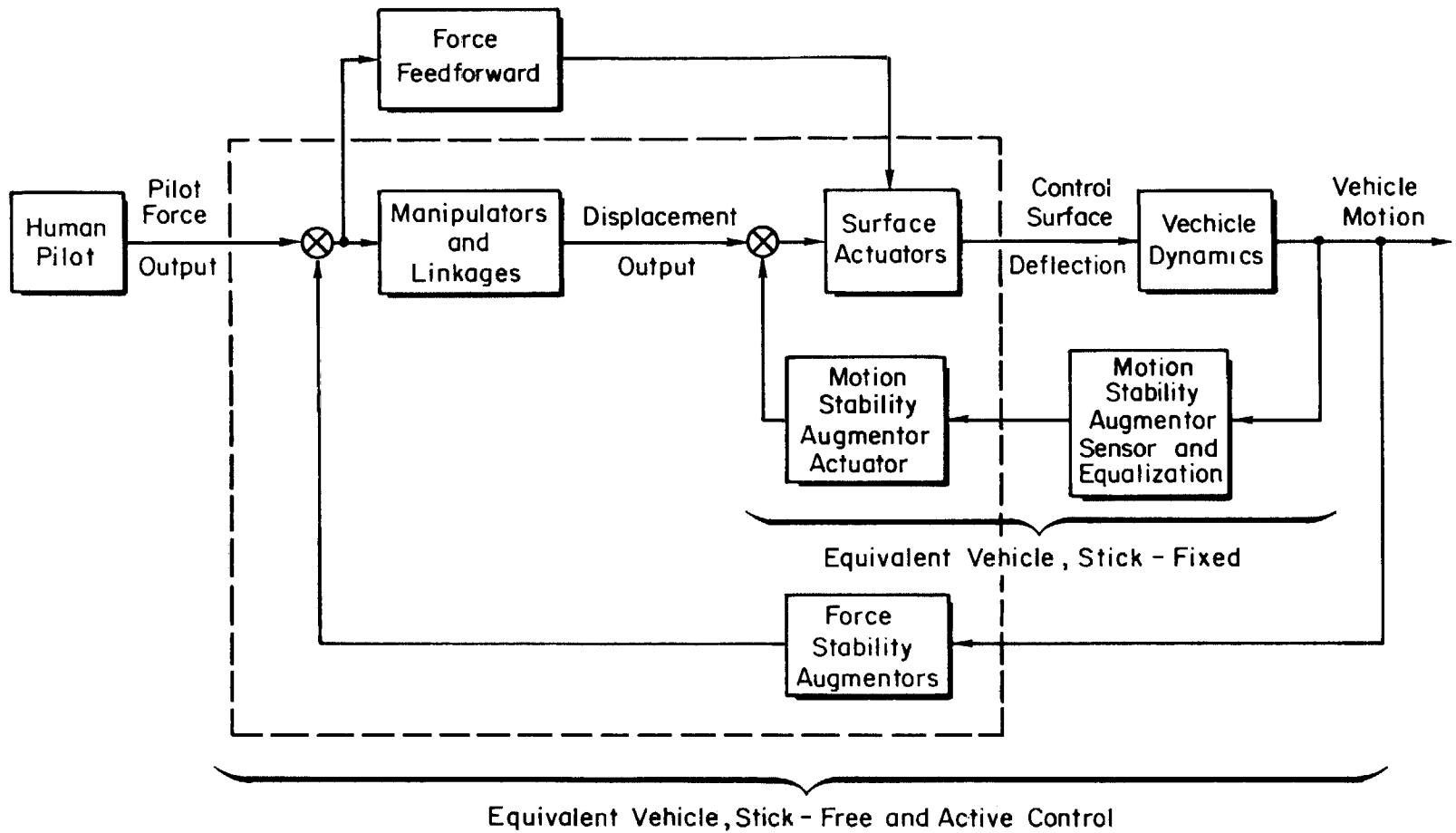


Figure 21. Pilot-vehicle Control System

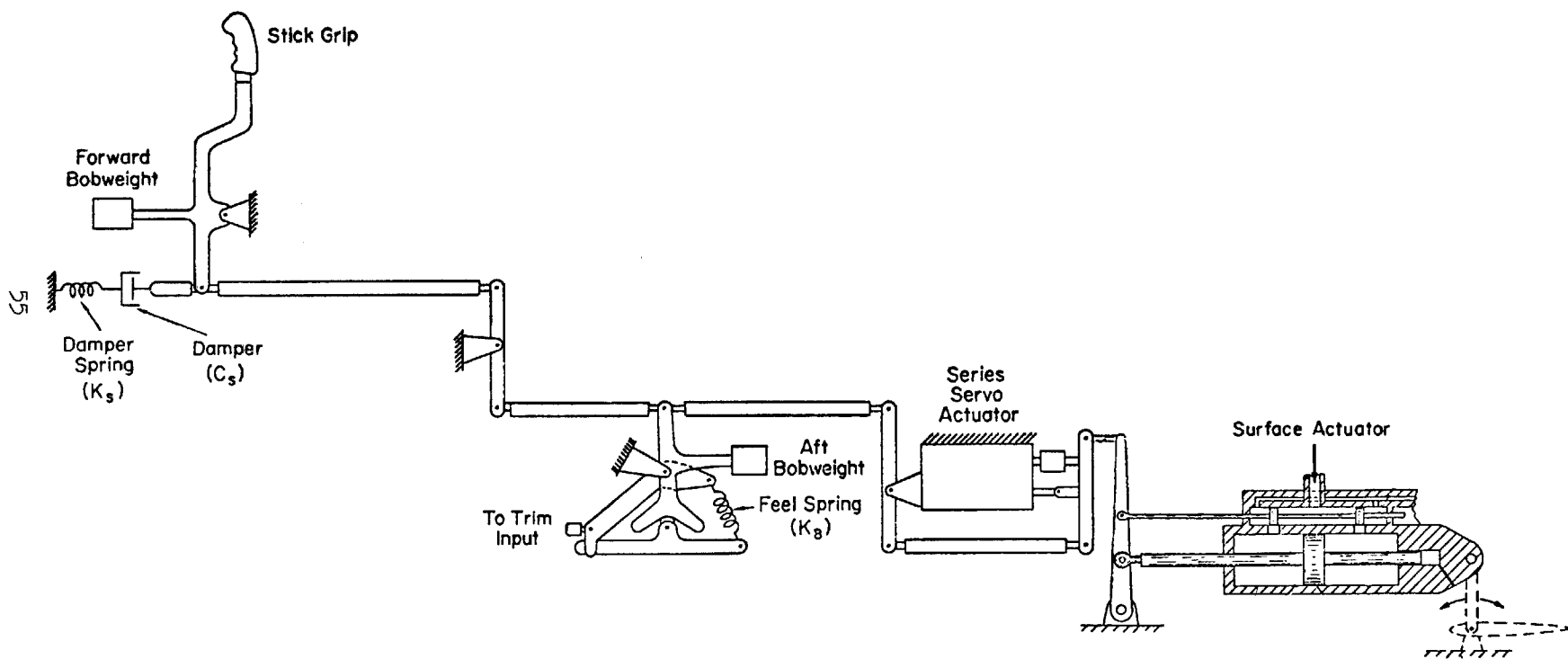


Figure 22. Control System Schematic

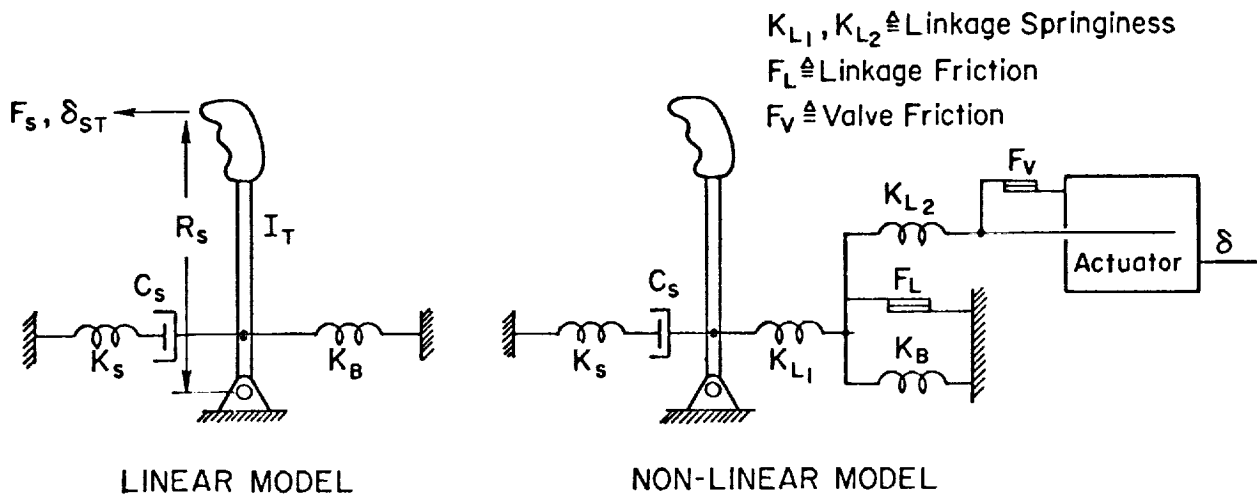


Figure 23. Detailed Characteristics of Typical Artificial Feel System

article. The various springs provide for: feel forces as appropriate functions of stick deflection; preload; stick centering; bobweight balance; etc. The linkage compliance itself is small (stiffness very large) so the constant  $K_{L1}$  can be lumped with  $K_B$ , and  $K_{L2}$  can be considered rigid in an analysis which emphasizes low-frequency behavior.

In good design practice the nonlinearities, linkage, and valve friction are minimized, and the control system characteristics approach those of the linear model shown on the left in Fig. 23. In the discussions below this linear system will be treated first, followed by a consideration of the more important nonlinear aspects.

### 1. Linear Dynamics

The transfer function relating stick displacement to stick force can be derived from equations based on Fig. 23. It is:

$$\frac{\delta_{ST}}{F_s} = \frac{R_s^2}{I_T} \frac{(s + K_s/C_s)}{\left( s^3 + \frac{K_s}{C_s} s^2 + \frac{K_B + K_s}{I_T} s + \frac{K_B K_s}{I_T C_s} \right)} \quad (40)$$

This can ordinarily be factored approximately in literal form as:

$$\frac{\delta_{ST}}{F_s} = \frac{R_s^2}{I_T} \frac{(s + K_s/C_s)}{\left[ s + \frac{K_B}{C_s} \left( \frac{1}{1 + K_B/K_s} \right) \right] \left[ s^2 + \frac{(K_s - K_B)}{C_s} s + \frac{(K_B + K_s)}{I_T} \right]} \quad (41)$$

Representative numerical values for a typical longitudinal control system are:

$$R_s = 1.75 \text{ ft}$$

$$I_T = 1.4 \text{ slug-ft}^2$$

$$K_B = 183 \frac{\text{ft-lb}}{\text{rad}}$$

$$K_s = 2000 \frac{\text{ft-lb}}{\text{rad}}$$

$$C_s = 50 \frac{\text{ft-lb}}{\text{rad/sec}}$$

When these are inserted in Eq. 41 the result is:

$$\frac{\delta_{ST}}{F_s} = \frac{26.25(s + 40)}{(s + 3.66)[s^2 + 2(0.481)(37.8)s + (37.8)^2]} \frac{\text{in.}}{\text{lb}} \quad (42)$$

This expression represents the input/output characteristics of the basic feel system exclusive of bobweight loop effects (i.e., stick fixed). It is not uncommon to assume that the feel system dynamics can be approximated by the second-order mode. However, for the system shown here with the damper note that the first-order lag dominates in the frequency band of interest in flying qualities. The lag time constant is approximated very well by  $C_s/K_B$ . It will later be seen that closure of the bobweight loop will reduce the lag somewhat.

The dynamic form of the typical stick force, stick displacement characteristic is shown in Fig. 24. This shows that: the stick force gradient is 5 lb/in. from zero to approximately 2 rad/sec; at 3.66 rad/sec it has increased 3 dB or 1.4 lb/in.; it crosses 10 lb/in. at about 7 rad/sec and increases approximately 1.49 (lb/in.)/(rad/sec) on out to about 40 rad/sec. Above the

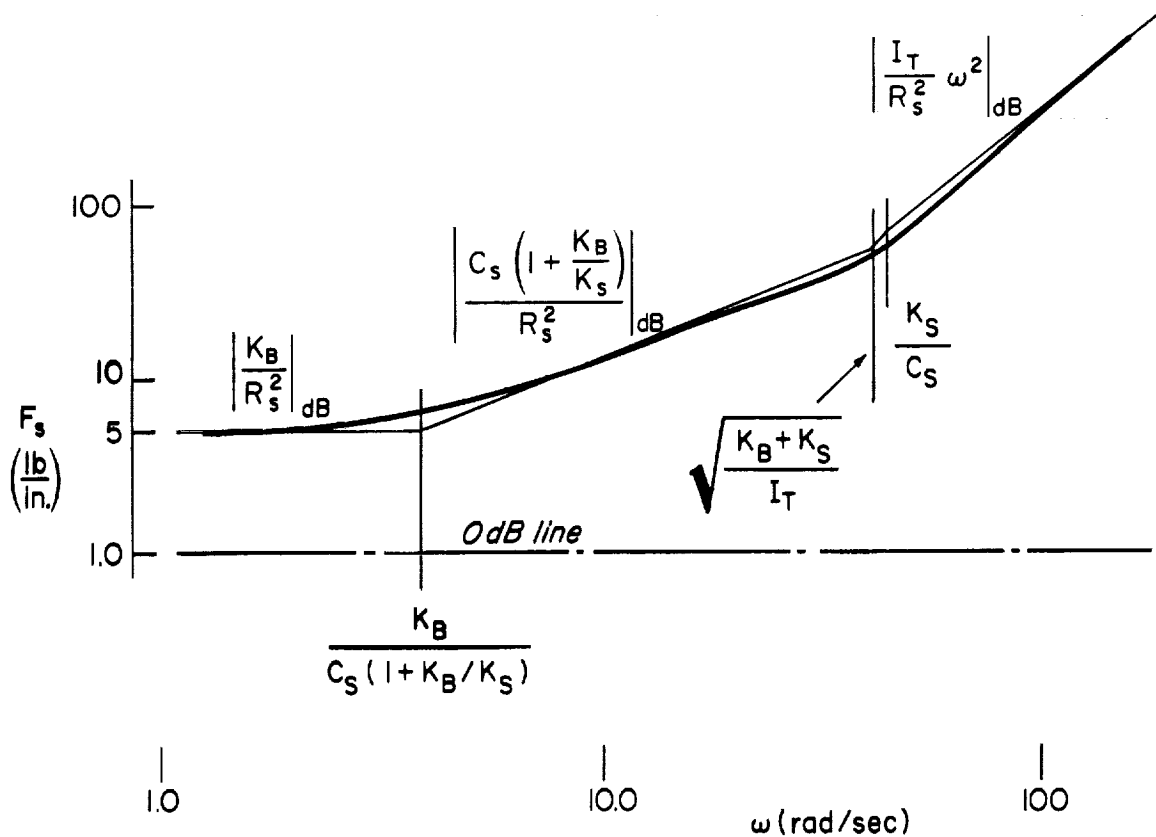


Figure 24. Dynamic Characteristics, Feel System

combined first- and second-order breaks near 40 rad/sec the gradient increases as the square of angular rate. Thus, the feel system causes the pilot to use more force for a given stick deflection (work harder) if he tries to close loops above 1 to 2 rad/sec. At the same time, viewed in terms of a pilot force input to the system, the feel system introduces a good deal of lag. In fact, at low frequencies the feel system can be approximated by a constant and pure delay, i.e., a linear phase shift with frequency:

$$\frac{\delta_{ST}}{F_s} \doteq \left( \frac{K_B}{R_s^2} \right) e^{-(C_S/K_B)j\omega} \quad , \quad \omega < \frac{K_B}{C_S} \quad (43)$$

This delay can adversely affect either the autopilot or pilot/vehicle system stability and performance.

Possible means of improving the situation can be deduced from Fig. 25. Decreasing  $C_s$  will directly reduce the effective delay and increase the first-order lag break frequency and damping of the second order. The plot shows that decreasing  $C_s$  moves the first-order lag to higher frequencies, but this is partially offset by the second-order becoming critically damped and hence contributing more phase lag at the lower-frequency region of interest. If  $C_s$  is reduced sufficiently, the feel system dynamics do become dominated by the second-order mode in the frequency bandwidth of interest.

The feel system d.c. gain and both second-order terms in the transfer function shown in Fig. 25 are directly affected by changes in feel spring ( $K_B$ ). A stiff spring moves the second-order contribution to higher frequency but also increases the stick force. The second orders can also be moved to higher frequency by decreasing the control system inertia. This has the additional benefit of not increasing steady-state stick force.

When the feel system is considered as a series link in the pilot/vehicle or autopilot system, its lags would ideally be made as small as possible. This implies that the damping,  $C_s$ , also be minimized. On the other hand, some aircraft designs place great reliance on force stability augmentation with dual or single bobweights. These, together with the other elements in the mechanical system, increase the system inertia and hence reduce the undamped natural frequency of the second-order characteristic. Because the value of the feel spring,  $K_B$ , is fairly tightly constrained by flying qualities requirements, the primary means for keeping the mechanical control system from undue oscillation when actuated by pilot inputs is the damper. But, as seen above, this has its inevitable consequence in increasing the low-frequency lag. Thus, it is apparent that control systems having large inertia (heavy bobweights) and low minimum feel spring gradients must be very carefully designed for proper interface operation with the autopilot and pilot.

$$Y = \frac{1}{C_s} \frac{K_s \left( s^2 + \frac{K_B}{I_T} \right)}{s \left( s^2 + \frac{K_B + K_s}{I_T} \right)}$$

$I_T = 1.4$      $K_B = 183$   
 $R_s = 1.75$      $K_s = 2000$

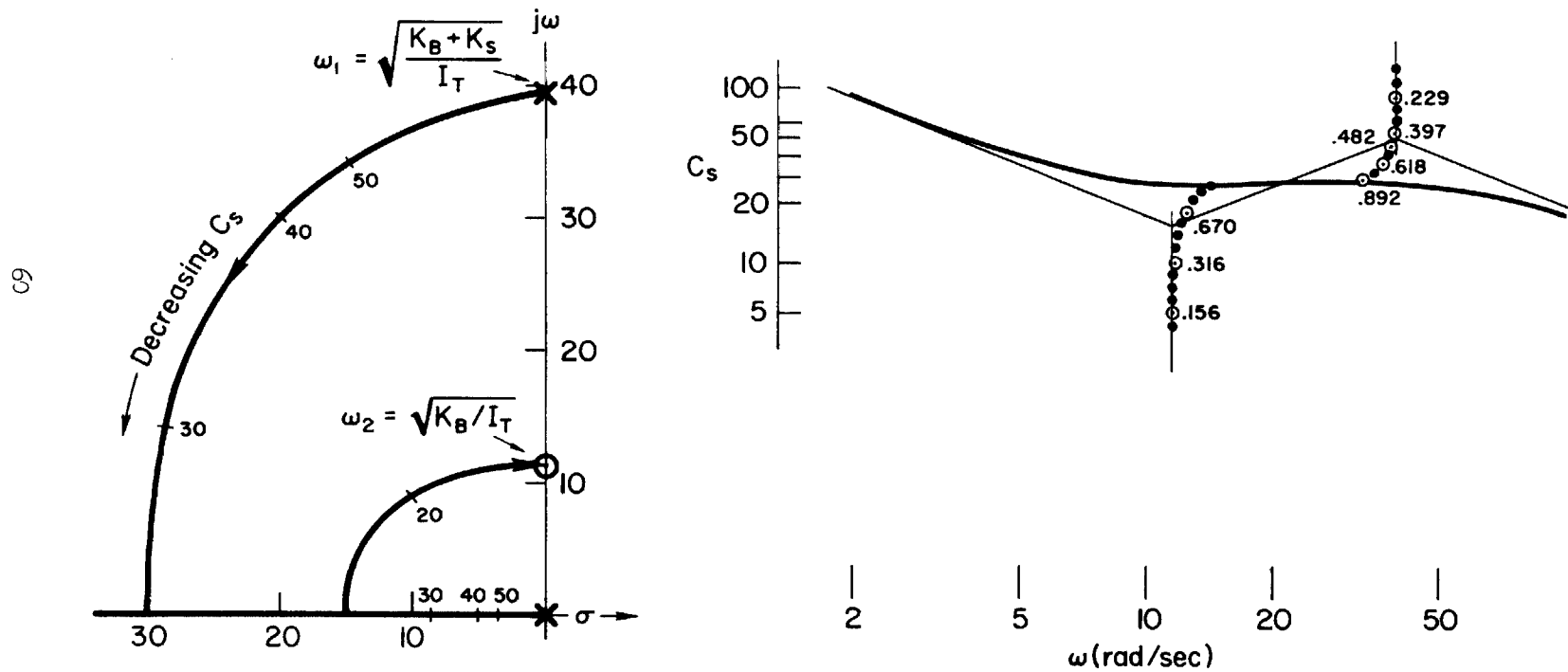


Figure 25. Survey of Feel System Poles with Change in Damping,  $C_s$

## 2. Nonlinear Behavior

The most commonly important small amplitude nonlinearities in mechanical control systems are preload and friction. The friction is unavoidable and minimized insofar as possible by design. Preload is introduced deliberately for a variety of purposes which includes partial offsetting of friction effects both statically, as in improving control system centering, and dynamically, as in reducing the effects of mechanical hysteresis caused by friction. Other deliberate nonlinearities, such as variation in feel spring characteristics with stick displacement, may be introduced to solve configuration-specific problems. These fall into a special category which are not general enough for us to consider here; but friction effects are ubiquitous and require consideration at a fundamental level.

Figure 26 shows a simplification to the nonlinear model of Fig. 23 in which only the low-frequency effects are present. The feel spring,  $K_f$ , here is the net spring gradient translated to the top of the stick (i.e., the contribution of  $K_B$  will be  $K_B/R_S^2$  and the linkage friction  $F_L$  is approximated by a Coulomb friction,  $-b \leq F_L \leq +b$ , also expressed as a stick force. The valve friction  $F_V$  will be considered subsequently; it is ignored for now.

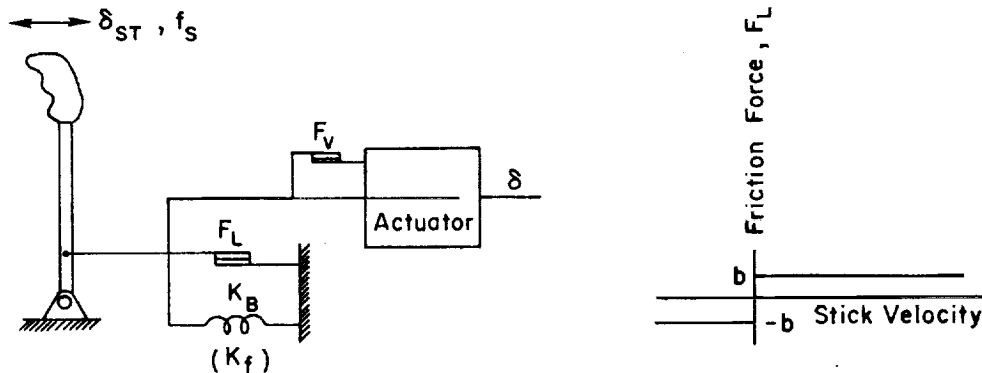


Figure 26. Feel System Characteristics at Very Low Frequencies

If a sinusoidal stick force,  $f_s = F_s \sin \omega t$ , is applied, typical waveforms of the forces and motion will be as shown in Fig. 27. The linkage will not begin to move until  $f_s > b$ , the Coulomb friction force. Thereafter, the deflection of the feel spring will be  $(f_s - b)/K_f$ . After  $f_s$  reaches its maximum value,  $F_s$ , and begins to decrease, the linkage will again stand still as the friction force which always opposes motion builds up in the opposite direction until the magnitude of the spring force,  $(K_f \delta_{ST})_{\max}$ , exceeds  $F_s + b$ . With  $F_s$  now decreasing further the linkage will move in the negative  $\delta_{ST}$  direction until  $F_s$  reaches its maximum negative value, at which point the linkage will again stand still. In terms of a transfer characteristic between the stick force,  $f_s$ , and the linkage deflection,  $\delta_{ST}$ , this motion is accounted for by the hysteresis loop shown in Fig. 28.

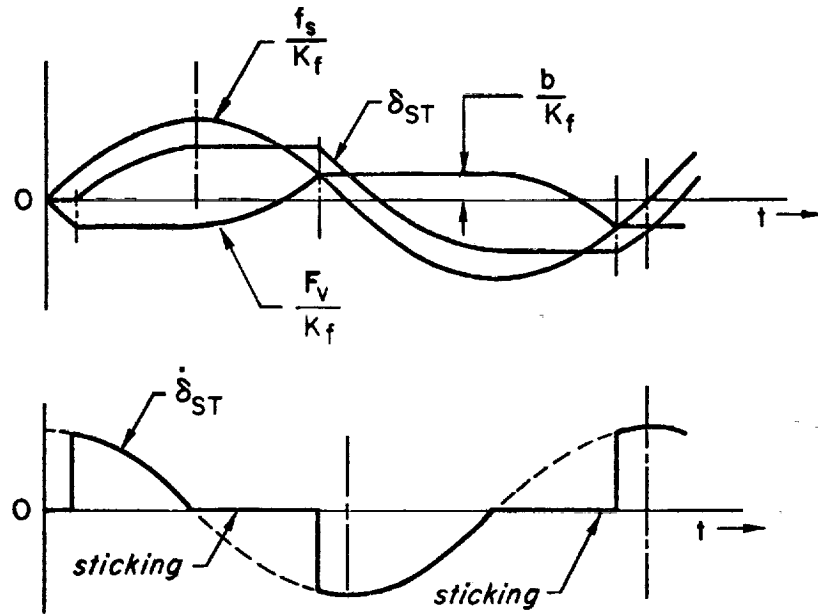


Figure 27. Waveforms in Artificial Feel System with Friction

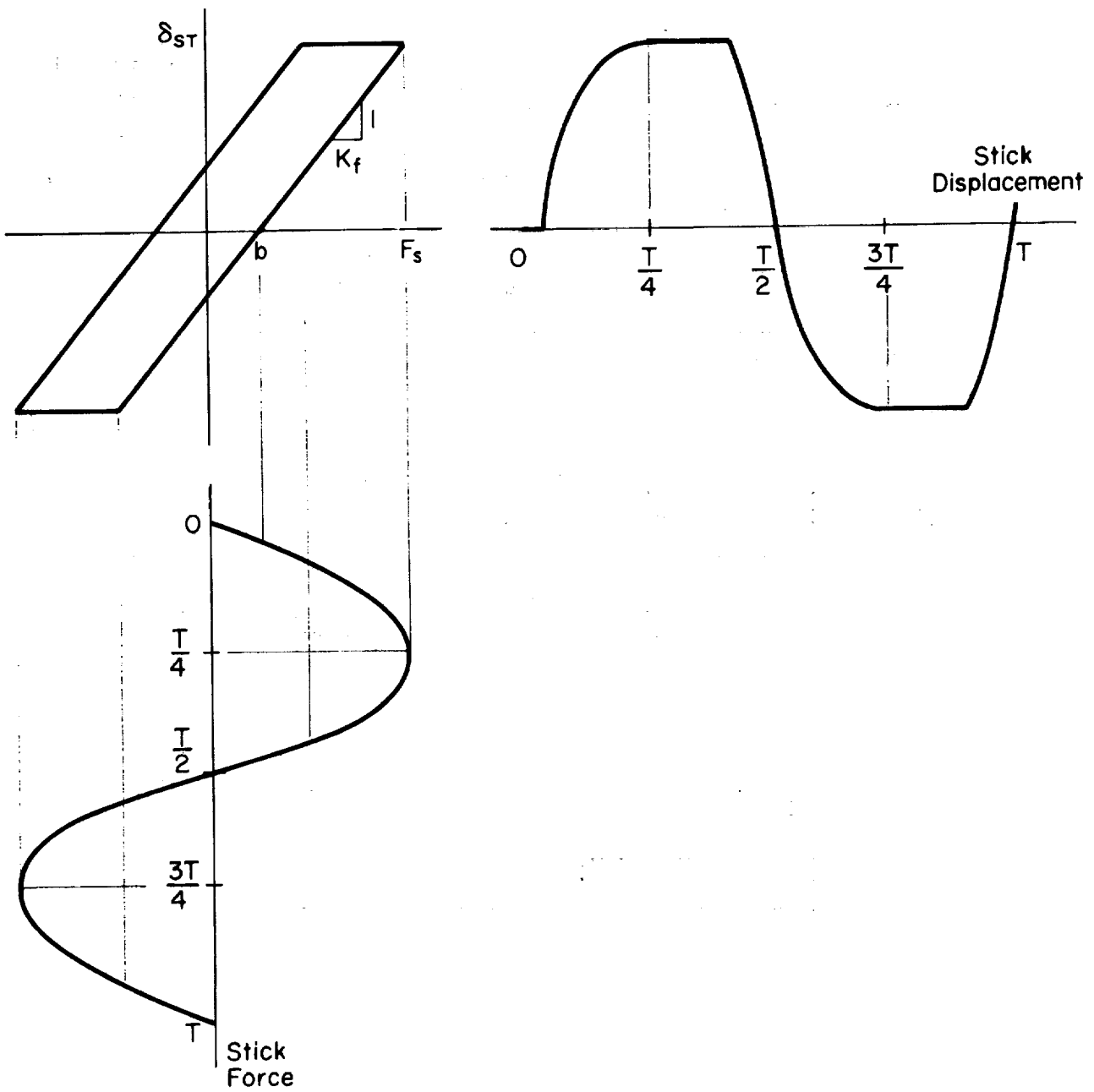


Figure 28. Mechanical Hysteresis Due to Coulomb Friction and Feel Spring

The sinusoidal describing function between  $\delta_{ST}$  and  $f_s$  is well known (e.g., Ref. 6). It can be expressed as:

$$\left| \frac{\delta_{ST}}{f_s} \right| = \frac{1}{K_T \pi} \sqrt{1 - u^2 + \left( \frac{3\pi}{2} - \sin^{-1} u \right)^2 + 2u \left( \frac{3\pi}{2} - \sin^{-1} u \right) \sqrt{1 - u^2}}$$

$$\angle \frac{\delta_{ST}}{f_s} = \tan^{-1} \frac{u^2 - 1}{\frac{3\pi}{2} - \sin^{-1} u + u \sqrt{1 - u^2}} \quad (44)$$

where

$$u = 1 - 2 \left( \frac{b}{F_s} \right) \quad ; \quad \text{when } u = 0 \text{ take } \sin^{-1} u = \pi$$

A graphical representation of this describing function is presented on the gain-phase plane as a negative inverse in Fig. 29. It indicates that the ordinary 0 dB, -180 deg phase point, which for non-minimum phase systems must be avoided to assure stability, is now a rather significant segment of the gain phase plane.

It may be desirable at this point to review the interpretation of the negative inverse describing function on the gain-phase plane as it is used to determine the possibility of a sustained oscillation. In a manner similar to the basic stability condition which underlies the theory of constant coefficient linear systems, the fundamental condition for stationary oscillations in a quasi-linear closed-loop system can be formulated as:

$$1 + \mu\beta = 0 \quad \text{or} \quad \mu\beta = -1 \quad (45)$$

where  $\mu$  and  $\beta$  are the forward path and feedback path transfer or describing functions, respectively. Now, if any part of either  $\mu$  or  $\beta$  is the describing function of a nonlinearity,  $N$ , and the remainder of the open-loop frequency response function is the linear term,  $G(j\omega)$ , the stability condition is:

$$NG(j\omega) = -1 \quad \text{or} \quad G(j\omega) = -1/N \quad (46)$$

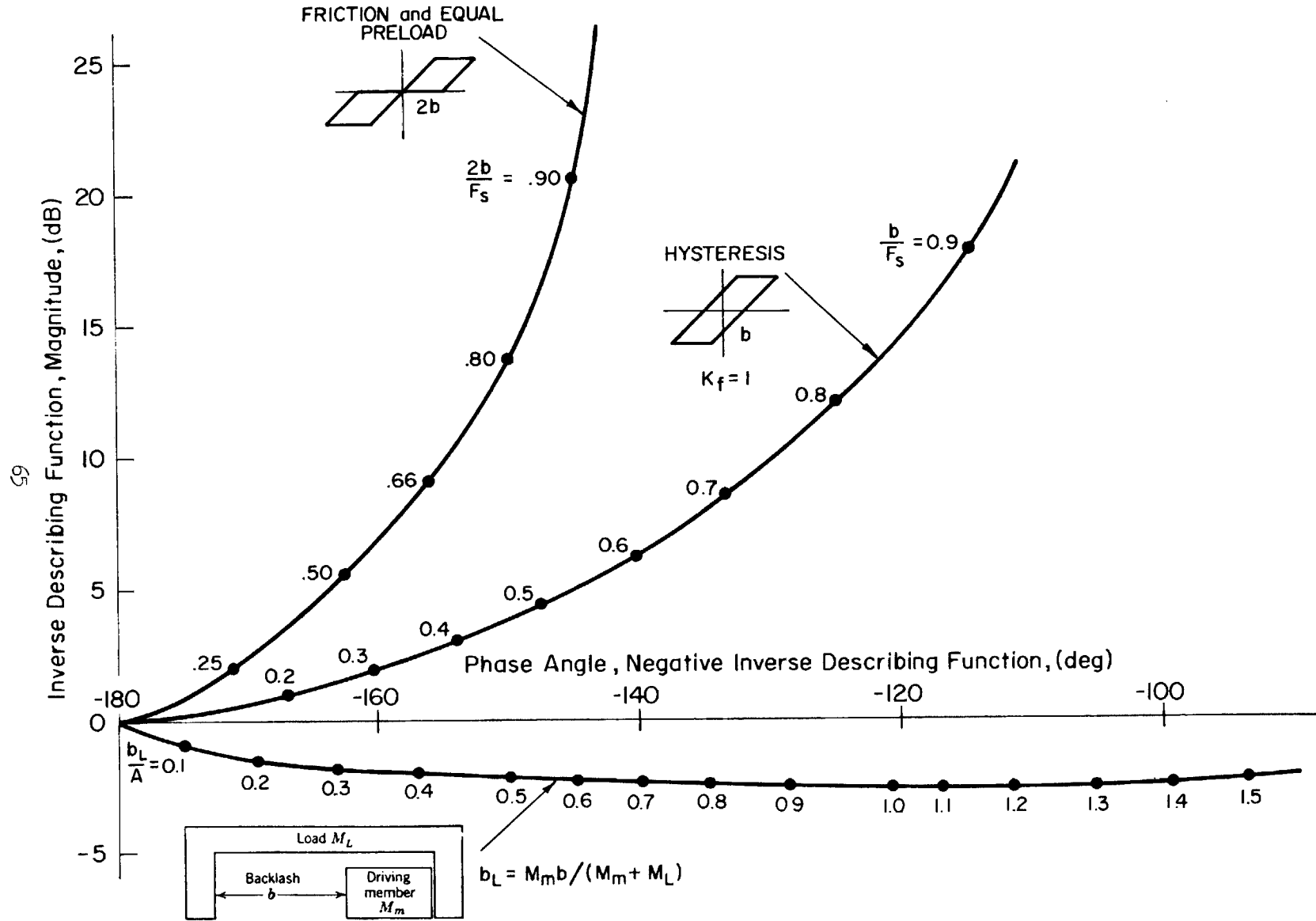


Figure 29. Inverse Describing Function for Hysteresis, Friction and Preload, and Backlash

Equation 46 indicates that if  $G(j\omega)$  and  $-1/N$  are plotted together on the gain-phase plane, intersections of the two curves will satisfy the equation. Intersections, therefore, will show the conditions for neutral oscillatory instability. In general,  $-1/N$  is an amplitude and frequency variant function, whereas  $G(j\omega)$  varies only with frequency. The values of the amplitude and frequency parameters at an intersection of the  $G(j\omega)$  and  $-1/N$  curves give the amplitude and frequency of the oscillation or limit cycle. This intersection is the critical point analogous to the point  $-1 + j0$  in the conventional polar diagram analysis of linear control systems or, in the gain-phase plane, the point 0 dB and  $-180$  deg phase angle. In this sense, the negative inverse describing function can be viewed as creating a critical region as an expansion of the critical point for linear systems. When a goodly region of the gain-phase plane is covered thereby, it is not uncommon to have several intersections of the linear locus with  $-1/N$ . Not all of these indicate stable limit cycles but as a practical matter all are to be avoided. Describing function analysis is an approximate procedure and can lead to inaccurate predictions when its implicit assumptions do not parallel those actually present. Nonetheless, it is an extraordinarily powerful and effective technique in practical engineering and nowhere has been more beneficially and extensively used than in flight control system design and analysis. For more details see Refs. 6, 7, and 8.

From this discussion it is apparent that the locus of the open-loop transfer function of either an autopilot or pilot-plus-vehicle system should avoid intersection with this inverse describing function to be assured of stability. As a practical matter, close approach gives warning of degraded closed-loop characteristics of a wandering-about, driftlike behavior. If gains required for control and stabilization purposes are so high as to actually cause an intersection with the inverse describing function, a limit cycle in the automatic system or a PIO under manual control can occur.

To reduce the change of dynamic problems of this character, the control system can be preloaded. This has the effect of shifting the hysteresis loop with a consequent marked attenuation and phase reduction in the describing function, as can be seen by comparing the hysteresis describing function with that for friction with equal preload (Fig. 29). A much smaller proportion of the gain-phase plane now constitutes a forbidden area, so the likelihood

of any closed-loop system oscillation from this cause becomes much less. This comparison indicates that not only is the preload useful for the purpose of returning the stick for a centered position but also beneficial in terms of dynamic stability.

The artificial feel system can contain other deleterious nonlinearities in unusual circumstances. For example, backlash can occasionally be present if a system is improperly rigged or if backlash preloading forces are exceeded. The backlash inverse describing function is much worse than that of hysteresis. As seen in Fig. 29, it in fact is almost impossible to avoid by any reasonable open-loop system transfer function locus. When backlash plus friction are considered together this becomes less serious, although the limiting case is that for hysteresis (see Ref. 6 for more details). While in this instance friction is beneficial, it should be emphasized that it also contributes to control system phase lag which is detrimental to closed-loop pilot-vehicle performance. Excessive control system friction can cause the pilot to operate as a positional rather than force controller and hence increase his phase lag. Thus friction should be kept to a minimum.

The location of the principal friction contributors within the control system can also have a strong influence on the consequences. When located in the control system cables or push rods it can have the beneficial (limited) influence noted above. However, if located in the hydraulic actuator input valve it can have very strong negative effects. This will be discussed in the next subsection.

The final nonlinearity to be mentioned here is stick-to-surface gearing. A common type of gearing is shown in Fig. 30. Here, the stick-to-surface gain increases as the horizontal tail deflection moves more trailing edge up (TEU). The gradient is nearly constant over the range of horizontal surface deflections required to trim the aircraft throughout the flight envelope. This gradient is selected to provide "good" control sensitivity for small stick deflections about trim (i.e., to provide low sensitivity in this region). However, for maneuvering requiring nearly full surface deflection, the gain between stick and surface is rapidly increased to prevent excessive stick deflection requirements.

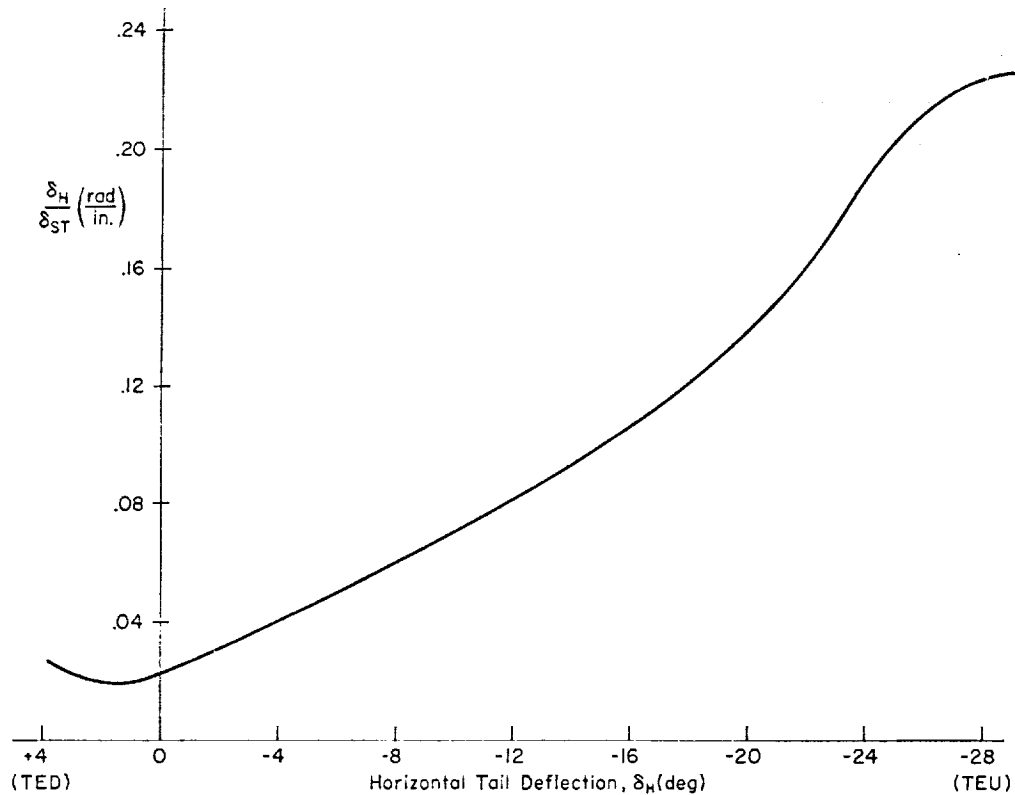


Figure 30. Stick-to-Tail Gearing Versus Tail Deflection

## B. ACTUATION DYNAMICS

Some of the more important linear dynamics of electrohydraulic and hydraulic actuation systems have been described in Section II. Although this emphasized actuator stability, the need for an adequate backup support structure was also mentioned. With stability augmentation installations in particular, the backup can be very tricky. Ideally, the series-installed actuator will move the surface actuator input without feeding back in any way to the stick. This requires the load as seen by the series servo looking toward the surface to be much less than that looking toward the pilot. Detents, system friction, preload, favorable mechanical advantages, and minimum series-servo-to-surface-actuator loads are elements in the compromises needed to

attain a satisfactory SAS installation. It is also important that the SAS limiting velocity be tailored to be consistent with that of the surface actuators so that surface actuator valve bottoming does not lead to series servo kickback to the cockpit controls. This characteristic can be almost inevitable when the surface actuators are holding substantial trim loads near the actuator stall. Under these circumstances, the surface rates attainable from the surface actuators are much less than maximum, whereas the stability augmentor limiting velocity is unaffected by the hinge moments. Consequently, full rate is still available to the SAS servo, while the surface actuator rate is much reduced. Although these practical design matters are fairly obvious and generally recognized, they have typically been independently discovered by new designers. At best, they tax design ingenuity to achieve a satisfactory compromise.

The series actuator backup problem in some systems is so difficult as to require alternative solutions. One concept which has other favorable properties is the use of a fully-powered hydraulic actuator inboard (on the pilot's side) of the series connection. This serves to isolate the series and surface actuators and all downstream friction and other nonlinearities from the cockpit controls. The major disadvantage is the increased complexity. Other approaches are to feed forward, as in Fig. 21, a signal proportional to desired control action. This provides command augmentation as well as an alternate pathway which can be used to offset some of series servo lost motion due to a soft backup. This type of system is inevitably highly calibrated on an individual basis and is seldom satisfactory except for experimental installations. Perhaps the ultimate solution to backup problems is to accomplish the series summing electrically, as in a fly-by-wire system. Then, of course, the SAS actuators are full authority and multiply redundant, leading to a different kind of flight control system with compromises of its own. Again, the subject of command augmentation will be elaborated upon in Section V.

An important feature of any mechanical input hydraulic servo installation is the effect of valve friction on other elements of the system. This particular friction is of a different category than that distributed along the mechanical linkages in that it is affected by the hydraulic system feedbacks. This is shown by the schematic diagram of Fig. 31. To emphasize the major effects introduced by this peculiar friction force, the feel system is

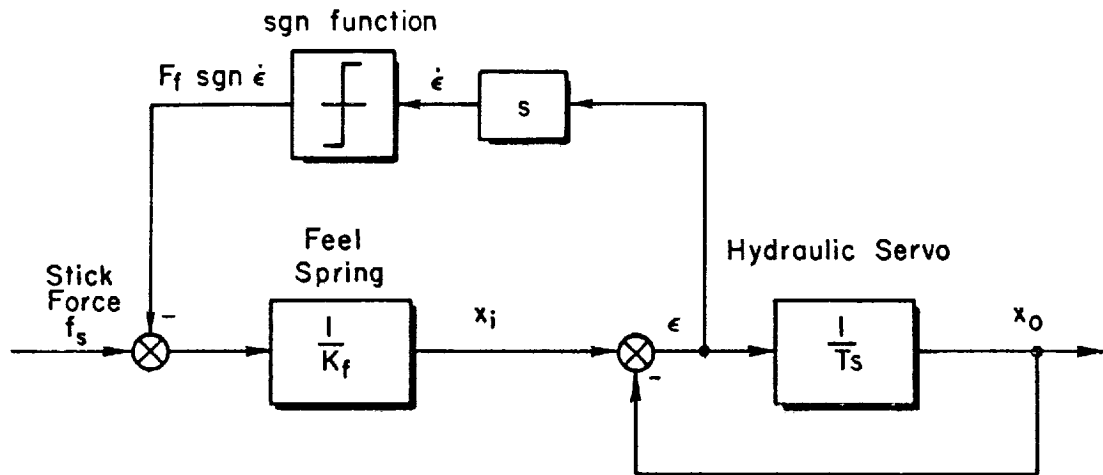


Figure 31. Block Diagram — Aircraft Control System with Valve Friction

represented only by the feel spring; and inertias, other frictional forces, dampers, etc., are neglected.

On a simple physical basis, we would expect that the friction at the outset of motion would act similarly to that normally in control linkages, but its position within the hydraulic servo feedback tends to maintain a valve error once this is established. Consequently, the servo will tend to go further and continue moving for a longer time than it would if the friction were not present. Qualitatively, then, the presence of the friction would be expected to increase the gain and lag of the hydraulic actuator as seen from outside this loop. Both of these features could be inimical to auto-pilot or human pilot control activity, resulting in limit cycles or PIO's, respectively.

The nonlinear properties of the actuation system cum valve friction which relate to periodic behavior are conveniently handled with describing function analyses. An appropriate describing function for this case has been derived (Ref. 8) and is given by:

$$\frac{x_0}{f_s} = \frac{1}{K_f} \left[ \frac{\left(1 + \frac{4F_f}{\pi F_s}\right)}{\left(1 + \frac{4F_f}{\pi F_s}\right) T_j \omega + 1} \right] \quad (47)$$

Notice that, as anticipated by the qualitative physics, the closed-loop sinusoidal describing function shows both gain and time constant are augmented by the factor  $(1 + 4F_f/\pi F_s)$ .

The actuator plus valve friction characteristics are shown in a gain phase plot as a negative inverse describing function in Fig. 32. It is important to recognize that the describing function is frequency-dependent. This means that intersections with the negative inverse describing function of the transfer function locus for the remaining elements in the loop must match in amplitude, phase, and frequency if an oscillation is to be present. It is apparent from Fig. 32 that the 0 dB, -180 deg criterion point for stability of the linear system is enormously extended by the valve friction effect. The nonlinearity represented by this type of describing function is thus very inimical to stability, particularly if the actuator time constant is fairly large or valve friction excessive. Indeed, the need to eliminate these effects as contributors to a serious stability problem is a major incentive in design efforts to minimize valve friction and actuator time constant.

### C. BOBWEIGHT EFFECTS

Many mechanical control systems have unavoidable or deliberately introduced bobweight elements. The situation shown in Fig. 22 is fairly general in that both fore and aft bobweights are present. For the illustrative longitudinal case, these alter stick force characteristics as a function of normal and pitching accelerations. These two bobweight feedback loops are represented in the Fig. 33 block diagram as a single path. The single equivalent loop is obtained by solving the following expression for bobweight stick force:

$$\begin{aligned} F &= B_N(a_z) = B_N(a_{z_{cg}} + l_x \ddot{\theta}) \\ &= B_N a_{z_{cg}} + B_P \ddot{\theta} \end{aligned} \quad (48)$$

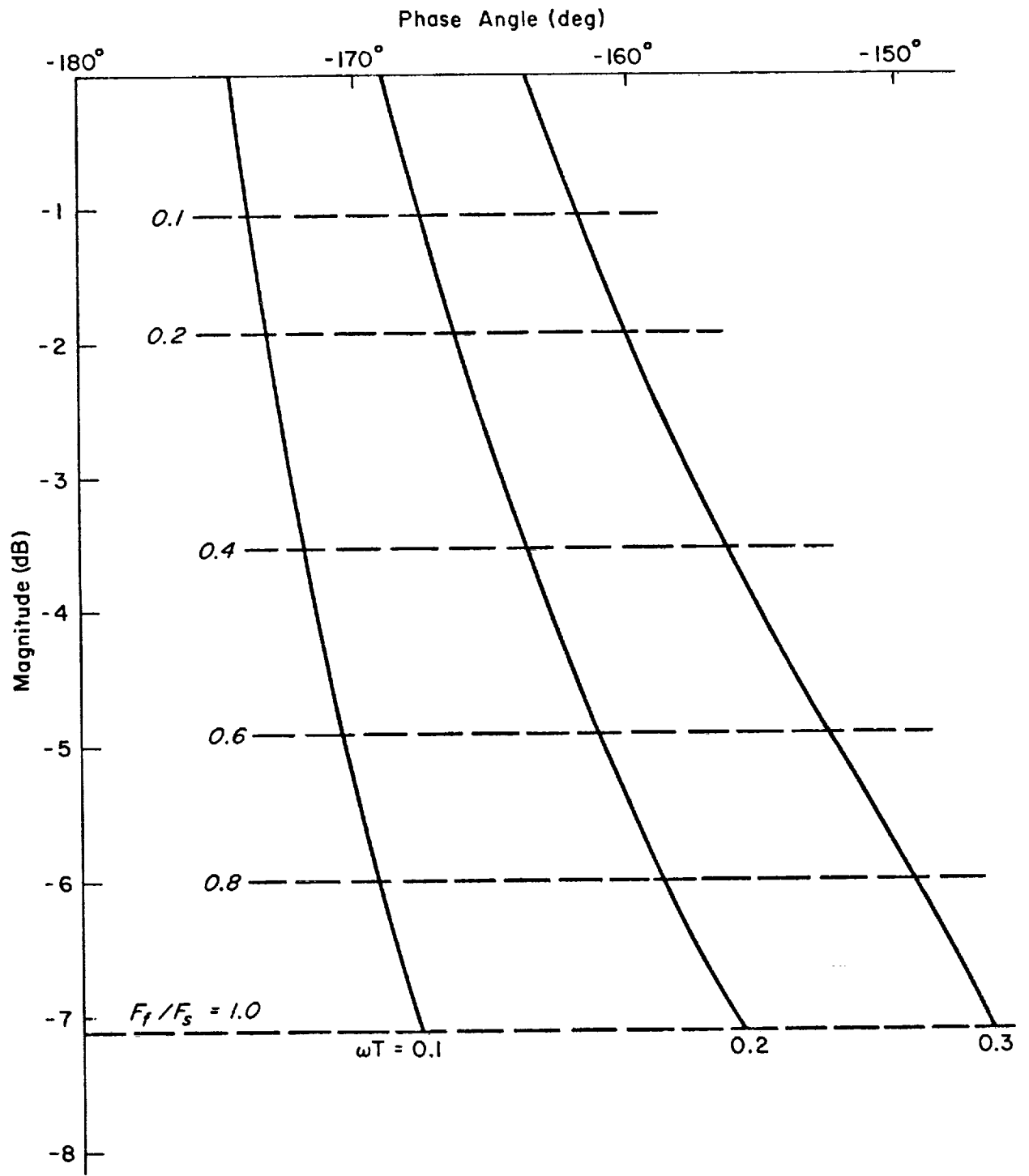
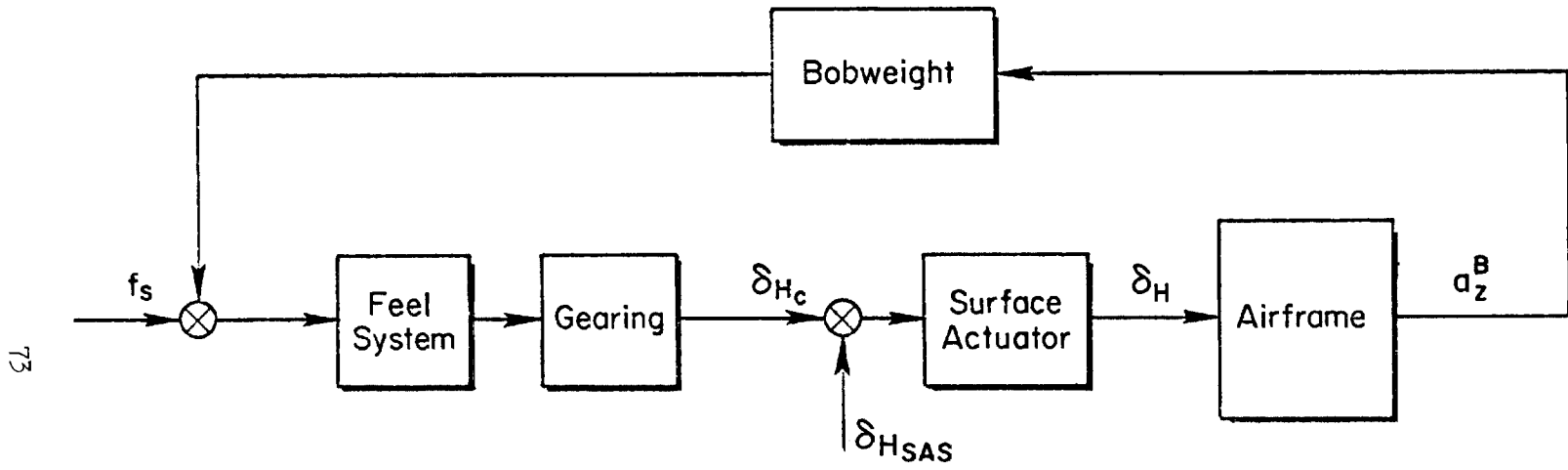


Figure 32. Negative Inverse Describing Function for a Control System with Valve Friction;  $K_f = 1$



$a_z^B$  is the normal acceleration at the effective bobweight moment arm

Figure 33. Block Diagram of Longitudinal Control System

This leads to the expression for the bobweight numerator which relates surface deflection to acceleration at an effective bobweight location:

$$N_{\delta}^{a_z^B} = N_{\delta}^{a_z^{cg}} + \frac{B_P}{B_N} N_{\delta}^{\theta} \quad (49)$$

Here  $a_z^B$  is the normal acceleration felt by an effective bobweight at some distance,  $l_B$ , from the c.g. It follows that  $l_B$  is simply  $-B_P/B_N$ .

The roots of the effective bobweight numerator,  $N_{\delta}^{a_z^B}$ , are the roots of the expression:

$$1 + \frac{B_P}{B_N} \frac{N_{\delta}^{\theta}}{N_{\delta}^{a_z^{cg}}} = 0 \quad (50)$$

or

$$\frac{B_P}{B_N} \frac{A_{\theta} s^2 (s + \frac{1}{T_{\theta 1}}) (s + \frac{1}{T_{\theta 2}})}{A_{a_z^{cg}} s (s + \frac{1}{T_{h 1}}) (s + \frac{1}{T_{h 2}}) (s + \frac{1}{T_{h 3}})} = -1$$

Figure 34 presents a survey of these roots as a function of effective bobweight arm ( $B_P/B_N = -l_B$ ). At  $B_P = 0 = -l_B$ , the zeros are coincident with those of the c.g. normal acceleration numerator,  $N_{\delta}^{a_z^{cg}}$ . At  $l_B \rightarrow \infty$  the zeros are coincident with those of the pitching acceleration numerator,  $N_{\delta}^{\theta}$ . For values of  $l_B$  between, the zeros lie on the loci shown in Fig. 34. The final form of the effective bobweight numerator is:

$$N_{\delta}^{a_z^B} = A_{a_z^B} s (s + 1/T_B) [s^2 + 2\zeta_B \omega_B s + \omega_B^2] \quad (51)$$

where

$$A_{a_z^B} = A_{a_z^{cg}} + \frac{B_P}{B_N} A_{\theta} = Z_{\delta} - l_B M_{\delta}$$

Approximate factors for an  $l_B$  range of typical interest are:

$$\frac{1}{T_B} \approx \frac{1}{T_{h 1}} \quad ; \quad \zeta_B \omega_B \approx \frac{1/T_{\theta 1} + 1/T_{\theta 2}}{2} \quad ; \quad \omega_B^2 \approx \frac{U_{\theta}}{l_B T_{\theta 2}}$$

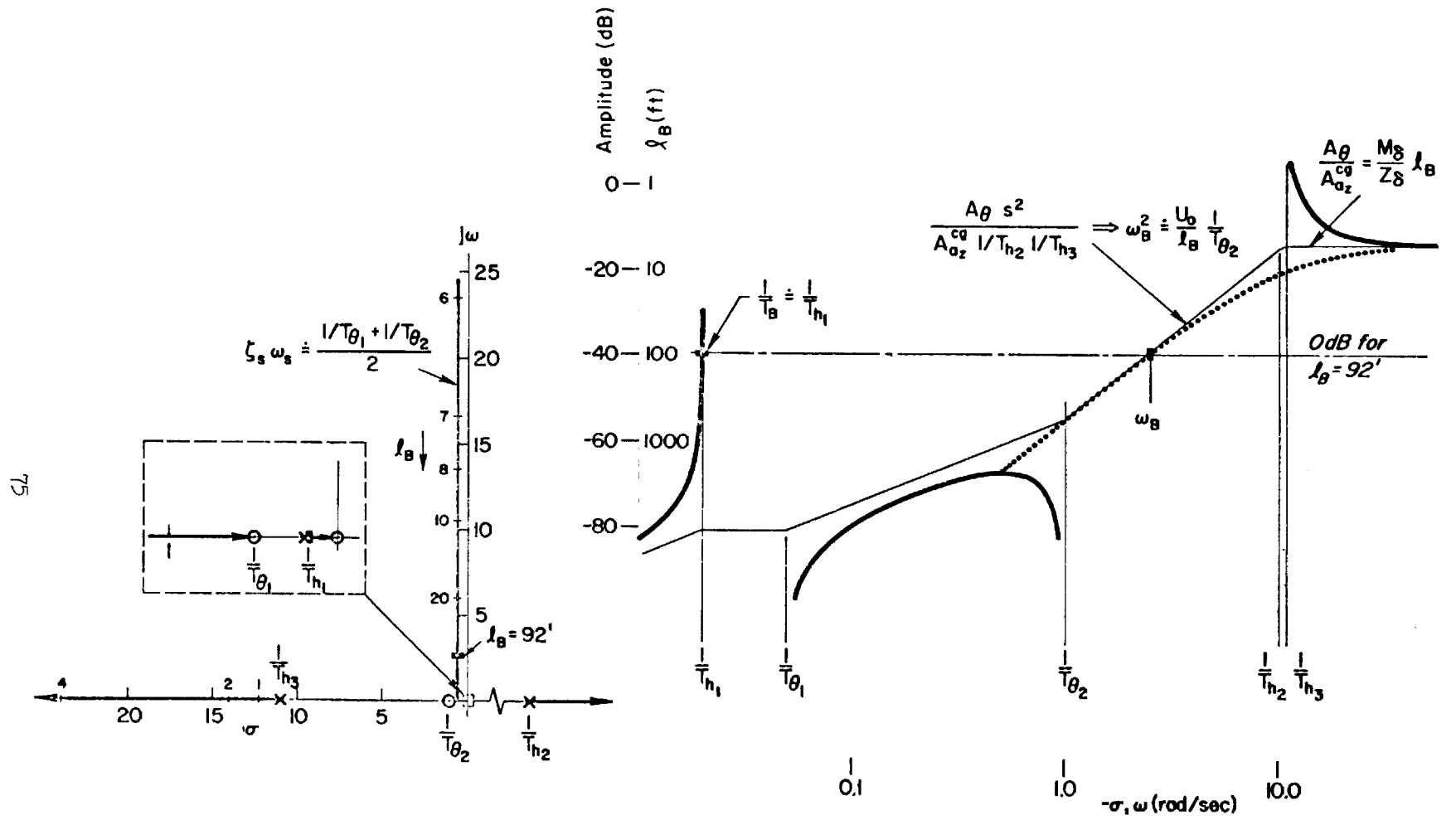


Figure 34. Root Survey for  $N_S^{aZ^B} = N_S^{aZ^{CG}} - l_B N_S^{\delta}$

Numerator root values for a fighter aircraft with an effective bobweight arm of 92 ft are identified in Fig. 34. It can be seen that  $1/T_B \doteq 1/T_{h_1}$  over a considerable range of  $l_B$ . Over most of this range the short-period equations offer a valid approximation to the principal bobweight effects. These are subsumed here in the second-order zeros which approach the vehicle short-period dynamics in the numerical example.

Ignoring stick breakout force (or assuming the stick is displaced from trim), the bobweight contribution to stick force dynamics for a representative case can be obtained from the loop closure of Fig. 35. Here, the airplane dynamics are represented by the short period alone. The short-period poles and the complex bobweight zeros, while typical, have been arbitrarily selected for demonstration purposes. The ratio of bobweight zeros to short period,  $\omega_B/\omega_{sp}$ , shown here as greater than one is usually close to unity. It can, in general, be either greater or less than unity. This is yet another example of the quadratic dipole situation discussed at length in Section II.

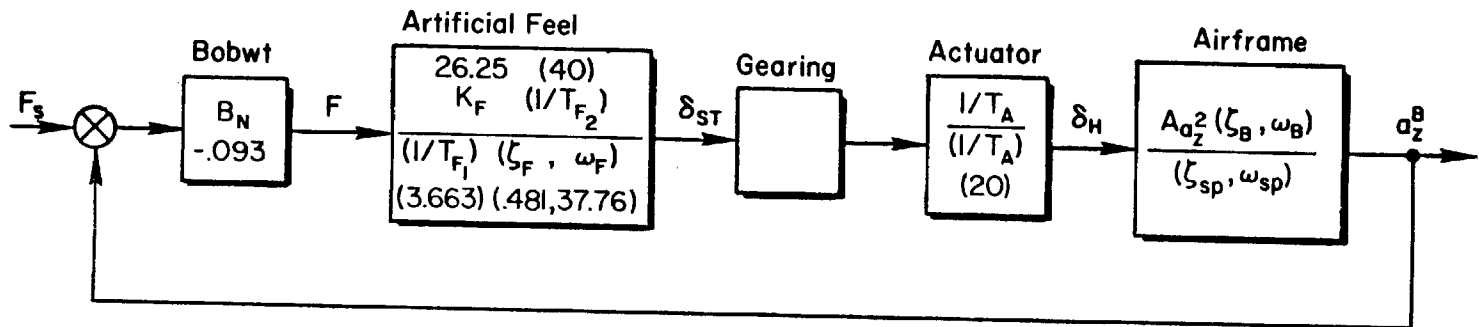
Two major contributions of the bobweight loop may be noted. First, the low-frequency root of the feel system (at 3.66 rad/sec) is moved to a higher frequency (identified as  $1/T_{F_1}$ ). Thus, the bobweight loop tends to reduce the low-frequency lag contribution of the feel system. Secondly, the short-period roots are driven toward the bobweight complex zeros. If we assume:

$$\frac{1}{T_{\theta 2}} \doteq -Z_w \quad ; \quad \zeta_{sp}\omega_{sp} \doteq -\frac{(M_q + M_{\dot{\alpha}} + Z_w)}{2}$$

$$\zeta_B\omega_B \doteq \frac{1/T_{\theta 2}}{2} \doteq -\frac{Z_w}{2}$$

it is readily seen that closure of this type of bobweight loop always results in decreased stick-free short-period damping. Taken to the extreme, i.e.,  $\omega_{sp}$  driven into  $\omega_B$ , the bobweight can cancel out that portion of the short-period damping due to  $M_q$  and  $M_{\dot{\alpha}}$ .

There are factors which can aggravate this situation. The first is increasing separation between  $\omega_B$  and  $\omega_{sp}$  when  $\omega_B/\omega_{sp} > 1$ . In this case the root locus between  $\omega_{sp}$  and  $\omega_B$  tends to blossom out toward the right half



77

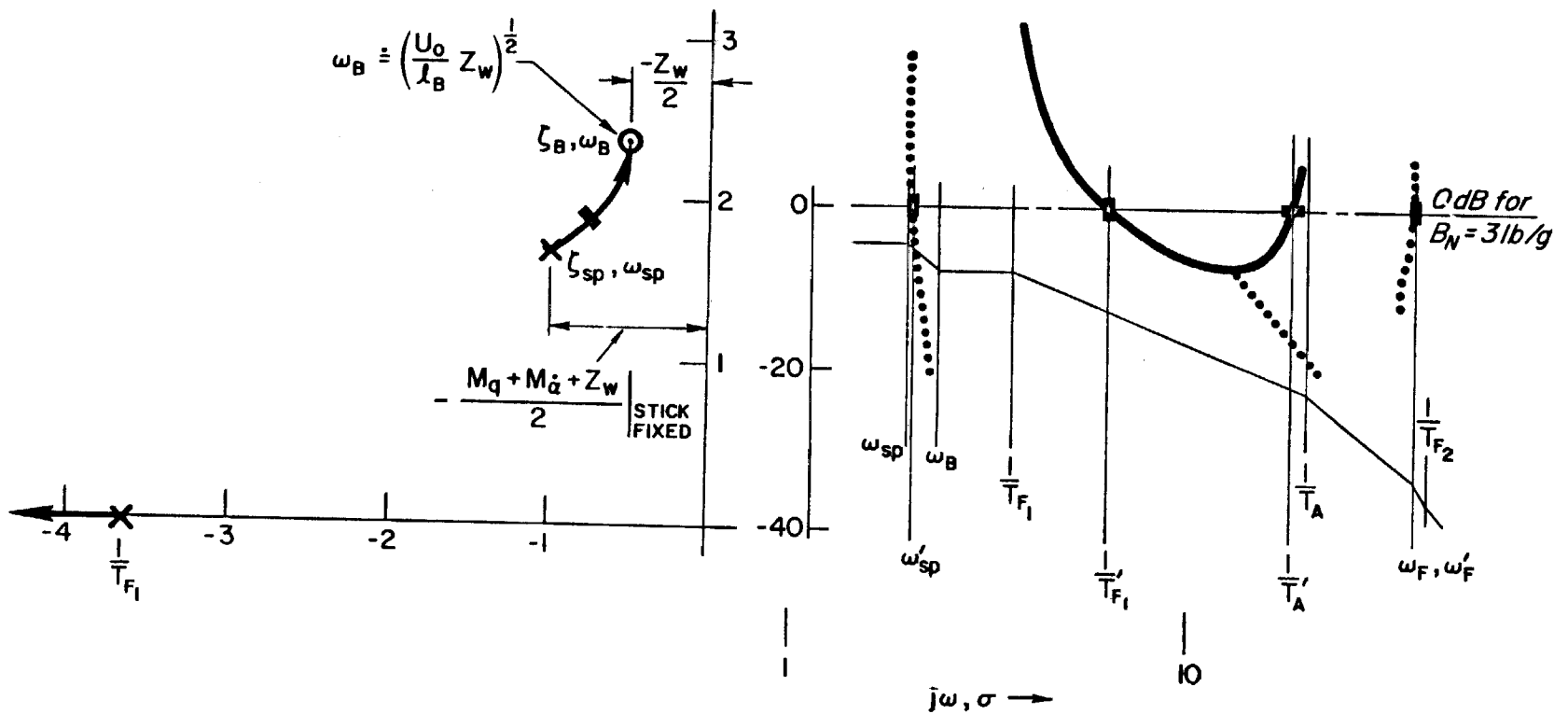


Figure 35. Bobweight Loop Closure

plane and the closed-loop short-period damping is reduced more rapidly for the same loop gain. A second is the introduction of lag in the region of the short period which also contributes to the blossoming. This can be due to  $1/T_{F_1}$  (the open-loop feel system pole) or by introduction of low frequency lags due to system nonlinearities (hysteresis). Either is demonstrated by the loci of Fig. 36. Note particularly the blossoming that results as the lag inverse time constant moves from 10 to 2.5. If this inverse lag is thought of as the artificial feel contribution, a potential detrimental interaction between the feel and bobweight systems becomes obvious.

If  $\omega_B/\omega_{sp} < 1$ , the locus between them rotates counterclockwise so that the closed-loop short-period damping tends to increase. While this may be beneficial at times, it must be noted that the effective short-period frequency is decreased simultaneously and this could be quite undesirable at times.

In summary, closure of the bobweight loop will either increase the effective airframe short-period frequency at the cost of reduced damping or increase the short-period damping at a cost of reduced frequency. The interaction between the feel system first-order lag and the bobweight loop is such as to increase  $1/T_{F_1}$  (and hence decrease the low-frequency lag contribution of the feel systems), but to decrease the closed-loop short-period damping. Any nonlinearities in this control loop will also tend to reduce the closed-loop short-period damping. Finally, it should be noted that friction and stiction in the bobweight system can cause the effective short-period dynamics to "jump" from the stick-fixed to stick-free values.

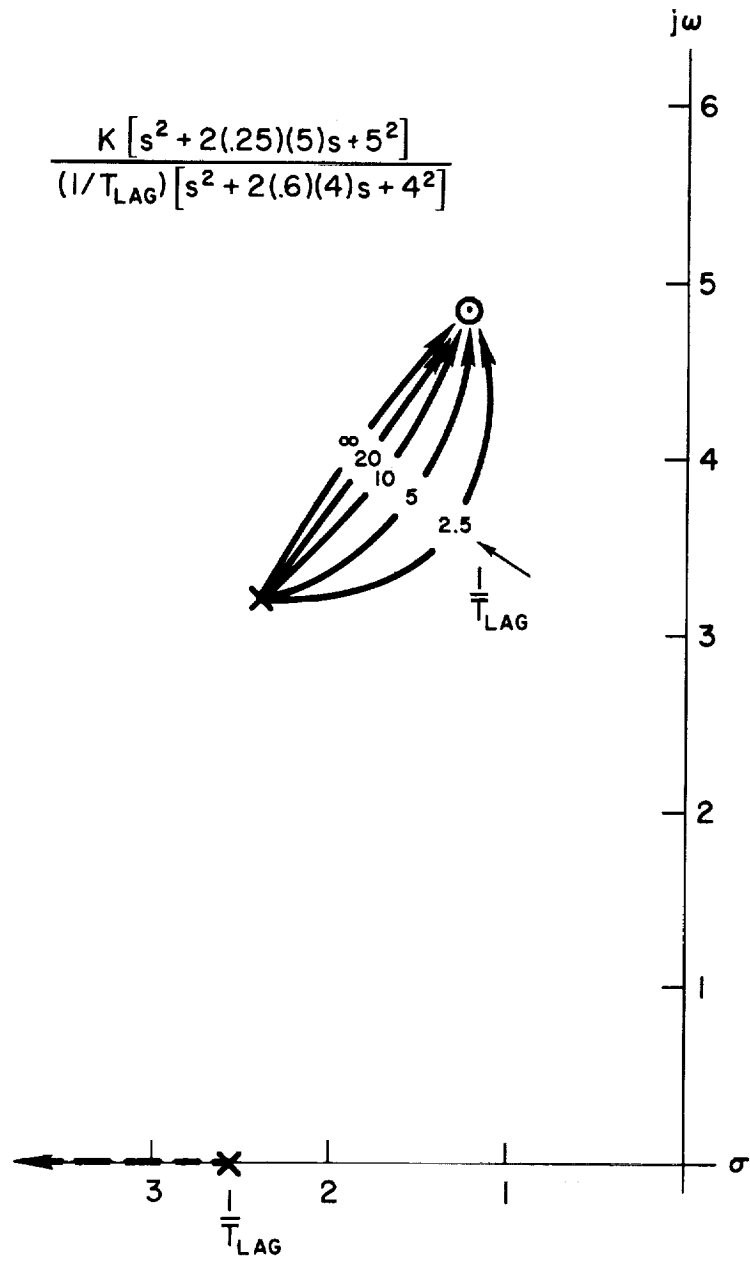


Figure 36. Effect of Increasing Control System Lags on Bobweight Loop Closure

## SECTION V

### AUGMENTATION AND STABILIZATION SYSTEM PROBLEMS

The previous section emphasized the predominantly mechanical aspects of the flight control system. These elements are always turned on in normal operation, and usually constitute the irreducible complete chain from pilot to surface. Accordingly, this collection of components is often called the primary flight control system. They constitute the milieu for the remaining flight control system elements which are predominantly automatic in nature and primarily feedback in character. These additional flight controls may provide damping, stability, or feel augmentation and other automatic control activities such as autopilot and command augmentation. Because their signal and equalization circuits are electronic, and thus highly flexible and versatile, these augmentation and stabilization systems offer great appeal as devices to modify and manipulate the controlled element characteristics and to accomplish other functions otherwise impossible to perform. Thus, they offer many promises. On the other hand, augmentation and stabilization systems also possess great potential for problems because they are integrative — and thereby must interface with the previously discussed mechanical control system, extensive sensor complexes and the pilot, and must react properly in conjunction with a highly variable response vehicle. Such integration is intrinsically synonymous with complexity. For example, Fig. 37 is a generic block diagram elaboration of Fig. 21 which shows the many interfacing elements possible in a Command Augmentation System (CAS) — as many as six interactive loops. Depending on the specific aircraft installation these elements may encompass parallel but non-identical pathways, multiple feedback loops, series and parallel actuators, coupling with the aircraft control feel and trim systems, etc. Figure 37 also shows the location and type of some of the more troublesome nonlinearities — friction, preload, threshold, limit, etc. These many factors will be discussed in this section. Major consideration will be given those augmentation and stabilization systems which provide both electrical and mechanical control parallel pathways from stick to surface. There are two reasons for this emphasis on command-type systems. First, the mechanization is more complex than a direct-wire electrical backup path

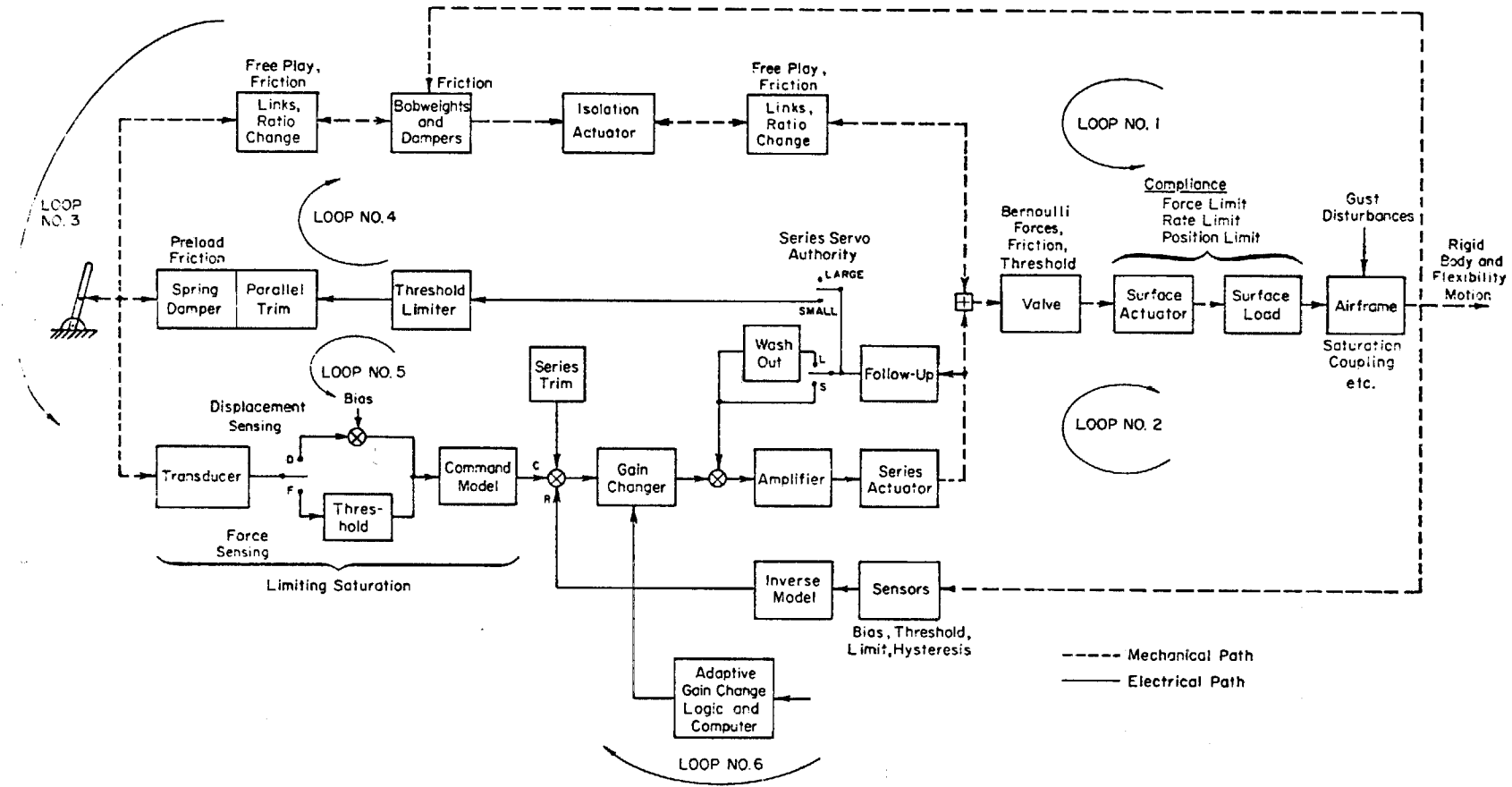


Figure 37. Generic Block Diagram for Command Augmentation Systems

(fly-by-wire system) and therefore has more potential problem areas. Second, although fly-by-wire control will become more common in the future, parallel mechanical-electrical CAS designs are currently predominant and will be for some time. However, it should be noted that total fly-by-wire mechanizations generally will have "direct wire" stick-to-surface-actuator backup modes and thus will also be prone to problems associated with dissimilar parallel paths.

The types of command insertion (input) and actuation (output) employed for the augmentation scheme will be discussed as the first topic. These CAS-mechanical control system interfaces are one of the central factors in command augmentation mechanization. Three input sensing and four actuation concepts are covered. These afford twelve potential system mechanizations. Rather than discuss each of these in detail, we shall divide the presentation on the basis of the four actuation schemes and make the command sensing a subset of these.

Command augmentation requires large effective actuation authority for the concept to be viable. The two most common means of achieving this are with full authority series positional servos\* or with limited authority series servos plus large authority parallel actuators. Full authority series is discussed first. The limited authority series mechanization is then presented with further breakdown as to parallel trim versus parallel boost actuation considerations. The fourth concept encompasses forward loop integration within the large authority series actuation means (otherwise known as velocity servos, automatic series trim, neutral speed stability actuation, etc.).

The three fundamental types of input command sensing covered are those that sense:

- a. Force directly at the pilot level input (stick force).
- b. Displacement of the force feel element (pseudo stick force).
- c. Displacement of the pilot lever input (stick displacement).

The attributes of these are discussed most fully in conjunction with the full authority positional series actuation and are not carried into the other

---

\*It should be noted that augmentation actuation functions may be provided by separate servos as reflected in Fig. 22 or incorporated into the basic surface actuator package via a multi-input scheme. In general, the conceptual problems are similar although the detail aspects may vary somewhat.

actuation schemes except as specifically altered by the actuation concept. This discussion of the three command sensing types within the framework of the four actuation schemes is a major part of the section because of the many inherent problems requiring coverage.

Attention is next turned to preshaping of the electrical command prior to differencing it with the feedback signal. Two forms of shaping are considered: lag (or low bandpass) and nonlinear gain.

The last article in the section is devoted to feedback sensor related considerations including location and orientation problems (gravity vector and aircraft response axis), influence of nonlinearities, and interaction of feedback, command, and actuation. Example mechanizations are also shown. This presentation is separated into separate discussions of each axis (longitudinal, lateral, and directional). Intentional coupling of lateral-directional motion, e.g., turn coordination, is not covered here but is the subject of Section VI.

The last article also briefly touches on problems related to the interaction of high-gain feedback systems and structural bending. Structural feedback and resonance has afflicted almost every high-gain system. Although structural modes are estimated as closely as possible, considerable cut and try generally has been required on the first few flights to finalize structural filter characteristics — sometimes resulting in different filter characteristics for ground and flight operations.

#### **A. COMMAND INSERTION/ACTUATION SUBSYSTEM COMBINATIONS**

Because CAS are integrations of many flight control subsystems they share the problems of their component elements. Nowhere is this connection more pervasive than with the actuation — the final common pathway of all flight control system action. We have already covered generally some features of actuators in previous sections, particularly dynamic stability, interfaces with load and backup structure, and some nonlinear aspects. Some of these features will be reiterated here in a more specific context. This repetition is inevitable as we proceed from general to specific considerations if coverage is to be reasonably complete.

The two basic types of actuation system installations are referred to as series and parallel. Series actuation results in control surface motion without motion at the control stick, whereas a parallel servo actuator moves surface and stick alike. It is desirable and common practice to isolate high-frequency signals from the control stick; hence, a SAS used for damping augmentation is accomplished by series-type actuation. Conversely, parallel operation is conventionally used for autopilot control of path, speed, and position and is often employed for control stick steering as well. Parallel actuation provides a direct indication of operation and thus from a safety standpoint provides the advantage of giving the pilot a means for monitoring the system.

As introduced previously, an extremely important characteristic of CAS is the need for high authority servo actuators to accommodate large command inputs as well as SAS operation. To avoid position limiting, most CAS systems provide servo authority which approaches full surface deflection. This complicates the problem of aircraft safety in the event of a system hardover malfunction. There have been several approaches to hardover protection. The most common technique for series actuators is limitation of actuator authority to command surface deflections sufficiently small to prevent structural damage in the event of failure. This restricted authority series servo is then used in conjunction with an automatic trim system which increases the low-frequency surface authority to full deflection. Another scheme which is becoming popular in actuation system fail safety is dual, triple, or quad redundancy. Yet another method is to employ parallel servos which provide the pilot direct indication of servo output and can be overridden by the pilot.

The special system component problems associated with redundancy, failure monitoring, etc., are highly mechanization-specific. They are peculiar to particular designs rather than generalizable to systems as a whole. Consequently, these will not be covered here. We will discuss, however, some of the fundamental system problems which can be and have been encountered when the large authority, redundant servos are functioning as intended.

## 1. Full Authority Series Actuation

Figure 38 shows a typical full authority series actuation system. As noted in Sections II and IV, for this system to function properly the mechanical impedance between the series actuator and the control stick must be much greater than that between the series actuator and the surface actuator valve. The backup impedance needed to act as a "ground" for the series actuator is provided by the feel system force breakout and spring gradient. In the absence of any free play between the series actuator and its ground, all motion of the actuator is transmitted to the surface actuator valve. The major forces with which the series actuator must contend are surface actuator valve friction, centering, and Bernoulli forces. If these are high, the backup forces needed may become excessive; then a separate power boost or fully-powered actuator may be incorporated between the series actuator and surface actuator.

If the surface actuator valve is "bottomed" (comes in contact with the actuator case) by the summed mechanical and series servo inputs, the impedance at the surface actuator valve becomes infinite and any subsequent series

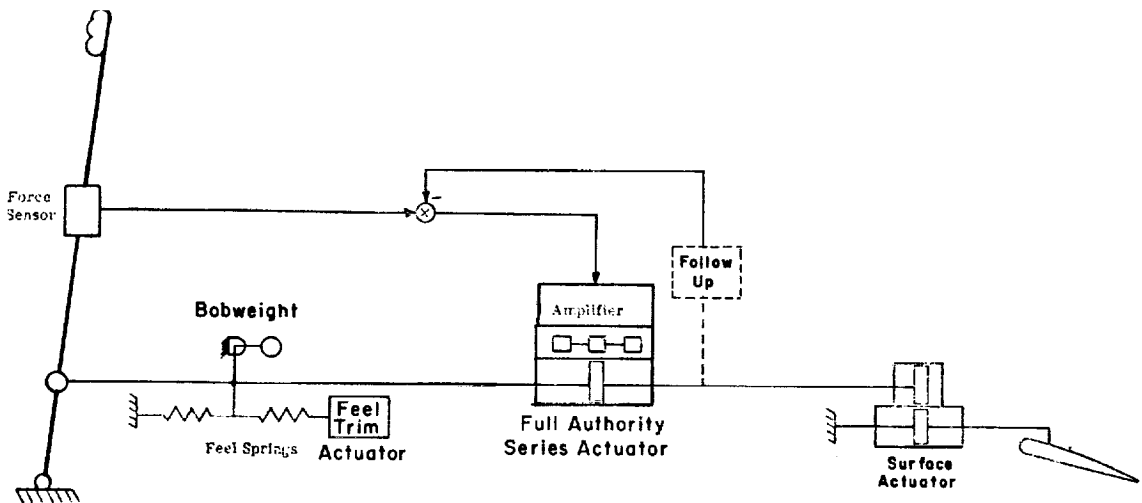


Figure 38. Full Authority Series Actuation

actuator deflection will be transmitted back to the stick. As noted previously, this "kickback" will occur when the actuator rates are incompatible, when sufficient surface actuator valve travel is not available to accommodate full stick travel (mechanical link) plus full series actuator travel, etc. This has been particularly troublesome in aircraft which employ the same control surfaces for pitch and roll control (e.g., elevons or rolling tail), because the combined inputs of partial roll and pitch stick can drive one surface to its limit while the other is still functional.

Most of the other characteristics of the full authority CAS series actuation are related to the type and location of the pilot input sensor used for the electrical path. This will be discussed next, classified as Stick Force, Pseudo Stick Force, or Stick Displacement, as appropriate for the sensor.

a. Stick Force

Figure 38 indicates a stick force sensor which detects stress due to forces (direct or reaction) applied at any point on the stick above the sensor location. This type of sensor is attractive for systems in which it is desired to provide essentially invariant stick force per g characteristics. The interaction of this sensing technique with the other elements of the control system has also created several potential problem areas as follows.

1) Feel System. Feel system integrity is a prime concern if this type sensing is to provide redundant stick-to-surface paths. If the mechanical link between the stick and feel spring is broken, both control paths are lost because there is no ground for the force sensor. Thus, to minimize the number of vulnerable parts and connections, the feel spring should be located as near to the stick as possible and the series servo as near to the power actuator as possible. On the other hand, if the mechanical link between the feel system and the series actuator is broken, both control paths are also lost because there is no backup for the series actuator.

In this same vein, the feel system (or stick) spring gradients should be selected to provide proper harmony between stick displacement, stick force, and

electrical output from the force sensor. A single gradient which achieves a satisfactory balance between stick displacements for gross maneuvering (large stick amplitude) and for precise control (small stick amplitude) conditions is hard enough to obtain without the complications added by the force sensor.

The familiar effective stick force breakout characteristic associated with the normal center stick is eliminated and/or replaced by entirely different characteristics which derive from friction forces within the stick/feel-system mechanism. It is common to incorporate an electrical threshold on the electrical force signal to match the ideal mechanical breakout (detent) threshold. The actual breakout characteristic as sensed by the force transducer is composed of the following elements sketched in Fig. 39. The friction

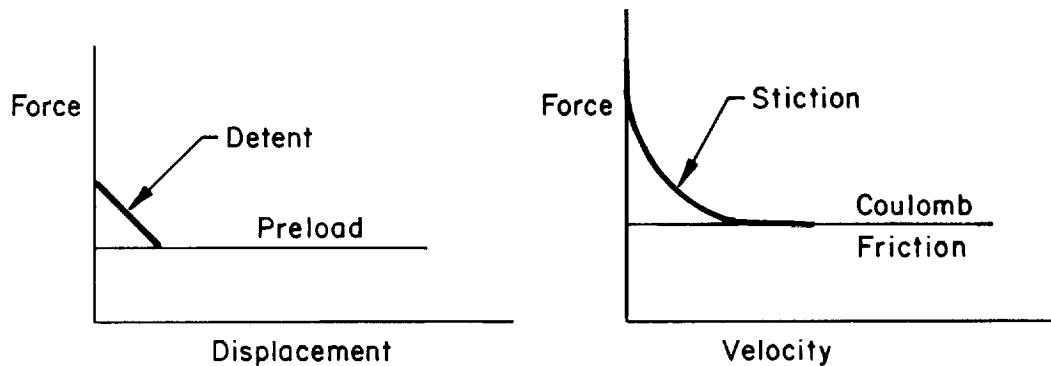


Figure 39. Breakout Characteristics

components can (and do) vary widely with production tolerances and with field usage (wear, corrosion, dirt, etc.); these variations are largely beyond the control of the systems designer. The stiction component results in a significant initial impulse or "dropback" characteristic at the series servo output (and hence power actuator) which can drastically affect control precision in the small stick deflection region (i.e., formation flying, aerial refuelling, etc.). If the electrical threshold is set sufficiently high to accommodate the stiction component, then problems arise because mechanical surface deflection occurs before the electrical response is commanded. Since the latter actually commands a specific aircraft motion response dependent upon the CAS feedback employed, this can result in effective control reversal in the small stick deflection area.

Poor stick centering characteristics due to friction and freeplay between the stick and feel springs (or within the detent) are improved by the preload, although they are relatively insignificant since the force sensor is unaffected by stick neutral position. Freeplay by itself is a temporary lack of ground and no power actuator command is generated through either the electrical or mechanical paths.

2) Trim System. It is very difficult for the pilot manually to trim stick force to zero via the feel trim actuator with this type sensor. If the pilot applies force to achieve a desired trim surface position and then actuates the feel trim motor to neutralize stick force, the series actuator retracts to neutral as stick force reduces and hence the surface deflection reduces. A constant stick movement which creates a series actuator movement equal and opposite to the trim motion is therefore required while trimming off the force in order to replace the retracting servo displacement with mechanical link displacement and hence retain constant surface position. This generally results in imprecise trial and error trimming and is greatly disliked by pilots. An alternative method is to introduce the trim command both to the feel trim actuator and, summed with the force sensor output, to the series servo such that the motion of one exactly cancels the motion of the other. This method is sensitive to production tolerances, wear, etc., on the trim motor rate.

Another method is to accomplish trimming via the series servo alone; however, this also introduces several problems. First, stick neutral is always at the same position regardless of flight condition. This destroys the relationship between stick position and surface position and hence removes a cue of vital importance to the pilot in maneuvering, landing, etc. Additionally, if the pilot attempts to trim off forces in, for example, a high g windup turn, he can be moving the stick forward while increasing the load factor. This is undesirable, to say the least. Finally, in the event the CAS cycles off for any reason (e.g., electrical power failure, redundant voting, etc.), the series trim is instantly lost and can provide dangerous, if not catastrophic, results. When used, this latter mechanization has often required the CAS to be turned off for approach and landing.

3) Kickback. If stick kickback is encountered, the stick force against the pilot's hand decreases and thus calls for decreased series servo deflection and a reduction in demand at the power actuator valve. The resulting motion may immediately jerk the stick from the pilot's hand or may cause a high-frequency "ratcheting" of the stick against his hand. This is most often encountered while the aircraft is on the ground but could be catastrophic if encountered in flight.

4) Bobweight Effects. Control system bobweight effects can be intentional to augment feel forces or unintentional due to mass imbalance in the control system (which almost always occurs to some extent at some trim conditions even if the control system is carefully mass-balanced). The intentional bobweight alters feel forces by increasing the force/displacement ratio as a function of load factor when the stick is out of the neutral position. Any bobweight contribution is sensed by the force transducer and transmitted to the augmentation system. The results depend upon the aircraft response (acceleration or attitude rate) feedback employed but, in general, the command will be for increased aircraft response via the series servo, will result in stick force lightening, and may provide a tendency to overcontrol.

Inadvertent mass imbalance can be either harmful or beneficial. Except for special situations such as catapult launch or massive control columns in climb or dive, mass balance is not usually considered to be important. However, a force-sensing CAS amplifies control system imbalance effects and can become crucial. The problem is quite difficult to avoid because the control system has distributed mass which is acted upon by a non-uniform force field (i.e., rotational and translational accelerations) dependent upon location of the masses within the aircraft and the initiating cause (stick input, gust disturbance, catapult, etc.). Any imbalance forces which reflect back to the pilot's hand will then be picked up by the CAS command sensor and cause immediate control surface deflection via the CAS.

As an example of the complexity of the problem, assume the control stick has appreciable mass above the pivot point and the control system has been mass balanced to zero stick force per g with the stick at the mid position of its travel. However, in flight the force neutral (trim) stick position can be forward (high speed) or aft (low speed) of the mid position and a

net moment arm may be present. The electrical signal obtained from the resulting action of the stick imbalance against the pilot's hand is stabilizing for the stick trimmed aft and destabilizing for the stick trimmed forward.

Bobweight effects of the pilot's arm also can be significant in creating unwanted inputs. This is especially true under high acceleration or deceleration situations such as catapult launch from aircraft carriers. The CAS of some Navy aircraft are generally turned off during launch for this specific reason. This same feature can cause severe bottoming of servos, surface actuators, etc., during hard landings, carrier arrestments, etc.

5) Structural Bending. Structural bending can modify the mechanical path length between the stick and power actuator. Like the series actuator, the effects of the resulting system inputs depend upon the effective control system impedances at the input locations. For a system with the feel package near the stick, any relative motion between the control run and structure should result in power actuator valve motion rather than stick motion. Thus, there should be no output from the force sensor (against the pilot's hand as ground). Conversely, if the feel package is located near the power actuator, the impedance looking toward the stick can be low so that any differential motion is reflected into stick deflection. In this case, a force signal can be developed against the pilot's hand.

6) Transducer Null. With this type of sensing, the transducer null (zero force output) is independent of any other elements of the control system. Therefore, once adjusted, it should require no further trimming.

7) On/Off Transients. The electrical path shown in Fig. 38 will provide series servo transients upon system engagement only if stick force is applied simultaneously. Disengagement transients can occur if either stick force or series trim is being used at the time of disengagement.

8) Transducer Vulnerability. A stick force sensor located near the top of the control stick is particularly vulnerable to damage and/or incorrect installation. The sensor is subject to damage resulting from various maintenance activities within the cockpit. A sensor which is integral with the stick grip is also vulnerable to specific maintenance actions involving any of the many switches mounted within the grip. Each removal and reinstallation, for

any reason, increases the probability of damage to electrical pin connections, inadequate securing, etc. One problem which has plagued some operational CAS is the failure of maintenance personnel to properly secure the stick grip which then works loose in flight and comes off in the pilot's hand!

b. Pseudo Stick Force

Pseudo stick force is obtained by installing a displacement transducer across the feel spring as shown in Fig. 40. A signal is provided to the

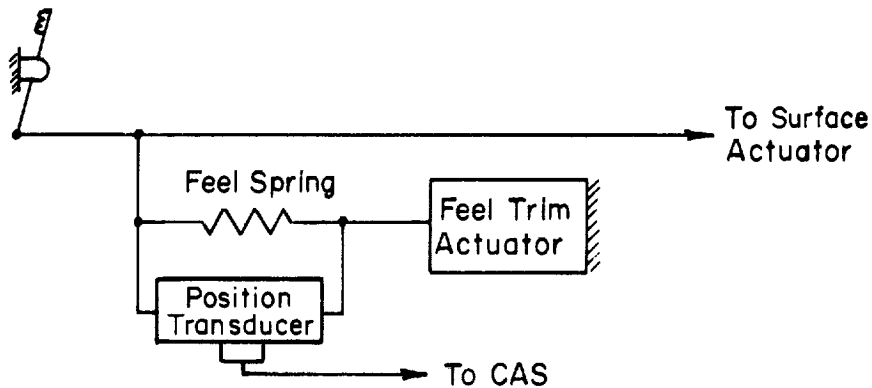


Figure 40. Pseudo Force Mechanization

series actuator of Fig. 38 whenever the feel spring is deflected. The interaction of this sensing technique and other elements of the control system is as follows.

1) Feel System. Feel system integrity requirements are the same as for the previously discussed stick force sensor.

The problem of feel system breakout characteristics is largely eliminated since this mechanization does not require an electrical threshold to match the mechanical breakout.

Feel spring centering and freeplay nonlinearities can become dominant. It is not uncommon for feel bungees to develop freeplay and high friction levels with wear and age. This will result in the spring and transducer not returning to neutral but instead stopping on one side or the other of

the freeplay. Thus, the transducer will have a bias (zero force at stick) output with magnitude dependent upon the mechanical system freeplay and friction level and with sign dependent upon the direction of the last stick input. Since the transducer commands aircraft motion response via the series servo, these nonlinearities in the feel system can result in imprecise control in the small stick deflection region and in trimming.

2) Trim System. Manual trim of stick force to zero via the feel trim actuator is subject to the same problems previously discussed for the stick force sensor.

3) Kickback. With this installation, kickback can cause the feel spring deflection to increase (over that initially commanded by the pilot) which, in turn, drives the series servo even harder. Thus, this system is divergent and, once started, will tend to drive the stick/feel-system to their stops unless alleviated by surface actuator movement sufficient to "unground" the surface actuator valve. The effect of kickback can be reversed if direction reversing links are judiciously employed in the control system.

4) Bobweight Effects. Intentional longitudinal bobweight activity is designed to increase stick force by introducing a moment to return the stick toward neutral. This has no effect on the pseudo-force transducer unless the feel spring is actually deflected (toward neutral position). In the latter case, the signal to the series actuator commands retraction which, in turn, decreases the maneuver command. Thus, both the mechanical and CAS paths increase stick force per g.

If the control stick or column has appreciable mass this system can also be sensitive to trim stick position. However, it makes little difference whether the stick is trimmed forward or aft of neutral since in either case the bobweight effect of the stick mass and the pilot's arm inertia will be in a direction to increase feel spring and transducer deflections.

5) Structural Bending. Structural bending effects should be nil since this sensor is located across the highest impedance component.

6) Transducer Null. Transducer null depends upon installation adjustment which generally will be non-zero. This null is further affected by feel system centering characteristics noted previously.

7) On/Off Transients. These are the same as for the stick force sensor.

8) Transducer Vulnerability. The sensor is generally located in an area which has little maintenance "traffic" and is well protected from inadvertent damage.

c. Stick Displacement

Stick displacement can be sensed by transducers located in any number of places within the control system. However, minimization of control system nonlinear effects generally dictates locating the sensor such that it is preloaded to eliminate as many nonlinearities as possible. One such location is across the feel system as shown in Fig. 41. The interaction of this sensing technique and other elements of the control system is as follows.

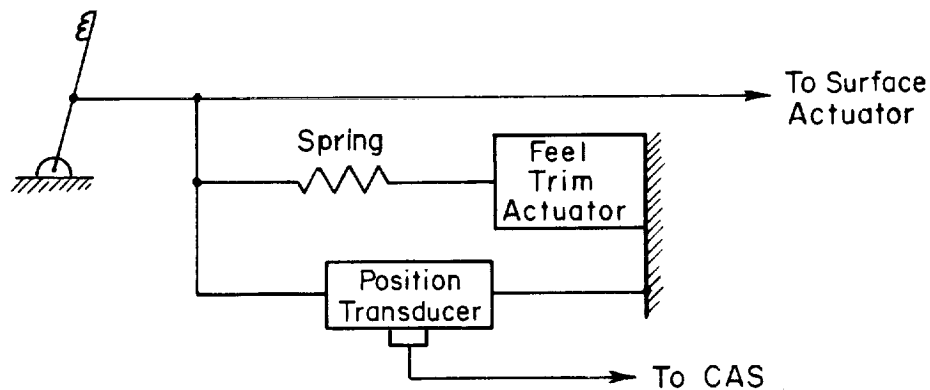


Figure 41. Control System Displacement Sensing

1) Feel System. Feel system integrity requirements for the installation shown are the same as previously discussed. However, the sensor can be located (e.g., directly from the stick to ground) such that mechanical integrity between the stick and the feel system is not required and hence the mechanical and electrical paths to the surface actuator are independent and, therefore, redundant.

This system also does not require an electrical threshold to match the mechanical breakout characteristics because there is no electrical output until the breakout is exceeded.

Feel spring centering and freeplay nonlinearity effects are the same as with the pseudo force sensing except that now those acting between the spring and ground through the trim actuator are also involved.

2) Trim System. Manual trim of stick force to zero via the feel trim actuator is considerably eased with this mechanization since the actuator only relieves spring loading and does not change control linkage displacement relative to ground. Thus, the pilot can hold the desired stick position and trim forces to zero at this position. If the pilot operates the trim without force applied to the stick, the trim actuator moves the entire control system including the stick command sensor and hence commands series servo motion (or CAS response) consistent with the direction of trim.

This mechanization is not compatible with introduction of separate, large trim signals to the CAS, since the latter will change the neutral position relationship between the stick (and stick transducer) and the surface. Small separate trim inputs can be inserted directly to the series servo, however, to offset stick position sensor bias, lack of centering, etc.

3) Kickback. The results of kickback are the same as with pseudo force sensing, i.e., can be favorable or divergent depending upon the usage of reversing links in the control system.

4) Bobweight Effects. Bobweight effects are the same as for the pseudo force sensor system.

5) Structural Bending. Structural bending effects are nil if the sensor is located across the high impedance feel package.

6) Transducer Null. Transducer null effects are the same as for the pseudo force sensor installation.

7) On/Off Transients. Engage or disengage transients are only obtained if the system is turned on or off while holding stick deflection from force neutral.

8) Transducer Vulnerability. Same as for pseudo force sensor.

## 2. Limited Authority Series Actuation With Automatic Parallel Trim

A typical mechanizational schematic for this system is shown in Fig. 42. As indicated previously, this mechanization stems from a compromise to obtain full surface authority for the CAS but without the fail safety problems of full authority series actuation. The limited authority series actuator accomplishes all stability augmentation functions. The parallel trim actuator is activated whenever the series deflection exceeds some preset amplitude and time duration limits. The full authority trim actuator then drives in a direction to relieve or recenter the series actuator. In this manner the series actuator is always operating about its center position and maximum authority can be set at a level which will prevent a hardover failure from producing structural failure.

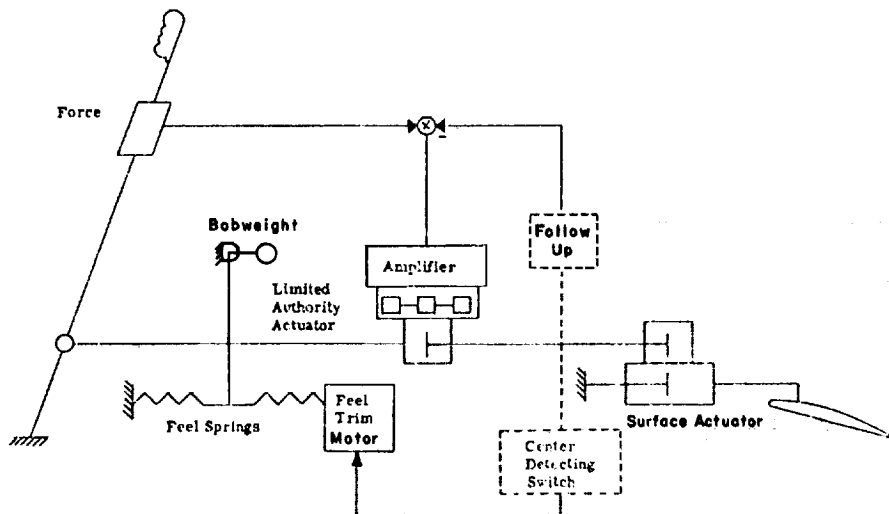


Figure 42. Limited Authority Series Actuation  
With Automatic Trim

This system exhibits the same characteristics discussed in the previous subsection for the three types of electrical sensing. In addition, it has other characteristics, which will be discussed next.

Because the surface actuator has much higher response rate than the trim actuator and the series servo has limited authority, the kickback tendency is reduced but not eliminated.

The center detecting switch unit must have a significant threshold about series actuator neutral to prevent undesirable chattering of the feel trim actuator.

During large extended maneuvers the system will attempt automatically to trim feel forces to zero. If maneuver forces are held in one direction for an extended period the stick force required will decrease as the trim system takes over command of the surface position. This results in stick force lightening in maneuvers which can be objectionable to the pilot. In addition, to return the surface to its initial, pre-maneuver, position, an opposite force must be applied to the stick until the trim actuator returns to its previous position. Thus, the pilot cannot establish a trim point, maneuver away from the trim point momentarily, and then just relax stick force to return to the trim condition. Instead, he must constantly "drive" the trim system via stick force. This:

- Increases pilot workload.
- Makes precise control difficult.
- Is especially objectionable at low q conditions where large surface (and hence stick) deflections are required for maneuvering.
- Makes stall and spin recovery more awkward.

The degree to which the above properties lead to control difficulties depends on trim actuator rate. The higher the trim rate, the greater the degradation in handling characteristics. Thus, a compromise in rate must be made between sufficiently high to prevent series servo bottoming and sufficiently low to prevent handling quality degradation.

The conflict between the pilot and the trim actuator can be reduced by incorporating a switching logic which disables the automatic trim during pilot-commanded maneuvers. However, this also removes the ability to trim stick force to zero at the pilot's discretion unless manual trim (via stick trim button) is also provided during such stick commands. This introduces the trim problems noted in the previous section. In addition, if the pilot attempts to use manual trim without deflecting the stick, the automatic trim will cancel the manual trim.

Finally, a small authority (easily saturated) series actuator with a large authority parallel autotrim gives the same result as command augmentation mechanized using parallel actuation alone.

### 3. Limited Authority Series and Parallel Actuation

A typical schematic for this type of mechanization is shown in Fig. 43. The limited authority series servo provides the high-frequency stability augmentation functions (damping, disturbance suppression, etc.). The parallel actuator provides the necessary authority to accommodate path control modes (i.e., autopilot control wheel steering, hold functions, etc.) and/or serves as a power boost for pilot stick or column inputs.

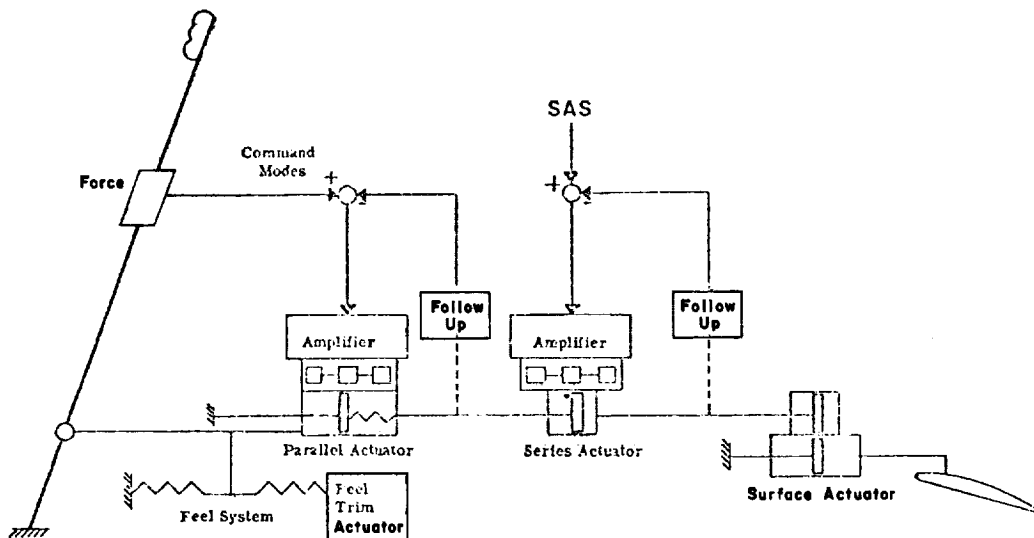


Figure 43. Full Authority Parallel and Surface Actuators With Limited Authority Series Actuator and Trim

Since the parallel actuator provides a rigid link to ground until it is overpowered, it acts as a very large mechanical preload or detent. Thus, position sensing is ineffective and true force sensing at the stick or column must be employed. The resulting force feel depends upon the ratio of feel system spring gradient, the parallel actuator spring gradient, and the electrical gain between the force sensor and the parallel actuator.

Although the parallel actuator is generally considered to have full surface authority, in reality it may not. The actuator output power is ordinarily limited so the pilot can overpower it in an emergency. In moving the entire control system, the actuator works against the feel springs, the power actuator valve forces, and other mechanical system friction, inertia, etc. Therefore, when the sum of these forces equals the parallel actuator overpower limit, it stalls and its surface authority is thereby limited. The authority is thus set by the pilot overpower limit. Another result of this limiting is that the actuator dynamics change as it approaches stall if the force limit is accomplished within the actuator itself instead of by virtue of an external clutch, bellville spring, or similar force-transmission limiting device. This introduces additional phase lag in the forward path for large pilot (or autopilot) commanded maneuvers.

The above force limiting effect can be reduced by incorporating an automatic crossfeed from the parallel actuator output to the trim actuator which operates to relieve feel system forces. However, this requires a fast trim rate to prevent the trim actuator from getting out of phase with the parallel actuator in large maneuvers and hence actually increasing the load on the parallel actuator. This is the same problem as just discussed for pilot/automatic trim opposition in large maneuvers. Another possibility is to use the trim actuator as the parallel actuator and hence reduce system complexity. In this instance, the stick force sensor signal is used to drive the trim actuator. Unfortunately, the pilot cannot overpower the trim actuator, and the actuator rates required then create a safety problem in the event of a runaway trim actuator.

Additional control system interface considerations include:

- a) Feel System. This system mechanization can retain complete control function even if the links between the parallel actuator and the feel system are broken. In this case, the feel system remains ground for the force sensor while the parallel actuator functions as ground for the series actuator. Thus, the electrical and mechanical paths are separate to some degree and hence redundant. Note, however, that if the parallel actuator is located between the stick and the feel system, no part of the mechanical system can be broken and still retain any control over the surface power actuator.

The force sensor requires some threshold to prevent inadvertent pilot inputs in turbulence or pilot movement within the cockpit. However, in this instance, there is no need to match the mechanical system detent, friction, and stiction characteristics since the parallel actuator acts as a power boost to overcome these nonlinearities. Similarly, feel system centering characteristics are of little concern.

- b) Trim System. The use of automatic trim has already been discussed above. Manual trim button control of the trim actuator to relieve maneuver stick force results in the same trim problems previously discussed in Subsection 1.a.2 for force sensing. Additionally, it is possible for the pilot to mistrim the system so the parallel actuator is working against a steady load and hence will have a lower stall limit in one direction. Thus, the use of manual trim is discouraged.
- c) Kickback. This mechanization is not subject to kickback if the surface actuator valve is bottomed because the resulting load will merely stall the parallel actuator. However, depending upon the stall force, kickback can result in damage to the control system or its support structure.
- d) Bobweight Effects. Any intentional or unintentional mass imbalance primarily adds to the loads seen by the parallel actuator. The system is subject to the same stick or column/force-sensor mass imbalance effects discussed in Subsection 1.a.4 for stick trimmed forward or aft of the neutral position.
- e) Structural Bending. Structural bending effects are nil.
- f) Transducer Null. Transducer null effects are nil.
- g) On/Off Transients. Disengage transients can be severe if the system is cycled off when the parallel actuator is holding trim position against the feel springs. Elimination of this possibility requires slaving the trim actuator to the parallel actuator. As discussed previously, this can create other problems.
- h) Transducer Vulnerability. Transducer vulnerability to damage is relatively high as discussed in Subsection 1.a.8.

#### 4. Series Actuation With Forward Loop Integration

Two additional actuation concepts which have been used are series CAS actuator with separate series trim motor and series CAS actuator with washed-out positional feedback. These two techniques, while generally used for different purposes, provide very similar dynamic characteristics, i.e., forward loop integration, as will be shown in the following.

a. Large Authority — Washout on Servo Actuator Feedback

This mechanization is used when the series actuator has large surface authority. The block diagram of the servo loop is shown in Fig. 44.

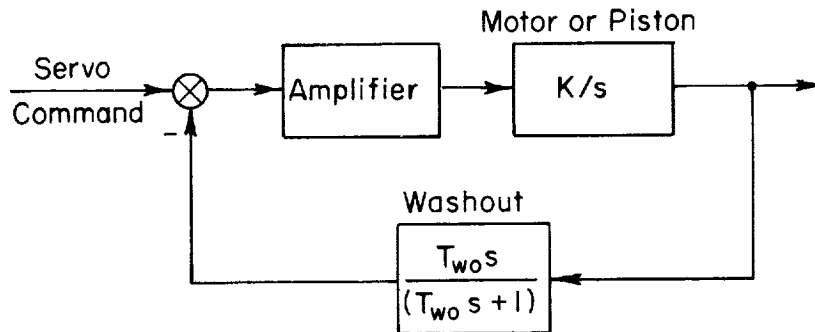


Figure 44. Forward Loop Integration With Large Authority Series Servo

The closed-loop transfer function is:

$$Y_c = \frac{K/s}{1 + \frac{KT_{wo}}{(T_{wo}s + 1)}} = \frac{1}{T_{wo}} \frac{(T_{wo}s + 1)}{s \left( \frac{s}{K} + 1 \right)}$$

where generally  $1/K \ll T_{wo}$  so the actuator acts as an integrator or rate servo at frequencies less than  $1/T_{wo}$  and as a positional servo over the broad bandwidth between  $1/T_{wo}$  and  $K$ . The integration prevents the necessity for command/feedback error offset to maintain non-zero actuation trim. This allows the actuator automatically to compensate for changing control surface effectiveness or trim surface deflection requirements with change in flight condition. However, it also changes the relationship between stick neutral and surface neutral. This, in turn, provides an airframe of apparent neutral speed stability, as will be noted later, because the pilot does not have to retrim stick position as speed changes. In the same manner, it masks airframe c.g. shift.

b. Limited Authority Series Actuator  
With Separate Series Trim

This mechanization is generally used when the series servo has small surface authority. The block diagram is of the form shown in Fig. 45.

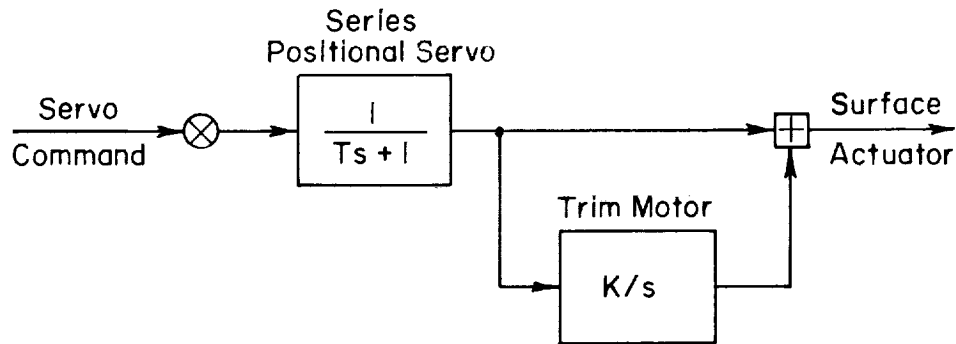


Figure 45. Forward Loop Integration With Small Authority Series Servo and Series Trim

The closed-loop transfer function is:

$$Y_c = \frac{1}{Ts + 1} \left[ 1 + \frac{K}{s} \right] = K \frac{(s/K + 1)}{s(Ts + 1)}$$

where, for this mechanization,  $T \ll 1/K$  and, again, the combination acts as an integrator or rate servo at low frequency and a positional servo at intermediate (maneuvering and short-period) frequencies. The low-frequency integration maintains the series servo operating about neutral at all times and hence helps prevent servo position saturation. As was noted in the previous discussion regarding use of the parallel trim servo for centering the series actuator, a centering threshold is needed between the series servo and the trim motor to prevent chattering or oscillation of the trim motor.

A schematic of a typical control system incorporating a series trim actuator to null the series SAS servo is shown in Fig. 46. The series servo displacement is sensed by the follow-up transducer and transmitted to the series trim actuator through a center threshold, as noted above. For

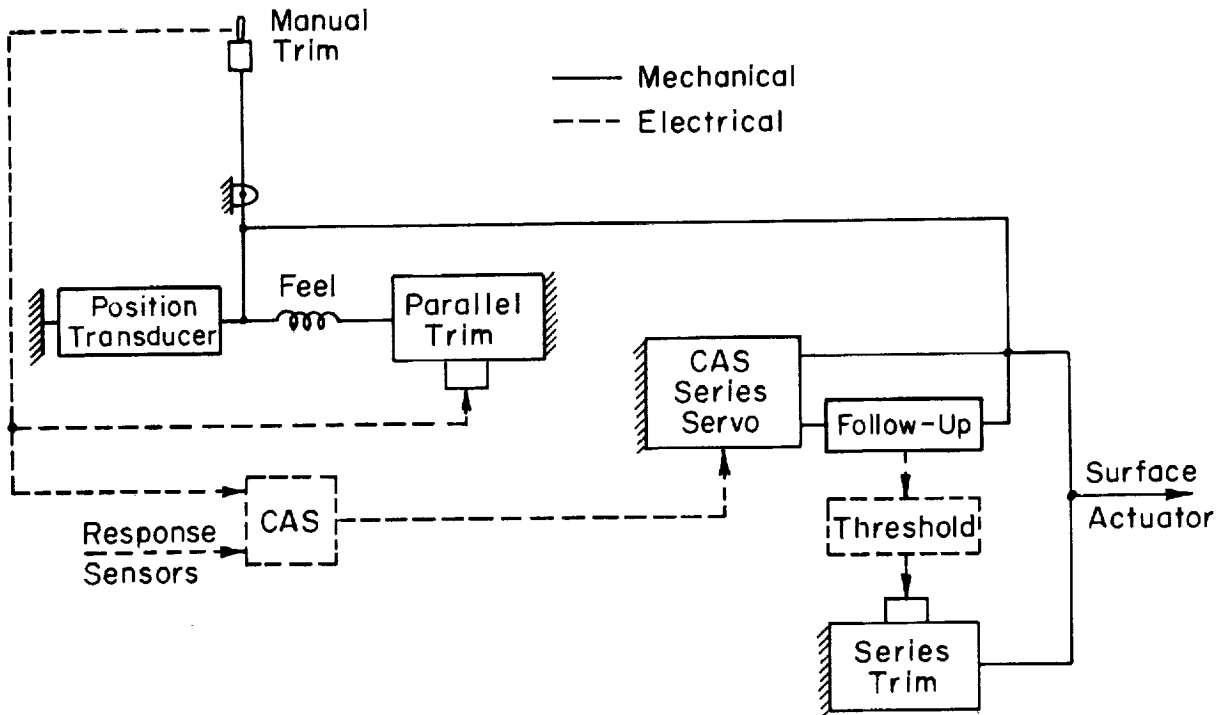


Figure 46. Typical CAS With Automatic Series Trim

normal maneuvering, stick position is sensed and used to command aircraft motion via the CAS. If the pilot operates the manual trim button which, in turn, operates the parallel trim, the surface is moved via the direct mechanical link and an electrical command is transmitted to the CAS. The latter commands a specific aircraft response which is in the same direction but may not coincide with that response which would be obtained from the mechanical surface deflection path. Thus, the series trim may be activated to augment or oppose the parallel trim. If, on the other hand, the pilot holds the stick at the desired position and trims off stick force via the parallel trim, neither the CAS command nor the mechanical link to the surface moves and precise trimming is achieved.

It should be emphasized that both of these mechanizations increase system low-frequency lags, complicate use of the conventional manual parallel trim, and, when coupled with SAS or CAS feedbacks, mask basic airframe speed

stability cues, mask longitudinal c.g. shift, and create other problems which depend upon the specific SAS or CAS feedbacks employed. These will be discussed subsequently.

## 5. Additional Notes

There are many variations on the themes of these CAS and CSS actuation systems. Reference 9 presents additional pertinent discussion of some of these. There also have been numerous largely unsuccessful attempts to use parallel actuation in past CAS and CSS designs, e.g., Ref. 10. Problems contributing to the lack of success include high-frequency motion of the stick, unnatural feel, etc. Parallel actuation has been so universally unacceptable that these mechanizations do not warrant further discussion.

### B. ELECTRICAL COMMAND PRESHAPING OR FILTERING

The essential property of a command augmentation system is the use of an electrical command to the augmentation system so that the augmentor acts as a booster on pilot actions. As shown in the typical system of Fig. 47, the

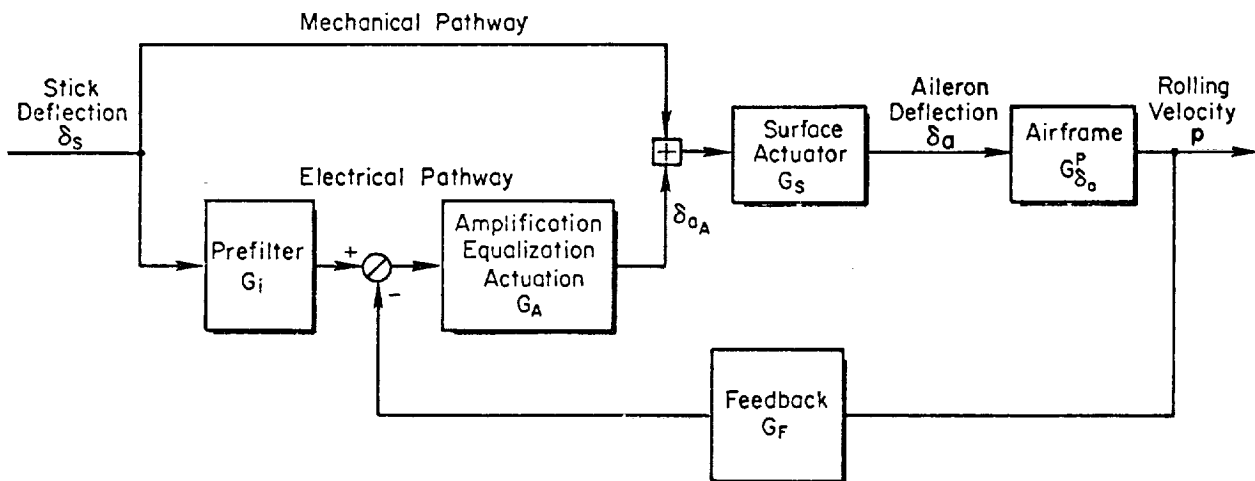


Figure 47. Rolling Velocity Command Augmentation System

two pathways to the surface, one electrical and one mechanical, offer a good deal of flexibility in tailoring the system. As a practical matter, the simplest approach will seldom serve and all the flexibility available is needed to provide desirable features. For instance, a simple command input to the augmentor which is linear with respect to stick force or displacement over the entire stick deflection range will often be unsuitable. This type of mechanization tends to provide an aircraft which is overresponsive for small stick inputs and underresponsive for large. Consequently, the history of most command augmentation system installations has an early phase with considerable diddling and fiddling.

To illustrate some of the factors involved, consider the rolling velocity command system of Fig. 47. The important transfer functions are given below.

Total Aileron:

$$\frac{\delta_a}{\delta_s} = \frac{(1 + G_i G_A) G_s}{1 + G_F G_A G_s G_{\delta_a}^P} \longrightarrow \frac{1}{G_{\delta_a}^P} \left( \frac{1 + G_i G_A}{G_F G_A} \right) \quad (52)$$

Aileron due to CAS

$$\frac{\delta_{aA}}{\delta_s} = \frac{G_A (G_i - G_F G_s G_{\delta_a}^P)}{1 + G_F G_A G_s G_{\delta_a}^P} \longrightarrow \left( \frac{G_i}{G_F G_s G_{\delta_a}^P} - 1 \right) \quad (53)$$

Rolling Velocity

$$\frac{p}{\delta_s} = \frac{(1 + G_i G_A) G_s G_{\delta_a}^P}{1 + G_F G_A G_s G_{\delta_a}^P} \longrightarrow \frac{(1 + G_i G_A)}{G_F G_A} \quad (54)$$

The righthand column shows the forms approached by the transfer functions over the frequency range where the open-loop gain of the augmentation system is very large. In choosing the form of the command feedforward  $G_i$  there are a number of key design considerations. We will mention the three most important.

The first consideration is that full aileron will be required for some flight condition(s) to get the most out of the airplane. Since the augmentation should not degrade the aircraft's capability, it is thus essential that for these flight conditions the aileron due to the augmentor should be equal to or greater than zero or it will otherwise subtract from the total aileron available. From Eq. 53 this is seen to require

$$\delta_{aA} \geq 0 \quad , \quad G_i \geq G_F G_s G \delta_a^P$$

or

$$\frac{G_i}{G_F G_s} \geq G \delta_a^P \quad \text{for large } \delta_s$$

A second design condition often imposed also relates to maximum aileron. In this instance, the maximum stick deflection is to provide a given maximum rolling velocity,  $P_{\max}$ . It follows from Eq. 54 that:

$$\frac{1 + G_i G_A}{G_F G_A} \doteq \frac{G_i}{G_F} \doteq \frac{P_{\max}}{\delta_{s\max}} \quad \text{for maximum } \delta_s \quad (55)$$

Finally, for good flying qualities about neutral there is an optimum airplane gain,  $K_{c\text{opt}}$ . This optimum gain is a strong function of the manipulator characteristics and is, in general, different for control wheels, center sticks, and side sticks. The optimum effective controlled element gain is essentially a compromise between too sluggish and too sensitive conditions. Equation 54 implies that:

$$\frac{1 + G_i G_A}{G_F G_A} \doteq \frac{G_i}{G_F} \doteq K_{c\text{opt}} \quad \text{for small } \delta_s \quad (56)$$

The first two conditions apply for large stick deflections, whereas the third is most important for small. As noted at the beginning of this section, conflict in desires is unavoidable unless, for example, Eqs. 55 and 56 are compatible.

There have been two basic approaches to the solution of command sensitivity dilemmas posed above. One is the introduction of low-pass filtering,

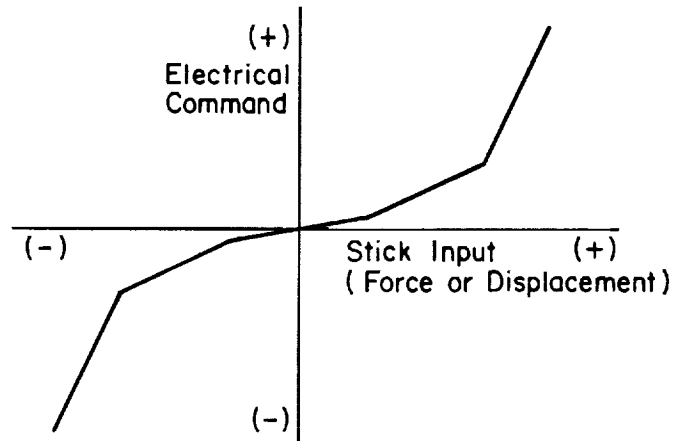
usually a first-order lag, for  $G_i$  and the other is nonlinear gain shaping in the prefilter  $G_i$  and sometimes in the feedback  $G_F$ . These are discussed anecdotally below.

### 1. Lag Shaping

This type of mechanization generally uses linear or nearly linear command sensor output with the electrical gain set to favor the full stick maneuver requirements. This signal is then put through a first-order lag (model) to reduce the gain of rapid (high bandwidth) stick motion and hence reduce control sensitivity in control situations where small rapid stick deflections may be required. Unfortunately, to be effective this requires a relatively low-frequency breakpoint which then introduces appreciable phase lag in the forward loop (similar to that previously discussed for the manual feel system). This phase lag then appears in all control loop dynamics and can appreciably degrade flight path control under certain conditions. For example, the first-order command filter in one high-performance aircraft has a lag time constant of over one-half second in both the lateral and longitudinal channels. This limits the tightness with which the attitude loops may be closed and hence limits precision of flight path control. In this case the CAS actually degrades carrier approach and landing performance of the aircraft. The extra phase lag can also contribute to PIO tendency when attempting to control flight path precisely at high dynamic pressure flight conditions. Such filtering or lags, if used, should not contribute appreciable phase lag at the highest short-period frequencies encountered in the flight envelope.

### 2. Nonlinear Gain Shaping

Another approach is to use nonlinear command gain shaping as a function of stick input. As represented by the sketch below, this provides a low command gradient around stick neutral and high gradient when near full stick deflection. In some past development programs a factor of 3 gain variation has been found desirable for fighter-type missions and control tasks. This type of gain shaping approximates the "softening" effect small distributed nonlinearities have on small stick deflection inputs with conventional mechanical control paths. Thus, it improves low stick amplitude command harmony at



the surface actuator between the electrical and mechanical paths, prevents excessive control sensitivity near stick neutral, and does not introduce phase lag to the control system in the frequency bandwidth of interest. It is still desirable to include some filtering in the region of the actuator response frequency to reduce unnecessary high-frequency overdriving of this component but this lag does not influence the flying qualities of interest to the pilot.

### C. FEEDBACK-RELATED PROBLEMS

This subsection is devoted to discussion of some widely encountered problems related to the type of response feedback employed, sensor location and orientation, feedback and feedforward mechanizations, etc. The common sensors (linear accelerometers, rate gyros, and attitude gyros) are considered. Emphasis is placed on large, rapid maneuvering aspects for two reasons: CAS's are most widely employed in high-performance military aircraft; and, for other aircraft, the consequence of possible inadvertent encounter with such conditions should be recognized. For an analytically thorough exposition and analysis of the basic effects of these and other feedbacks on the aircraft dynamics the reader is referred to Chapters 7, 8, and 11 of Ref. 1. Those aspects relating to the longitudinal axis will be discussed first, followed by the lateral (roll) axis and, finally, the directional axis.

## 1. Longitudinal Axis

The different types of sensors and their location and orientation influences will be discussed first. This will be followed by brief descriptions of some specific mechanizational shortcomings not previously considered.

### a. Linear Accelerometers

Normal acceleration feedback generally is used in a CAS to stiffen the aircraft and/or to provide direct augmentation of stick force per g characteristics. The accelerometer is rigidly mounted in the aircraft with its sensitive axis perpendicular to an aircraft reference line or axis which is roughly horizontal when the aircraft is in nominal cruise conditions. The accelerometer sensitive element is biased to offset a 1 g gravity input and thus to sense deviation from level 1 g flight. The static output of the sensor is

$$n_z \doteq 1 - \cos \Theta_0 \cos \Phi_0$$

where  $\Theta_0$  is the steady-state pitch angle of the accelerometer relative to the gravity vector. Thus, a  $(1 - \cos \Theta \cos \Phi)$  feedback signal is obtained in unaccelerated non-level flight and stick command (force or position) must be maintained to prevent the feedback from producing surface deflection to return the aircraft to a 1 g flight path. The sign of the feedback is selected to provide aircraft nose-up surface deflection when the sensed normal acceleration is less than 1 g and nose-down surface deflection when the sensed normal acceleration is greater than 1 g. For unaccelerated, nose-down descent, the feedback will tend to make the aircraft level off. However, for unaccelerated climb the feedback will tend to further increase the climb attitude. This effect can be particularly insidious if automatic trim actuation or other forward loop integration is also present, for then a divergence in flight path and speed can be created which can end, ultimately, in aircraft stall. The necessity for holding stick inputs in such steady flight situations can be overcome by washing out the very-low-frequency sensor output or by incorporating an electrical trim command input. However, for aircraft in highly maneuvering flight it is impractical to keep introducing a trim signal to offset the change in gravity component, and this must be accomplished via the stick

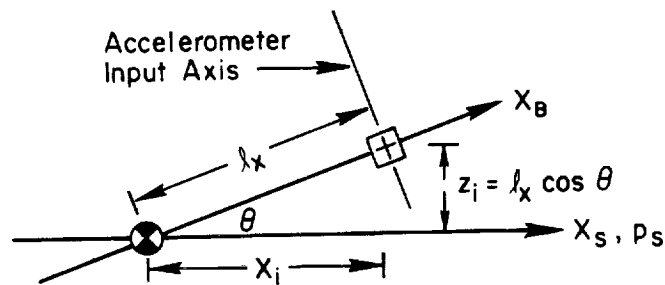
command. Therefore, in constant  $g$  maneuvers this feedback causes considerably more longitudinal stick activity by the pilot. This may be readily appreciated by considering 360 deg rolls.

Another aspect of acceleration sensing concerns sensor location relative to the aircraft c.g. The combined static and dynamic output of the biased accelerometer in  $g$  units is (neglecting bending modes)

$$n_z = 1 - \cos \theta \cos \varphi + \frac{a_{zcg} + (pr - \dot{q})x_i + (qr + \dot{p})y_i + (q^2 + p^2)z_i}{g}$$

where  $x_i$ ,  $y_i$ ,  $z_i$  are distances between the sensor and the aircraft c.g. measured in the stability axis. Generally, the sensor can be located in or near the aircraft x-z plane so the lateral offset term ( $y_i$ ) is small. The major problem arises with the  $x_i$  and  $z_i$  terms and, in particular, the  $-\dot{q}x_i$  and  $+p^2z_i$  contributions. Recognizing that the accelerometer is an electrical bobweight, we may refer back to the discussion of Section IV-C. The zeros of the feedback numerator are controlled by the bobweight arm, i.e.,  $x_i = l_B$ . It may be noted in Fig. 34 that if the accelerometer is located such that  $x_i = l_B = Z_B/M_B$  then the high-frequency zeros (one of which is non-minimum phase) are effectively moved out the  $\sigma$  axis to infinity. This is the location at which elevator deflection produces rotation without translation, i.e., the center of rotation for which the elevator is a center of percussion. It may be noted from Fig. 35 that movement of the zeros (i.e.,  $\omega_B$ ) to very high frequency will greatly attenuate the high-frequency amplitude asymptote and thus greatly reduce the potential of instability of high-frequency, lowly damped modes (e.g., bending or actuator). This location also minimizes the requirement for complex low-frequency lead-lag shaping to maintain loop stability. For further discussion the reader is again referred to Chapter 6 of Ref. 1.

Since most aircraft roll about an axis near the stability x axis, when the aircraft is at high angle of attack, an accelerometer mounted ahead of the vehicle c.g. along the fuselage reference axis can be a considerable distance above the vehicle roll axis (i.e.,  $z_i$  can be appreciable). This can result in significant coupling of lateral motion into the longitudinal axis in highly maneuverable aircraft:



The acceleration in sensor axis is  $p^2 z_i \cos \theta = p^2 l_x \cos^2 \theta$ . One important aspect of this is that an oscillatory roll rate is rectified because  $\cos \phi$  and  $p^2$  are even functions. The  $\cos \theta \cos \phi$  term always results in an up elevator signal, and the  $p^2 l_x \cos^2 \theta$  term will also give rise to up elevator feedback when the accelerometer is above the aircraft roll axis. This can be pro-stall at high  $\alpha$  (wing rock condition) and anti-recovery in oscillatory spins.

Related and specific fundamental problems encountered with  $n_z$  feedback include:

- The stick (command) motion to maintain a constant load factor in combat maneuvering through 360 deg in pitch and/or roll complicates the pilot control task.
- If the command exceeds the feedback capability for any reason (past  $C_{L_{max}}$  in maneuvering, feedback saturation, takeoff rotation, etc.) the resulting error signal to the servo causes increased surface deflection which provides, for example,
  - stick force lightening and/or aircraft pitch-up
  - over rotation and PIO in takeoff
  - pro-stall, anti-spin-recovery surface
- The system increases the rate of speed and/or path divergence in backside operation.
- The system opposes any input to the aircraft other than the electrical command which tends to alter aircraft flight path; therefore, trim must be accomplished as an electrical command to prevent the pilot holding stick displacement (force) in steady turns.
- A high-gain system can cause standoff error in the altitude capture and hold mode of an AFCS.

All of the above are magnified or intensified if the system incorporates integration in the forward loop, e.g., actuation mechanizations using feedback washout or automatic trim. Several aircraft have been lost because of inadvertent aft c.g., normal acceleration feedback, and an auto trim feature.

Finally, the use of this feedback generally requires some means of gain scheduling since the loop gain changes as the square of dynamic pressure.

b. Rate Gyro

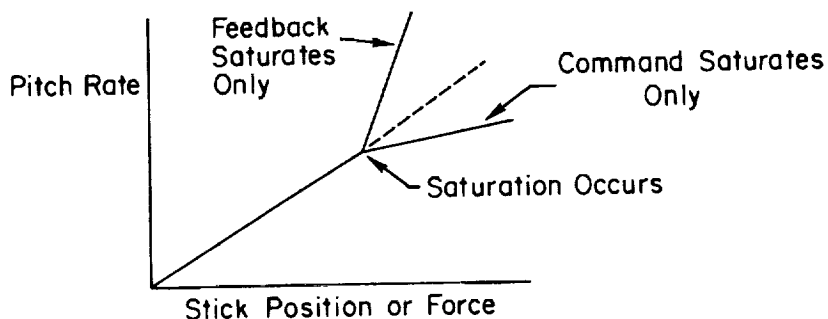
Aside from structural elastic mode considerations there are few problems in locating and aligning pitch rate gyros. This feedback is generally employed to augment short-period damping (i.e., augment  $M_q$ ); however, with gain scheduling of either the feedback or the stick command, this type CAS has also been employed to augment stick force characteristics since  $n_z \sim U_o q$ . Either approach has certain drawbacks. The basic aircraft stick force per g tends to lighten at high dynamic pressure flight conditions. To augment stick force requires either increasing the feedback gain and thereby decreasing the forward loop gain or maintaining the feedback relatively constant and decreasing the command. Scheduling an increase in feedback gain as a function of  $U_o$  rapidly leads to instability problems because the total loop gain is then proportional to:

$$U_o M_{\delta} = \frac{U_o \rho S U_o^2 c}{2 I_y} C_{m_{\delta}} \sim U_o^3$$

The high-gain pitch rate CAS can provide unusual landing characteristics. For example, one aircraft gave the impression it did not want to land. Generally, an aircraft will tend to balloon at the completion of flare and, as it enters the ground effect region, the nose will drop as airspeed decreases, and the aircraft will settle to a landing. A high-gain pitch rate CAS, however, prevents the pitch attitude from changing during the ballooning phase and subsequent bleedoff of airspeed. The pilot therefore has to keep "pushing" the nose down via stick commands to make the aircraft approach the ground as speed bleeds off. This appears to the pilot as a negative  $F_s/u$  characteristic and is particularly disconcerting. Pilots have overcome the tendency by trimming the aircraft nose down before starting the flare and then keeping positive

force on the stick to counter the mistrim. This technique will work where the trim is accomplished through the CAS series servo, but it is not possible when automatic or separate manual trim is used.

In the analysis, synthesis, and simulation of augmentation systems the effect of sensor and/or transducer saturation limiting is often neglected. This can result in surprises in flight if both command and rate feedback do not limit or saturate at the same value. Typical responses for either path reaching saturation first are shown in the following sketch.



It is assumed here that the series servo is not saturated and the aircraft is at a flight condition where the basic vehicle rotation capability is somewhat higher than that commanded via the electrical path. Command saturation results in the system behaving as a pure rate damper system and suddenly reduces maneuver performance at a time when the pilot is using large stick inputs presumably to obtain maximum maneuvering capability. Feedback saturation without simultaneous command saturation results in a sudden error command to increase the maneuver. This can produce pitch-up, stick force per g lightening, loss of pitch rate damping, etc. These occurrences are encountered in rapid maneuvering situations where they can be awkward at best and catastrophic at worst. As noted previously, the use of forward loop integration (rate servo or automatic trim) will further aggravate this situation because the input error will continue to drive the actuators in a direction to maintain system saturation.

c. Blended Normal Acceleration and Rate Gyro

Blended feedbacks are employed to provide nearly invariant handling and transient responses throughout the aircraft flight envelope. The specific responses are dependent upon the ratio of feedback gains. These are usually selected such that the system is essentially pitch rate command at low dynamic pressure and normal acceleration command at high dynamic pressure. The idiosyncracies previously discussed for each feedback still apply (e.g., accelerometer location), although they are modified somewhat. The pitch rate feedback opposes the undesirable characteristics of normal acceleration in non-zero pitch, roll, or flight path angle and backside operation. The normal acceleration feedback opposes the pitch-up effects of limiting in pitch rate feedback. However, limiting of normal acceleration feedbacks for any reason (past  $C_{L_{max}}$ , not yet airborne, etc.) can still result in stick force lightening and pitch-up tendencies because the total stick command then calls for more pitch rate.

Stall warning is often greatly decreased with this type of CAS because the combined feedbacks maintain "good" vehicle handling characteristics up to the point of stall. One method of countering this problem is to decrease the electrical command path gain as a function of angle of attack or dynamic pressure. This effectively increases the stick force per g as the stall is approached. Unfortunately, once the stall is achieved both feedbacks oppose the natural tendency for the aircraft nose to drop. Thus, the pilot must command a nose-down attitude by forcefully pushing on the stick. The decreased command path gain then requires a greater stick displacement and/or force for stall recovery which is quite objectionable to pilots. Yet another problem experienced with this means of introducing stall warning is a pitch-up command upon failure or disengagement of the warning system if CAS gains are returned to normal upon such failure.

d. Attitude and Attitude Rate

Autopilot control wheel steering modes generally are attitude-hold type with either pitch rate or attitude rate command. For control at large bank angles it is important to note the differences between body axis rates (rate gyro) and Euler axis rates (vertical gyro):

$$\text{Body axis rate } q = \dot{\theta} \cos \varphi + \dot{\psi} \cos \theta \sin \varphi$$

or

$$\text{Euler axis rate } \dot{\theta} = q \cos \varphi - r \sin \varphi$$

Thus, at large bank angles body axis and Euler axis rates are not equivalent and, more important, cannot simultaneously be zero. Thus, a mixture of body rate command and attitude hold functions which perform properly for wings-level condition can be quite different in turns. Also, if attitude (Euler) rate command is used, operation of the system must be restricted to within limited roll attitudes. This is due to the decrease in Euler angle pitch rate for a given elevator deflection as roll angle increases. Thus, the feedback decreases, the CAS effective forward loop gain increases, and stick force per g lightening is obtained.

Other problems associated with such mechanizations may be readily visualized with the aid of Fig. 48. This shows a blended rate command, attitude hold system which was actually developed and flown in a fighter aircraft. This mechanization has several shortcomings. First, precise control of pitch attitude is difficult when the stick force switch is set to a low threshold, because the system "locks onto" a  $\theta$  reference whenever stick force is less than the preset switching value. This is frequently referred to as "nibble." It is not possible to arrive at the desired  $\theta$  with  $q = 0$  and  $F_S > X$  lb. If pitch rate is appreciable, a "pitch back" is experienced and control becomes a trial and error process. The  $\theta$  error cannot be removed via the basic manual trim system because the autotrim function will oppose any non-electrical trim command. By increasing the force switching threshold, a stick force less than the switching value can be transmitted to the attitude synchronizer and thus serve as an attitude rate to obtain vernier control of the reference attitude. However, caution must be exercised in using such attitude rate commands because the attitude being commanded is an Euler angle, not an integral of a body axis rate, and this results in the previously mentioned stick force lightening with increasing bank angle.



e. System Complexity

This last problem is really associated with the summation of the foregoing and might well be entitled the "complexity trap." Several aircraft and CAS development and production programs have followed the route outlined below:

<u>FEATURE DESIRED</u>	<u>INCORPORATE</u>
<ul style="list-style-type: none"> <li>● Nearly invariant flying qualities throughout aircraft flight envelope</li> <li>● High disturbance suppression</li> </ul>	<ul style="list-style-type: none"> <li>● High authority CAS</li> <li>● <math>n_z</math> feedback for <math>F_s/g</math></li> <li>● <math>q</math> feedback for damping</li> <li>● Adaptive gain change (maintain <u>high</u> gain at low dynamic pressure)</li> <li>● Redundancy for fail safety</li> </ul>
<ul style="list-style-type: none"> <li>● Neutral speed stability (relieve pilot of necessity to trim)</li> </ul>	<ul style="list-style-type: none"> <li>● Washout on actuator feedback or series autotrim</li> </ul>

The result is a system with almost complete lack of feel, response, or stick position cues to the pilot concerning aircraft speed, dynamic pressure, angle of attack, elevator position, remaining maneuver potential, etc. The aircraft provides little or no stall warning and is stall prone. To rectify this, additional complexity is incorporated:

<u>FEATURE DESIRED</u>	<u>INCORPORATE</u>
<ul style="list-style-type: none"> <li>● Stall warning</li> </ul>	<ul style="list-style-type: none"> <li>● Pedal/stick shaker (ineffective because of high buffet levels)</li> <li>● <math>\alpha</math> feedback to <u>decrease</u> CAS command gain so as to <u>increase</u> <math>F_s/g</math></li> <li>● Redundancy to preclude failure which could cause pitch-up or loss of control</li> </ul>

The latter, while providing stall warning, was shown previously to actually increase the initial pilot effort to effect stall recovery, since he still must actively push the aircraft nose down and the decreased command then requires greater stick force on deflection to do so.

## 2. Lateral Axis

Lateral CAS mechanizations are not as varied as are longitudinal. Roll axis systems are invariably roll rate command and differ primarily in the number and type of non-equal parallel paths between pilot input and surface deflection (Figs. 49 and 50). The most prevalent feedback sensor is a rate gyro although derived rate and roll attitude have been used successfully in the autopilot Control Wheel Steering modes of transport-type aircraft

### a. Rate Gyro

The major problem regarding sensor location is minimization of structural mode effects. The gyro generally is rigidly mounted with its sensitive axis aligned with the aircraft centerline axis. Since most aircraft are flown to roll about an axis near the aircraft velocity vector (stability axis), the misalignment between sensor input axis and vehicle roll axis is directly related to vehicle angle of attack. The rate gyro output is:

$$p_g = p_s \cos \alpha - r_s \sin \alpha$$

Generally,  $r_s \sin \alpha \ll p_s \cos \alpha$  so that  $p_g \approx p_s \cos \alpha$  and angle of attack merely modulates the loop gain.

Since command augmentation systems are generally employed in high performance fighter and attack aircraft where rapid roll is essential to rapid maneuvering, there is a strong tendency to make the system high gain. Also, since the yaw axis SAS is generally employed to maintain stable dutch roll characteristics and correct airframe dynamic deficiencies (e.g.,  $\omega_\phi/\omega_d$ ), it is often possible for the roll rate CAS to be fixed gain even on aircraft with Mach 2+ capability. Therefore, most of the problems encountered have been associated with high gain, e.g.:

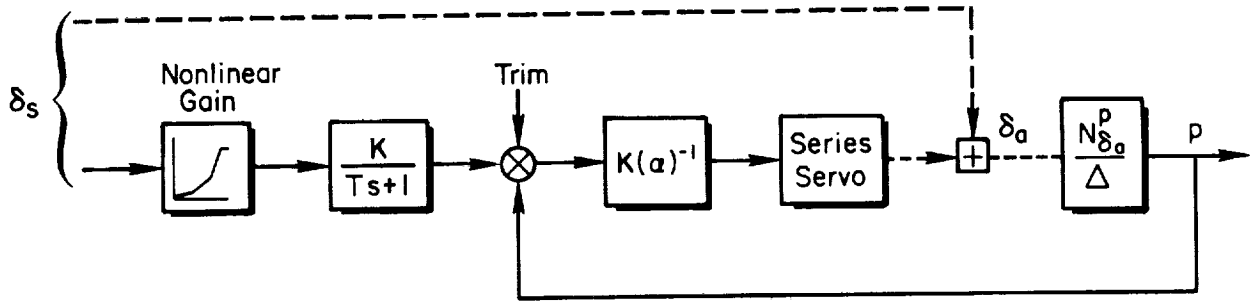


Figure 49. Simplified Roll Rate CAS — Fixed-Wing Aircraft

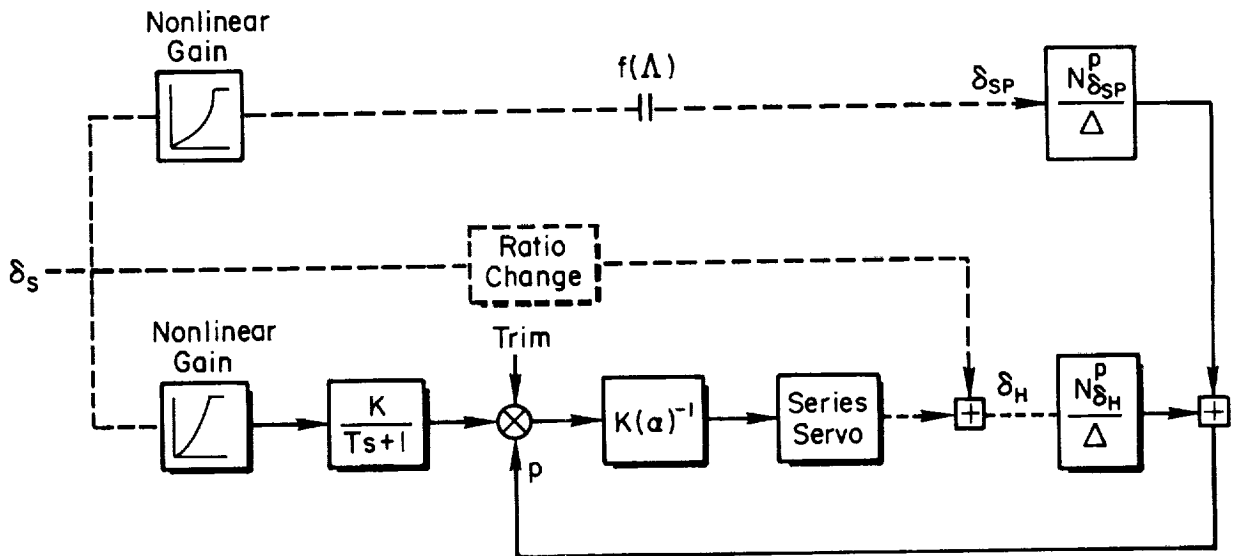


Figure 50. Simplified Roll Rate CAS — Swing-Wing Aircraft

- Gain shaping of command is crucial; oversensitivity to small stick deflection inputs leads to PIO in precise tracking tasks; undersensitivity at large stick deflection leads to restricted performance.
- Command or feedback limiting is more prevalent (than for longitudinal); at low  $q$  (landing) slow aircraft response leads to large stick inputs and command (or servo) limiting; at high  $q$  aircraft response can be so rapid that feedback limiting is encountered.
- System gain (command and feedback) must be drastically reduced on swept wing aircraft as stall is approached to prevent introduction of large pro-departure surface deflections.
- The system prevents control of bank angle via rudder (S-turns in landing, rudder roll in air combat maneuvering).
- Returning of control stick to neutral ( $p_c = 0$ ) following high roll rate maneuver results in abrupt stopping of aircraft roll but inertia of pilot's head and body gives head snap, inadvertent control input, etc.
- Rough ride qualities in turbulence and/or lateral PIO.
- Large lateral control deflections commanded by the system tend to emphasize "aileron yaw" characteristics.

Other problems which have been encountered include the use of automatic parallel trim to augment series servo authority. For steady roll, aileron displacement must be maintained and this requires a finite error between  $p_c$  and  $p$ . If the error signal operates the autotrim then the previously noted stick force lightening (if series trim), stick "wander" (if parallel trim), and excessive stick motion to stop the maneuver are encountered. Also, rudder maneuvering causes a roll rate error and hence the autotrim to operate.

Response models generally are first-order lags placed in the command path. More complicated "inverse models" have been placed in the feedback of some systems; however, these have not met with much success. The "inverse model" is introduced as lead in the feedback. This requires accompanying lags and results in the type of behavior discussed in Section III-B. In addition, since lateral trim must be introduced as an electrical command in CAS's, the

dynamics of the "inverse model" feedback result in imprecise, trial and error trimming.

The advent of swing wing aircraft introduced another set of potential problems. These aircraft generally have differential moving tail surfaces for roll control throughout the aircraft performance envelope. Therefore, the roll rate CAS operates through these surfaces. The wings typically contain spoilers which augment the rolling tail control power when the wings are forward of some nominal sweep angle (e.g., 45-50 deg). Therefore, three parallel but different roll command paths (as indicated in Fig. 50) can exist over a significant segment of the aircraft flight envelope and at a range of wing sweep angles. A number of countering factors immediately come into play.

First, the wing spoilers are highly effective but usually highly non-linear roll moment producers. They also produce favorable (proverse) yaw moment. Second, except at high speeds, the differential tail generally is not a highly effective roll moment producer and, further, the differential deflection allowable is generally restricted to avoid interference with longitudinal control requirements. Differential tail deflection does produce large adverse yaw moments. If the control path through the spoilers and the direct link (mechanical) to the differential tail provide greater roll rate than is commanded via the CAS, then it is possible for the spoilers and differential tail to provide opposing roll moments but with yaw moments summing. Such complicated interactions can result in widely varying  $\omega_p/\omega_d$  characteristics unless gains in all paths are carefully matched over the complete flight regime.

#### b. Roll Attitude and Attitude Rate

It was mentioned previously that derived rate, roll attitude command has been successfully employed in transport-type aircraft. On these aircraft the low frequency of the structural bending modes makes it difficult to separate (filter) rigid and flexible body modes in the rate gyro signal while the conservative bank angles and rates employed in typical maneuvering allows use of vertical gyro or platform outputs. Direct attitude command systems (attitude proportional to control wheel deflection) also have been successful because of the conservative maneuvering and the fact that the pilot can maintain control wheel displacement without appreciable arm fatigue. While frequently proposed

as special control modes for specific weapon delivery tasks in high performance, stick controlled aircraft, these mechanizations have not proven acceptable in flight trials because it is extremely tiring for the pilot to maintain the side force necessary to hold lateral stick displacement in turns (of even a few seconds). Also, because of stick deflection limits, it is necessary to limit the maximum bank angle that can be commanded. Again, command sensitivity conflicts arise between maximum bank angle that can be commanded and oversensitivity to small stick inputs. Finally, it is highly desirable that such mechanizations revert to roll rate response systems if, and when, an emergency should arise requiring bank angle greater than the bank command limit.

In the lateral control system, the difference between sensing axis, when using mixed sensors, can be more significant than for longitudinal control because large angle of attack can be involved. The general expression for the difference in angular rates between two axis systems is:

$$\dot{\phi} = p + r \tan \theta \cos \phi + q \tan \theta \sin \phi \doteq p + r \tan \theta$$

where  $\theta$  is the angle between the appropriate axis systems for the two sensors, e.g., body rate gyro input axis and vertical gyro reference axis, body rate gyro input and inertial platform roll axis, or vertical gyro reference axis and inertial platform roll axis. If the command involves one axis and the attitude hold function another, then "spring back" or "roll back" can be experienced where the system "locks" to the instantaneous roll attitude while still having appreciable roll rate.

Another manifestation of this problem is the so-called "roll coasting" that can occur if the command augmentation system utilizes body axis roll rate and the pilot is flying by reference to the Euler axis all-attitude indicator. In roll maneuvers, a roll rate is commanded by the pilot until he nears the planned roll attitude as shown on the all-attitude indicator. At this time the rate command is removed and the augmentor maintains body axis rate at zero. However, at large  $\theta$  and/or turn rate the Euler rate  $\dot{\phi}$  is not necessarily zero and so the display attitude continues to build.

### 3. Directional Axis

The conventional functions of this axis include dutch roll damping augmentation, increasing directional stiffness, combatting yaw disturbances (aileron yaw, engine out moments, gusts, etc.), and turn coordination. When these are accomplished satisfactorily with a relatively small authority system there is little need for the yaw axis to be a CAS. If the performance of these functions requires a large, or full, authority yaw SAS, then pedal command capability is required to allow the pilot necessary uncoordinated maneuvers (rudder S-turns in landing or rudder rolls in air combat maneuvering, sideslip in crosswind landing or formation flying). The significant problems, however, do not involve the command path but rather the feedback sensing which then also encompasses fundamental SAS problems and turn coordination. The latter is the topic of the next chapter and will not be discussed here. The principal sensing problems to be discussed here relate to lateral accelerometer placement and gain scheduling, and angle of attack influence on yaw rate gyro orientation and washout effectiveness.

#### a. Lateral Acceleration

Similar to the longitudinal case, the rigid-body motion sensed by an accelerometer fixed in the aircraft is:

$$a_{y_i} = a_{y_{cg}} + (pq + \dot{r})x_i - (p^2 + r^2)y_i + (qr - \dot{p})z_i$$

Analogous to the longitudinal case, it is desirable that the sensor be located on the aircraft x axis at the center of rotation for which the control surface deflection — in this case rudder — is a center of percussion. This is a distance  $x_a = -Y_{\delta_r}/N_{\delta_r}$ , ahead of the aircraft c.g. for aft rudders. Assuming for the moment all other motion quantities to be small, Ref. 1 shows:

$$a_{y_{cg}} + x_a \dot{r} = Y_v v + Y_{\delta_r} \delta_r + x_a \dot{r} \doteq Y_{\beta} \beta$$

Thus, the accelerometer located at  $x_a$  closely approximates a sideslip sensor and is effective in augmenting the directional stiffness derivative,  $N_{\beta}$ .

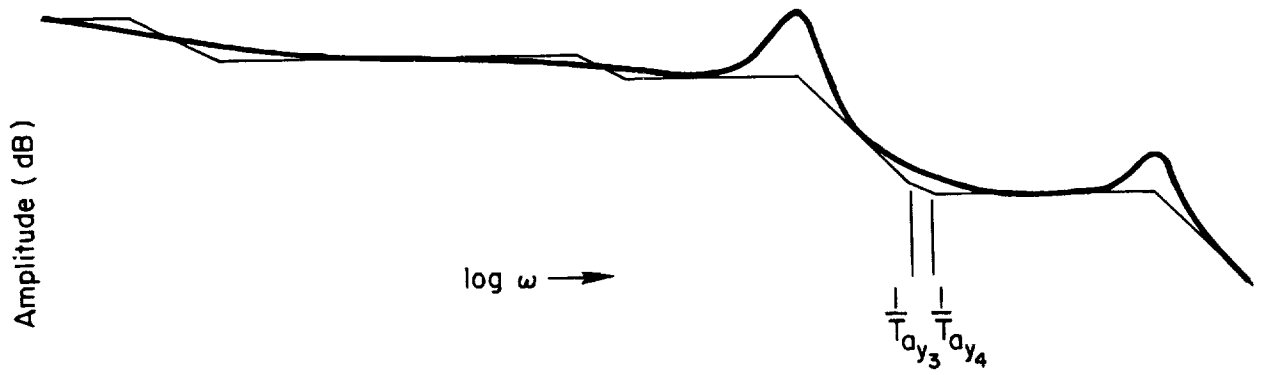
Because both center of rotation and vehicle c.g. can shift appreciably with changes in Mach number and loading, a serious practical problem is finding an accelerometer location which is adequate for all flight and loading conditions. Figure 51 indicates the effect of sensor location on the high-frequency zeros of the  $a_y/\delta_r$  numerator. For accelerometer locations at the center of rotation one zero goes to infinity and the other is at a very high frequency. Therefore, the high-frequency asymptote is maximally attenuated and the likelihood of higher-frequency mode instability (actuator or structure) is reduced. The possibility then exists for introducing lead-lag equalization in the vicinity of open-loop  $\omega_d$  so the closed-loop frequency can be increased without incurring instability.

For accelerometer locations forward or aft of the center of rotation, the high-frequency zeros move toward  $\omega_d$  and hence raise the high-frequency asymptote with the attendant danger of actuator or structural resonance or instability. The potential of lead equalization is also reduced because this further increases the high-frequency asymptote. It should be noted that for accelerometer aft of the center of rotation one high-frequency zero is non-minimum phase and introduces another example of the right half plane zero problem described in Section III. For accelerometer locations ahead of the center of rotation, the complex zeros,  $\omega_{ay}$ , are in the left half plane and provide some lead equalization for higher-frequency modes.

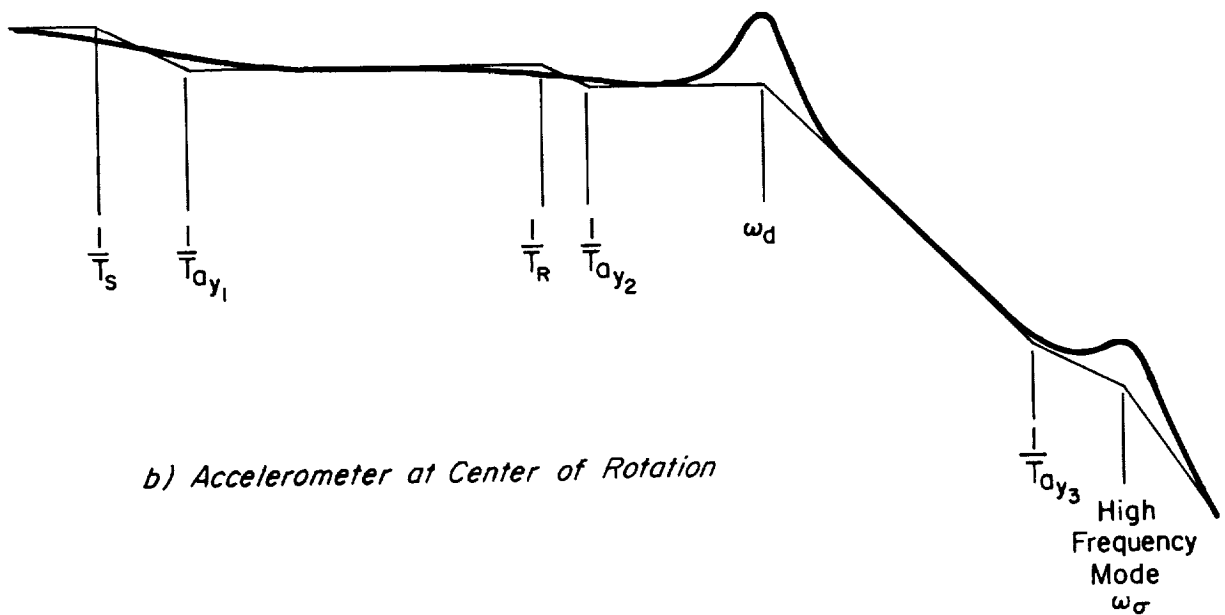
Another problem related to that of sensor location is the gain limitation posed by the high-frequency modes. In the absence of any gain adjustment mechanization, the loop gain will vary as:

$$Y_{\beta} N_{\delta_r}' \sim \frac{\rho a^2 U^4 C_{y\beta} C_{n_{\delta_r}}'}{m I_z}$$

Thus, gain compensation the inverse of this is required if this feedback is to be stable and effective throughout the aircraft flight envelope. However, more refined equalization adjustments (i.e., lead-lag) are desired. To develop these, attention is directed to the exact expressions for the various asymptotes called out in Fig. 52 for an accelerometer plus lead-lag equalization ( $1/\tau$  and  $a/\tau$ ) and servo ( $\omega_G$ ). The aircraft dutch roll in this example is



a) Accelerometer Aft of Center of Rotation



b) Accelerometer at Center of Rotation



c) Accelerometer Forward of Center of Rotation

Figure 51. Typical  $a_y \rightarrow \delta_r$  Bode Diagram

generalized in that it can be either stable and underdamped ( $\omega_d$ ) or overdamped ( $1/T_{d1}$ ,  $1/T_{d2}$ ) even to the realm of instability ( $1/T_{d2}$  negative). Similarly, the accelerometer location can be either ahead ( $\omega_y$ ) or behind ( $1/T_{y3}$ ,  $1/T_{y4}$ ) the center of rotation. The asymptotes of major interest are those for the flat regions preceding  $\sqrt{|\omega_d^2|}$  and  $\omega_\sigma$ , and the section of  $-20$  dB/decade slope lying between. The expressions for these three asymptotes are invariant with interchange of neighboring break frequencies, except for the high-frequency flat region which requires  $\omega_\sigma$  to be greater than all the other break frequencies (in particular,  $\omega_\sigma > \omega_y$ ). However, the frequency regions over which the three asymptotes apply are not invariant with such interchanges. These ranges are summarized below:

- 1) Low-frequency asymptote,  $A_y K_y \omega_y^2 / \omega_d^2$ .  
High-frequency end limited by either  $\sqrt{|\omega_d^2|}$  or  $1/\tau$ , whichever is smaller.
- 2) Mid-frequency asymptote,  $A_y K_y \omega_y^2 \tau / a$ .  
Low-frequency end limited by larger of  $\sqrt{|\omega_d^2|}$  or  $1/\tau$ .  
High-frequency end limited by smaller of  $a/\tau$  or  $\sqrt{|\omega_y^2|}$ .
- 3) High-frequency flat asymptote,  $A_y K_y a$ .  
For existence requires  $\omega_\sigma > \omega_y$ .  $\omega_\sigma$  is always high-frequency limit.  
Low-frequency end limited by larger of  $a/\tau$  or  $\sqrt{|\omega_y^2|}$ .

To insure adequate dutch roll damping and/or stiffening requires that the gain crossover be made in an amplitude ratio region which has a reasonable length of roughly  $-20$  dB/decade slope. Another way of saying the same thing is that a reasonable phase margin is required at crossover. Thus, the zero dB line should cross the asymptotic plot (at  $\omega_c$ ) somewhere along the mid-frequency asymptote. For this crossover region even to exist,  $\sqrt{|\omega_d^2|}$  and/or  $1/\tau$  must be less than  $a/\tau$  or  $\sqrt{|\omega_y^2|}$ ; and for good closed-loop servo mode ( $\omega_\sigma$ ) damping to be possible this "less than" must be modified to "much less than."

The existence of the region can be assured by controlling the values of  $1/\tau$  and  $a$ . Generally speaking,  $1/\tau$  less than  $\sqrt{|\omega_d^2|}$  is preferable since it results in higher potential phase margin. For a reasonably large value of  $a$ ,

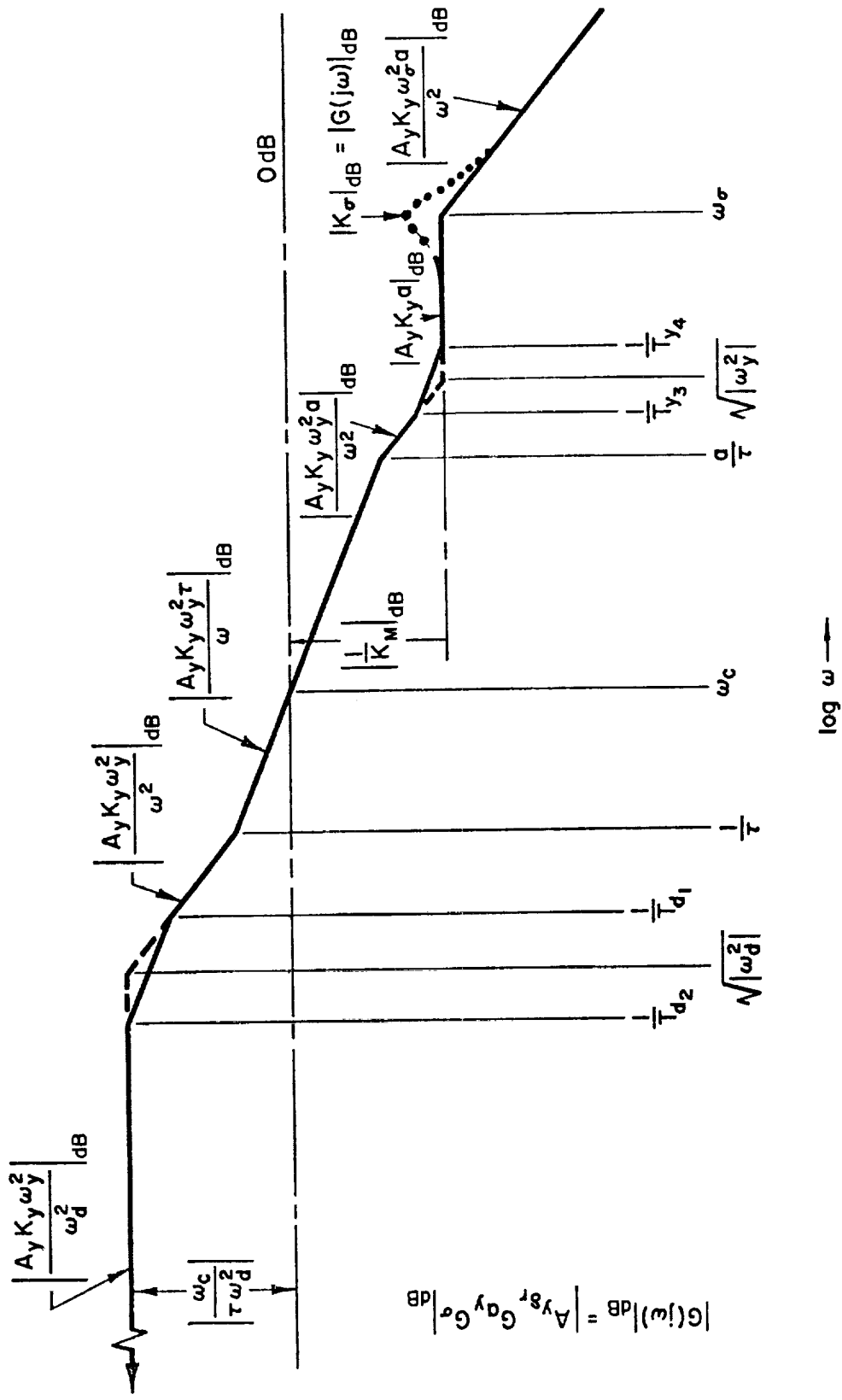


Figure 52. Mid- and High-Frequency Portion of Bode Plot for  $f(a_y) \rightarrow \delta_r$  Loop

however, it is sufficient to specify simply that  $1/\tau$  be near the dutch roll roots.

From damping considerations, a fairly large value of  $a$  is needed; otherwise the lead effect of  $1/\tau$  would be largely canceled. Also, for a nominal case,  $\sqrt{|\omega_d^2|} < 1/\tau$  and  $a/\tau < \sqrt{|\omega_y^2|}$ , a large value of  $a$  allows plenty of margin in which to meet the stiffening requirement. By virtue of this desire for relatively large values of  $a$ , it can be inferred that a reasonable location for  $a/\tau$  is somewhere in the vicinity of  $\omega_y$ .

It appears therefore that the "proper equalization" is quite closely tied to the basic transfer function factors,  $\omega_d$  and  $\omega_y$ , which vary with flight condition and c.g. location. In order then to maintain the virtues of this system for all flight conditions, the location of the lead-lag pair, as well as the gain, will very likely have to be automatically adjusted.

The above discussion shows that the significant vehicle parameters involved in the final adjustment of gain and equalization are  $A_y$ ,  $\omega_y^2$ , and  $\omega_d^2$ . Using the definition of  $x_a \equiv -U_0 Y_{\delta_r}^* / N_{\delta_r}$ , these quantities are given in terms of dimensionless derivatives by:

$$A_y = -Y_{\delta_r} \frac{\Delta l_x}{x_a} = \frac{qSb\Delta l_x}{I_z} C_{n\delta_r}$$

$$\omega_y^2 \doteq -\frac{x_a}{\Delta l_x} \left( N_\beta - \frac{Y_v N_{\delta_r}}{Y_{\delta_r}^*} \right) \doteq -\frac{qS}{m\Delta l_x} C_{y\beta}$$

$$\omega_d^2 \doteq N'_\beta = \frac{qSb}{I_z} C'_{n\beta} = \frac{qSb}{I_z} \frac{\left( C_{n\beta} + \frac{I_{xz}}{I_x} C_{l\beta} \right)}{\left( 1 - \frac{I_{xz}^2}{I_x I_z} \right)}$$

$$\Delta l_x = l_x - x_a = l_x + \frac{U_0 Y_{\delta_r}^*}{N_{\delta_r}} = l_x + \frac{k_z^2}{b} \frac{C_{y\delta_r}}{C_{n\delta_r}}$$

The aerodynamic parameters involved in these expressions represent two very different levels of predictability and "computational" difficulty. The values of  $C_{n_\beta}$  and  $C_{\ell_\beta}$  entering into  $\omega_d$  are very strong functions of angle of attack, in addition to Mach number, and are not easily measured or extrapolated to full-scale conditions. On the other hand,  $C_{y_\beta}$ ,  $C_{y_{\delta_r}}$ , and  $C_{n_{\delta_r}}$  are measured in body rather than stability axes for the specific calculation of  $\omega_y$ , and as such are essentially completely independent of  $\alpha$ . Also, for varying c.g. and inertia,  $\ell_x$  and  $k_z^2$  vary; and  $C_{y_{\delta_r}}/C_{n_{\delta_r}}$ , which depends on the effective rudder arm, is also a weak function of Mach number (due to shifts in the rudder center of pressure). Finally,  $C_{y_\beta}$  is a moderately strong function of Mach number, but is relatively easy to measure experimentally.

As an example of how complex the system compensation may be, assume that the dimensionless aerodynamic derivatives are constant as is  $\ell_x$  and  $k_z^2$  (e.g., over some restricted flight regime). The variation of the pertinent system parameters with dynamic pressure and equalization is then as follows:

<u>PARAMETER CONTROLLED</u>	<u>PARAMETER VARIED</u>
$A_y K_y a = \text{Constant}$	$K_y \propto \frac{1}{aq}$
$\omega_c = A_y K_y \omega_y^2 \tau$	$\omega_c \propto \frac{\tau}{a} q$
	$\frac{\omega_c}{\tau \omega_d^2} \propto \frac{1}{a}$
	$\tau \sqrt{ \omega_d^2 } \propto \tau \sqrt{q}$
	$\frac{\tau}{a} \sqrt{ \omega_y^2 } \propto \frac{\tau}{a} \sqrt{q}$

The effects of various possible equalization adjustments on these parameters are summarized in Table 2. The last column of the table indicates the basic mechanism of equalization adjustment. For example, the variation of  $K_y$  may be accomplished by a servo-driven potentiometer; therefore, additional suitably "shaped" potentiometers on the same servo shaft can be used to vary the equalization time constants as the desired function of  $K_y$ .

TABLE 2. EFFECTS OF IDEALIZED ADJUSTMENTS OF  $f(a_y) \rightarrow \delta_r$  CONTROLLER PARAMETERS

ASSUMED EQUALIZATION ADJUSTMENTS	VARIATIONS, WITH DYNAMIC PRESSURE, OF					EQUALIZATION VARIATION WITH $K_y$
	Controller Gain, $K_y$	Crossover Frequency, $\omega_c$	Low Frequency Gain, $\omega_c/\tau a_y^2$	Relative Lead Location, $\omega_d \tau$	Relative Lag Location, $\omega_y \tau/a$	
1) $a, \tau$ fixed	$\frac{1}{q}$	$q$	Constant	$\sqrt{q}$	$\sqrt{q}$	None
2) $a$ fixed $\frac{1}{\tau} \propto \sqrt{q}$	$\frac{1}{q}$	$\sqrt{q}$	Constant	Constant	Constant	$\tau, \frac{\tau}{a} \propto \sqrt{K_y}$
3) $a, \frac{1}{\tau} \propto \sqrt{q}$	$\frac{1}{q^{3/2}}$	Constant	$\frac{1}{\sqrt{q}}$	Constant	$\frac{1}{\sqrt{q}}$	$\tau \propto K_y^{1/3}$ $\frac{\tau}{a} \propto K_y^{2/3}$
4) $\tau$ fixed $a$ (or $\frac{a}{\tau}$ ) $\propto \sqrt{q}$	$\frac{1}{q^{3/2}}$	$\sqrt{q}$	$\frac{1}{\sqrt{q}}$	$\sqrt{q}$	Constant	$\tau$ fixed $\frac{\tau}{a} \propto K_y^{1/3}$
5) $\frac{1}{\tau} \propto \sqrt{q}$ $\frac{a}{\tau}$ fixed ( $a \propto \frac{1}{\sqrt{q}}$ )	$\frac{1}{\sqrt{q}}$	$q$	$\sqrt{q}$	Constant	$\sqrt{q}$	$\tau \propto K_y$ $\frac{\tau}{a}$ fixed
6) $a$ fixed, $\frac{1}{\tau} \propto q$	$\frac{1}{q}$	Constant	Constant	$\frac{1}{\sqrt{q}}$	$\frac{1}{\sqrt{q}}$	$\tau, \frac{\tau}{a} \propto K_y$

Of the possibilities listed, Cases 1 and 5 can be eliminated immediately because a variation of  $\omega_c$  proportional to  $q$  is too drastic. Case 2 has the most promise of working over the entire flight regime because of its lead and lag location characteristics, although a variation of  $\omega_c$  with  $\sqrt{q}$  is not desirable. Case 3 has the desirable characteristic of  $\omega_c \doteq \text{constant}$ , but also has the undesirable features that the low-frequency gain decreases with an increase in  $\sqrt{q}$  and the dynamic range of  $K_y$  variations is very large. Also, the lag,  $a/\tau$ , is likely to depart too drastically from  $\omega_y$ . Case 4 does not suffer this last defect, but  $K_y$  variations again are large and crossover frequency is proportional to  $\sqrt{q}$ . Case 6 has desirable characteristics on all counts, except lead and lag location variations which may be too drastic.

The net conclusion to be drawn from Table 2 is that no one of the "simple" equalization adjustments is likely to suffice over an entire flight envelope. Also, the real variations in vehicle dynamic characteristics not taken into account will substantially modify the "idealized" conclusions stated above.

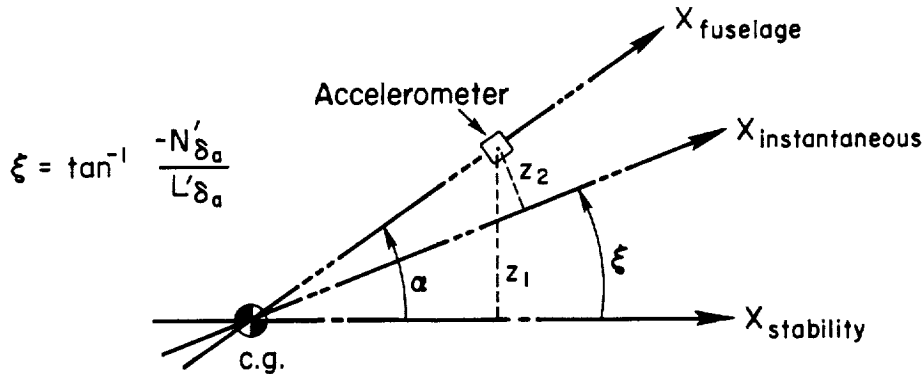
As a result of the foregoing, it is not uncommon for the lateral acceleration loop gain to be fixed value and selected so that this feedback does not cause adverse effect throughout the aircraft flight envelope. This generally results in an almost totally ineffective feedback in the low speed, low dynamic pressure flight regimes.

Returning now to the more general aspects of motions sensed by a lateral accelerometer, the actual sensor location is usually a compromise. Generally it can be located such that  $y_i$  is small and the sensed acceleration reduces to

$$a_{y_i} \doteq a_{y_{cg}} + (pq + \dot{r})x_i - \dot{p}z_i$$

For highly maneuvering aircraft all of these terms can be significant:  $pqx_i$  in rolling pullouts,  $\dot{r}x_i$  for rudder deflection, and  $-\dot{p}z_i$  for aileron deflection. In the latter case it should be noted that the  $z_i$  for aileron input can be different for the initial and steady rolling motions. This is because the initial roll axis is defined by the moment producing terms

$L'_{\delta_a} \delta_a$  and  $N'_{\delta_a} \delta_a$ . At high angle of attack, assuming adverse aileron yaw and stability axis derivatives, the relationship between the axis systems of interest is as follows.



Thus the instantaneous roll acceleration lever arm is defined by the angle  $(\alpha - \xi)$ . If this is large (i.e.,  $N'_{\delta_a} \neq 0$  or positive) then the initial lateral acceleration sensed (by accelerometer or pilot) can be very large in full aileron rolls. For example, initial lateral accelerations exceeding one g have been obtained on some high performance fighters with sudden application of full aileron deflection. The sign of the sensed feedback to rudder is such that, for the example sketched above, the resulting initial rudder deflection would uncoordinate the maneuver.

Another source of large lateral acceleration is sudden loss of engine thrust in aircraft with engines mounted a considerable distance outboard from the aircraft centerline. Again magnitudes greater than one g have been experienced. The possibility of such large accelerations should be taken into account and precautions taken to prevent amplitude or rate saturation anywhere within the system causing phase lags which might lead to system instability.

#### b. Rate Gyro

The yaw rate gyro is the most common of the directional axis sensors. The fundamental problem of this sensor is orientation with respect to aircraft stability axes. The yaw rate sensed by the rate gyro ( $r_g$ ) can differ considerably from the stability axis perturbation yaw rate ( $r_s$ ) of the aircraft, i.e.,

$$r_g = r_s \cos(\alpha + \theta_T) + p_s \sin(\alpha + \theta_T)$$

where

$\alpha$  = angle between aircraft stability axis and aircraft reference axis

$\theta_T$  = rate gyro tilt from aircraft reference axis

$(\alpha + \theta_T)$  = sensor angle of attack =  $\epsilon$

At low sensor angle of attack  $r_g \doteq r_s$ ; however, at large positive  $\alpha$  and/or  $\theta_T$  a significant roll rate component is obtained. It is commonly recognized that this roll rate component destabilizes the dutch roll. The reason for destabilization is that the angular velocity numerator quadratic's undamped natural frequency,  $\omega_{rg}$ , increases as the sensor axis is inclined above the stability axis (the usual case). Thus  $\omega_{rg}/\omega_d$  approaches unity with the consequent reduction in damping attainable as explained in Section II-B. The shift in sensor zeros with gyro tilt may be observed from the survey plot of Fig. 53 which derives from

$$N_{\delta_r}^{rg} = N_{\delta_r}^{rs} \cos(\alpha + \theta_T) + N_{\delta_r}^{ps} \sin(\alpha + \theta_T)$$

$$\text{zeros of } N_{\delta_r}^{rg} = \text{zeros of } 1 + (N^{ps}/N^{rs}) \tan(\alpha + \theta_T)$$

For a typical fighter aircraft at 5 g, 0.8 m, and 20,000 ft the trim  $\alpha$  is 16 deg and

$$\frac{N^{ps}}{N^{rs}} = \frac{-0.0924 (0) [0.97, 37]}{-0.43 (1.39)[-0.285, 0.9]}$$

At this condition  $\omega_d = 3.64$  rad/sec, therefore, from Fig. 53:

$\theta_T$	$\omega_{rg}$	$\zeta_{rg}$	$\omega_d$	$\zeta_d$	$\omega_{rg}/\omega_d$	$1/Tr_g$
-16 deg (stability axis)	0.9	-0.285	3.64	0.2	0.247	1.39
-6 deg	2.25	0.2	3.64	0.2	0.619	0.23
-0 deg (FRL axis)	2.70	0.2	3.64	0.2	0.742	0.16
+4 deg	3.25	0.2	3.64	0.2	0.893	0.11

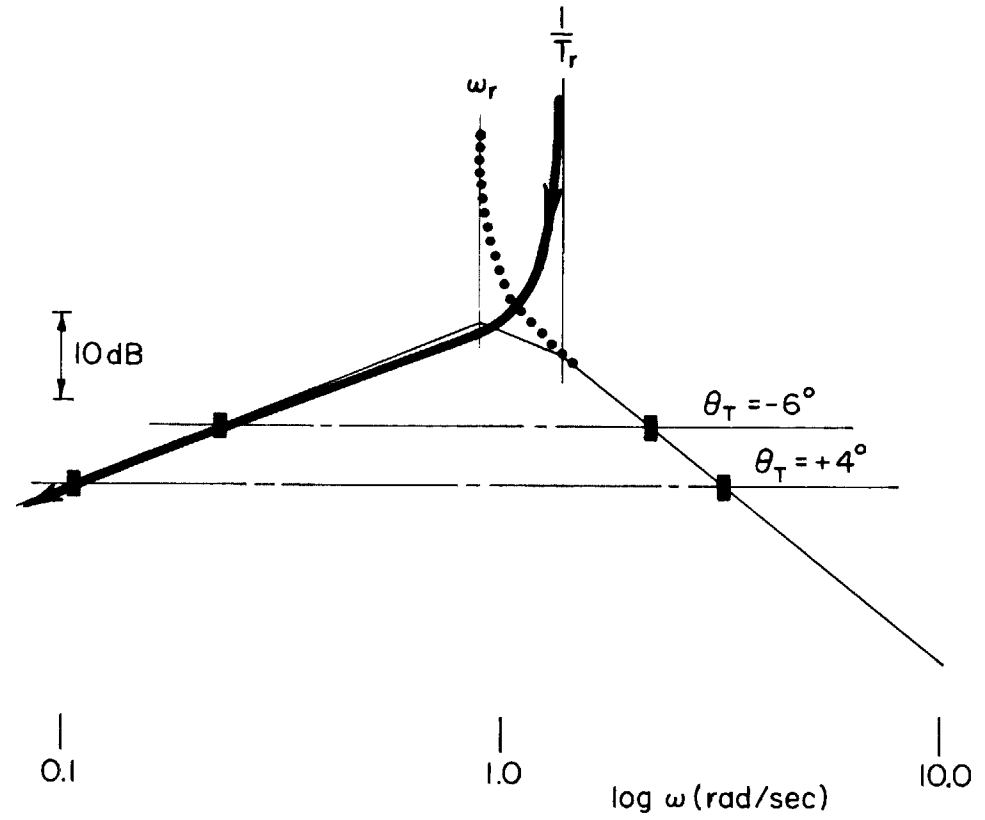
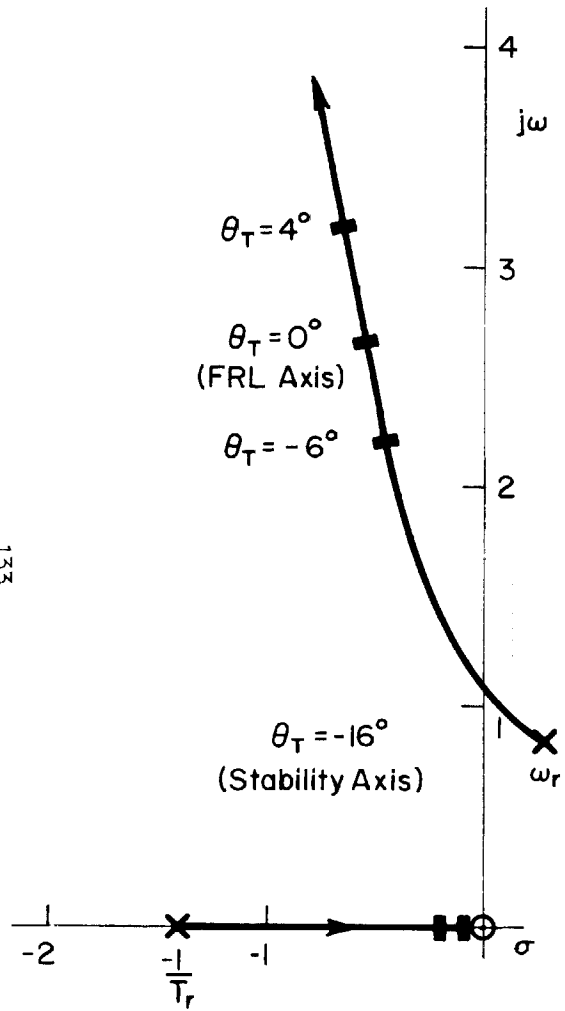


Figure 53. Roots of  $(N^D s / N^R s) \tan (16 + \theta_T) = -1$

It is readily apparent that gyro inclination with respect to stability axis has a strong effect on  $\omega_{rg}/\omega_d$  and hence the effectiveness of this feedback in damping dutch roll.

Another aspect, not so well recognized, is the dramatic influence this shift in  $\omega_{rg}$  has on the effectiveness of the yaw rate feedback washout. The washout time constant is selected to attenuate sensing and feedback of frequencies below the dutch roll and, in particular, the yaw rate of steady turns. Typically this is 0.5 to 1 rad/sec. However, for the  $\alpha = 16$  deg example case the dramatic shift in  $\omega_{rg}$  results in the closed-loop survey plot of Fig. 54. The movement of  $\omega_{rg}$  toward  $\omega_d$  causes the low-frequency amplitude to be increased and hence to counter the washout. The nominal gain line passes below the amplitude ratio plot and indicates the yaw damper will actively oppose aircraft motion in this bandwidth (i.e., any yaw). Such opposition at high  $\alpha$  is recognized by many pilots who turn yaw dampers off prior to engaging in air combat maneuvering.

The above shift in numerator zeros can be counteracted in several ways. One is to tilt the yaw rate gyro so the sensitive axis is nearly coincident with the vehicle stability axis. For a fixed gyro mounting, this involves compromising system performance at both high and low  $\alpha$ . Tilting the gyro down tends to move  $\omega_{rg}$  farther into the right half plane and can rapidly lead to system instability. However, on one aircraft two rate gyros were employed. One was aligned with the fuselage reference line (approximately) for up and away flight, and the other was aligned with stability axis for nominal approach and landing conditions. Sensing was switched from one gyro to another as a function of flap position.

A third way to combat the  $\omega_r$  shift is the previously discussed (Section II-B) augmentation of  $L_p$  [since  $\omega_r^2 \doteq (g/U_0)(L_B/L_p)$ ] with a roll rate-to-aileron feedback capability of the yaw rate damper. However, this method is limited to those flight conditions and configurations where use of aileron is both effective and safe. On aircraft which require fading out the roll SAS or CAS at high  $\alpha$ , this method would be totally ineffective. Yet another technique is to crossfeed roll rate to rudder to cancel the component sensed by the yaw rate gyro. However, to be truly effective this

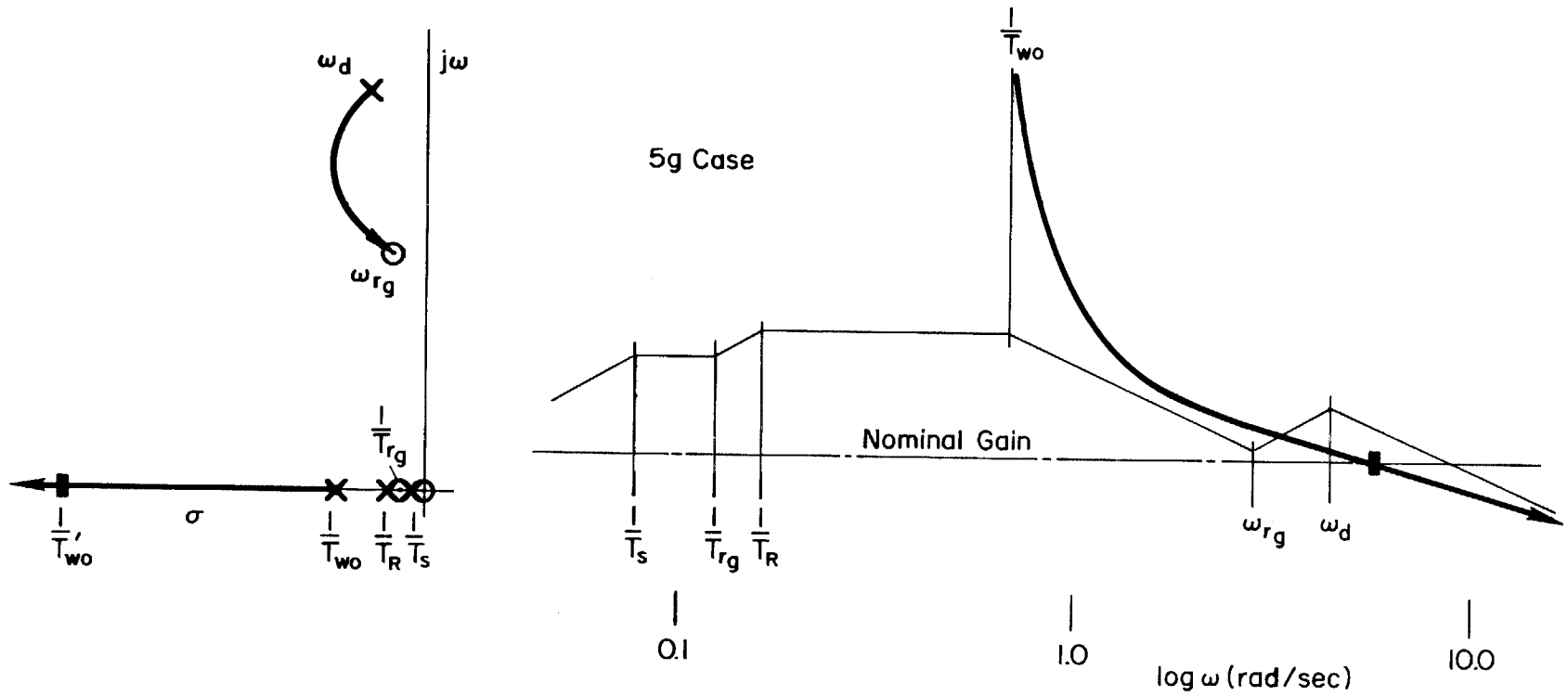


Figure 54. Yaw Rate Damper Effectiveness at  $\alpha = 16$  deg

also requires multiplying the roll rate signal by  $\alpha$  so that  $p\alpha \doteq p \sin \alpha$ . Despite problems associated with sensing  $\alpha$ , this corrective term recently has proven very effective and safe at  $\alpha$ 's approaching stall.

c. **Blended Lateral Acceleration and Yaw Rate**

It is common for lateral acceleration and yaw-rate feedback to be employed together, especially in supersonic aircraft. Yaw rate is employed primarily to augment dutch roll damping and lateral acceleration to augment directional stability at supersonic conditions. As indicated previously the gain of the lateral acceleration loop varies as  $q_0^2$ , therefore it often is optimized and fixed for the high speed condition. The effectiveness rapidly decreases at lower dynamic pressures and provides little benefit at low speed. On the other hand, maximum yaw-rate feedback gain is generally required at low dynamic pressure flight conditions and, since loop gain again is directly proportional to dynamic pressure, system gain can become too high at supersonic speeds. Therefore it has been common to vary this gain as an inverse function of indicated airspeed, true airspeed, Mach or some system parameter (i.e.,  $M_0$ ) which is a function of dynamic pressure. More recently, to reduce complexity and improve reliability, there has been a tendency to employ a fixed, compromise gain or, at most, a step change in gain for landing and take-off.

## SECTION VI

### TURN COORDINATION

In general, coordinated flight implies minimum roll-yaw coupling which can be quantified in many ways, some of which are:

- Zero sideslip angle ( $\beta = 0$ )
- Zero lateral acceleration at the c.g.
- Turn rate consistent with bank angle and speed  
( $r = g\phi/U_0$ )
- Zero lateral acceleration at the cockpit (ball in the middle)

The first three are equivalent when the side force due to aileron,  $Y_{\delta_a}$ , and due to turn rate,  $Y_r$ , are very small, which is usually the case. The last is complicated by pilot location effects which are mainly associated with ride qualities. Based on these considerations sideslip angle is the appropriate indicator of turn coordination. If a good sideslip sensor (or sensor complex) were available, this feedback would certainly be preferred as the most straightforward and simple. Unfortunately, such is not the case. Sideslip sensing is plagued by many problems not the least of which are local flow anomalies and sensor vulnerability. In fact the most significant problem in turn coordination is that of obtaining an approximation to direct sideslip sensing which is practical yet adequate throughout the aircraft flight and maneuver envelope.

Three means of approximating sideslip are discussed here: directional stiffening ( $a_y$  augmentation of  $N_\beta$ ), control crossfeeds (lateral stick or aileron to rudder), and roll feedbacks ( $p, \phi$  to rudder). For the most part, the theoretical aspects of directional stiffening have been discussed in the preceding section and will be touched lightly here.

#### A. DIRECTIONAL STIFFENING

As noted previously, if an accelerometer is located at the center of percussion for rudder inputs, the lateral acceleration sensed, exclusive of other nonlinear kinematic effects, is:

$$a_y = a_{y_{CG}} + x_a \dot{r} \doteq Y_{\beta} \beta$$

Thus a properly located lateral accelerometer is a relatively simple approximation to sideslip from a sensing standpoint. If the aircraft dynamic pressure is relatively small, it can be quite effective as a turn coordination means. It does suffer, however, from complex gain and shaping compensation problems for applications involving extended flight regimes, again as previously discussed.

The integral of lateral acceleration has been used in some aircraft. This introduces phase lag which compounds the previously discussed gain and shaping problems. In addition, the integration feature must be cut-out when the aircraft is on the ground to prevent pre-takeoff ground maneuvering or aircraft tilt (uneven landing gear struts, runway tilt, etc.) from causing full rudder deflection at takeoff. Also as mentioned previously, this form of auto-trim makes intentional sideslip maneuvers (crosswind landing, formation flight, etc.) more difficult.

#### B. CONTROL CROSSFEEDS TO RUDDER

The principal source of sideslip in initiating or terminating lateral maneuvers is aileron yaw,  $N'_{\delta_a}$ . Therefore another means of accomplishing turn coordination is to remove this source by supplementing the directional axis augmentation systems with an aileron to rudder crossfeed. This is sometimes attempted via a fixed or variable gain interconnection. However, for modern aircraft, the sideslip excitation can change significantly with airframe dynamic modes and flight conditions. The ideal aileron-rudder crossfeed to maintain zero aileron and roll-rate induced sideslip was developed in Section II where it was shown to require dynamic shaping to accommodate contributions of the various airframe dynamic modes and augmentation systems. Generally this shaping can be approximated by a first order lag-lead or, at most, two first order lags and leads with fixed time constants. However, the gain requires adjustment with flight condition. Equation 13 indicates the gain to be proportional to

$$KCF \sim \frac{N'_{\delta_a} T_r}{N'_{\delta_r}} \doteq \frac{N'_{\delta_a}}{N'_{\delta_r} L'_p}$$

The influence of flight condition is more readily seen by expressing the gain in coefficient form and with the ratio of yaw coefficients in aircraft body rather than stability axis, viz.,

$$C'_{n\delta_{as}} = C_{n\delta_{aB}} \cos \alpha - C_{l\delta_{aB}} \sin \alpha \doteq -C_{l\delta_{aB}} \sin \alpha \quad \text{at high } \alpha$$

$$C'_{n\delta_{rs}} = C_{n\delta_{rB}} \cos \alpha - C_{l\delta_{rB}} \sin \alpha \doteq C_{n\delta_{rB}} \cos \alpha$$

$$L'_p = \frac{\rho S U_b^2}{4 I_x} C'_{l_p}$$

Thus

$$K_{CF} \sim \left( \frac{1}{U_0} \right) \frac{C_{l\delta_{aB}}}{C_{n\delta_{rB}}} \tan \alpha$$

The ideal crossfeed gain is thus proportional to angle of attack and inversely proportional to aircraft velocity. The sign of crossfeed might also vary with aircraft configurations (i.e., swing wing aircraft).

It should also be noted that the foregoing applies only to aileron induced maneuvers for which turn coordination is desired. There are situations where non-zero sideslip maneuvers are necessary (e.g., crosswind landings). For such cases, the addition of a washout on the crossfeed will allow unopposed steady sideslip maneuvers.

As indicated in Section II, aileron to rudder crossfeeds have been employed on many aircraft. None, however, have been formulated on the basis of the foregoing total system approach and therefore have met with varying degrees of success. Table 3 summarizes a few of the configurations used.

TABLE 3. SUMMARY OF CONFIGURATIONS UTILIZED

ARI FORM	AIRCRAFT/SYSTEM	MECHANIZATION
Fixed gain	F-4	Electro-mechanical, stick rudder
	F-14	Mechanical, stick-rudder
Variable gain	B-58	Electro-mechanical, aileron-rudder $f(m, h)$
	A-7	Electro-mechanical, aileron-rudder $f(\delta_e \text{ trim})$
Fixed gain and compensation	F-4/TWead I	Electronic $r_c = \frac{K(s+5)}{(s+.3)(s+10)} \delta_a$
Fixed compensation variable gain	F-4/TWead II	Electronic $r_c = \frac{K(\alpha)(s+5)^2}{(s+.3)(s+10)}$
Variable gain and compensation	F-89	Electronic $\delta_r = \frac{K(q^{-1})}{(s+1)} \delta_a$
	F-4/SFCS	Low speed $r_c = \frac{K_1 s}{(s+.2)} p_c$
		Mid speed $r_c = \frac{K_2 s}{(s+.2)(s+.5)} p_c$
High speed $r_c = 0$		

Fixed gain crossfeeds generally are employed to overcome a specific airframe deficiency and/or improve turn coordination in a limited portion of the flight envelope — usually landing. These mechanizations are then engaged upon lowering flaps or gear. Mechanical systems have often proven quite troublesome because of the considerable uncertainty in prediction of key stability derivatives and parameters before actual flight and the inherent problems in changing a mechanical system after the aircraft starts flying.

The variable gain crossfeeds for the B-58 and A-7 are designed to reduce, but not eliminate, aileron yaw. The B-58 nominally had strong proverse aileron yaw. An adverse yaw mechanical  $\delta_a - \delta_r$  interconnect was used to cancel the major portion of this yaw. A relatively small authority electrical crossfeed with gain and sign a function of Mach and altitude was then employed as a vernier adjustment to the mechanical interconnect. The adverse yaw ARI interconnect, however, aggravated control in engine out situations where it is necessary to hold aileron opposite to the engine out. Therefore it was necessary to also include a high gain feedback of lateral acceleration to rudder to overcome the rapid yaw that could develop under engine out conditions. Unfortunately, the peculiarities of this aircraft required the use of a rather large rudder authority coordination system.

The A-7 aircraft exhibits adverse aileron yaw at high angle of attack and proverse at low angle of attack. Therefore the ARI crossfeed is scheduled with trim elevator position to reduce the variation in aileron yaw rather than actually provide turn coordination.

The TWeaD I ARI mechanization is very close to the form derived in Subsection A preceding although the specific compensation time constants were derived through pilot selection in flight test. The low frequency lag is slightly lower than the yaw damper washout [ $(1/T_{wo}) = 0.5$ ] while the high frequency lag is probably somewhat higher than the augmented roll subsidence ( $1/T_R^*$ ). This fixed gain system provided "good" turn coordination over the speed ranges from low subsonic to low supersonic.

The TWeaD II ARI mechanization again was selected on the basis of flight trials but with emphasis on optimizing turn coordination in high angle of attack maneuvers, air-to-air, and air-to-ground tracking tasks. This flight

test covered a slightly larger portion of the aircraft flight envelope than did the TWeaD I development program, and again the maneuver coordination was praised by the pilots as providing excellent flying qualities. It should be noted that this ARI together with the yaw SAS mechanization afforded a relatively close approximation to the  $\dot{\beta}$  equation, viz.,

In stability axis:

$$\dot{\beta} = r_s + Y_v \beta + Y_{\delta_r}^* \delta_r + Y_{\delta_a}^* \delta_a + (g/U_0) \varphi \cos \theta_0$$

The TWeaD II mechanization:

$$\delta_r = \frac{K_1 T_1 s}{(T_1 s + 1)} (\alpha p_g - r_g) + K_2 a_y^i + \frac{K_3 (\alpha) (s + 1/T_2)^2}{(s + 1/T_3)(s + 1/T_4)} \delta_a$$

Noting that

$$(\alpha p_g - r_g) \doteq -r_s \quad \text{and} \quad \frac{a_y^i}{U_0} \doteq Y_v \beta + Y_{\delta_r}^* \delta_r$$

In steady turns the lateral accelerometer also senses the gravity vector component due to  $\varphi$  and therefore also accounts for the last term in the  $\dot{\beta}$  equation. Thus the shaped ARI reduces or eliminates sideslip excitation on turn entry or exit and the SAS provides the vernier adjustment throughout the maneuver.

The SFCS employs crossfeed proportional to roll rate command rather than aileron deflection. The system also has a high gain roll rate CAS. This mechanization tends to coordinate only commanded maneuver entry and specifically does not coordinate maneuver recovery. In the latter, the maneuver command is zero as soon as the stick is returned to neutral. The high gain system then provides large aileron deflection to stop roll rate but there is no accompanying crossfeed to rudder. Hence a large aileron yaw results upon termination of the maneuver. This is particularly disconcerting to the pilot, because it is unexpected (after the initial maneuver is coordinated) and disturbs the tracking precision at termination of the commanded maneuver.

The F-15 also has an ARI. The specific mechanization is not known but some characteristics have been revealed in Ref. 11. It apparently has two ARI associated problem areas: one is high  $\alpha$  ride qualities, the other is crosswind landing. The ARI operates through a mechanical path and through the CAS and is designed to provide zero sideslip combat maneuvering in order to decrease the possibility of departure. The large authority ARI gain is scheduled as a function of  $\alpha$  and the lateral stick to aileron gain is an inverse function of  $\alpha$ . Thus as  $\alpha$  increases, lateral stick deflection produces less aileron and greater rudder deflection. In achieving essentially zero sideslip rolling maneuvers, the aircraft rolls about the velocity vector. At high  $\alpha$  the pilot is above the velocity vector and the high roll acceleration of the aircraft results in a large  $l_{z\dot{p}}$  acceleration on the pilot during full stick deflection rolls. Thus a situation exists where zero-sideslip turn coordination is not the best from a ride quality standpoint. The second problem, crosswind landing, required modification of both the mechanical and CAS systems to change control system configuration with lowering of the landing gear and with wheel spin-up. Full stick to aileron gain is returned upon lowering the landing gear and both the mechanical and CAS ARI paths eliminated upon wheel spin-up.

### C. ROLL CROSSFEED TO RUDDER

Turn coordination generally is mechanized along the lines of the previously discussed blend of washed-out yaw rate, lateral acceleration, and/or aileron crossfeed to rudder. The yaw rate and lateral acceleration signals usually require some high frequency filtering to attenuate structural modes. The latter are usually sufficiently separated from vehicle rigid body modes of interest that the structural filters do not interfere with performance of the yaw damper. Very large, highly flexible vehicles pose several problems however. First, yaw rate wash out requirements for maneuvering may conflict with dutch roll damper performance due to very low frequency rigid body dynamics. Second, the bending modes may be sufficiently low frequency and large amplitude to preclude use of lateral acceleration feedback. Third, very low frequency surface actuator dynamics can preclude high gain, closed-loop minimization of lateral-acceleration or sideslip.

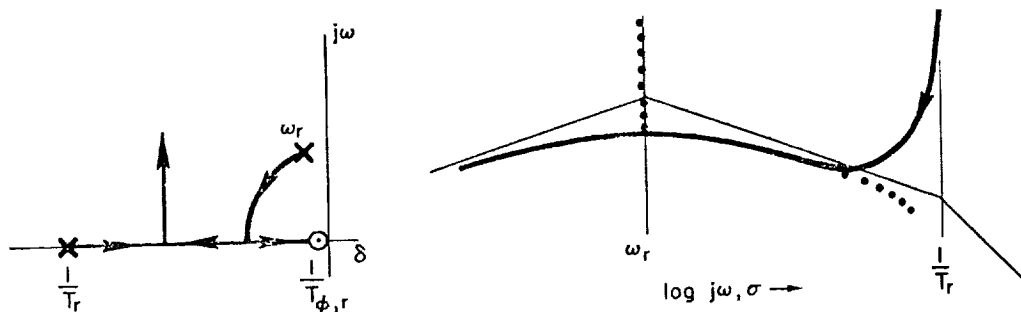
In such situations bank angle-to-rudder has been used as the basic turn coordination loop. This feedback is appropriately gain compensated with dynamic pressure and introduced to the damper loop as the zero sideslip yaw rate command  $r_c \doteq (g/U) \phi$ . Roll rate is also fed to rudder to provide lead. A system survey sketch for these feedbacks is presented in Fig. 55. Note that the spiral is greatly destabilized since the system commands rudder to convert any bank angle that develops (e.g., due to gust) into a coordinated turn. Also note these feedbacks increase dutch roll damping. The resulting yaw axis turn coordination and damper block diagram is shown in Fig. 56.

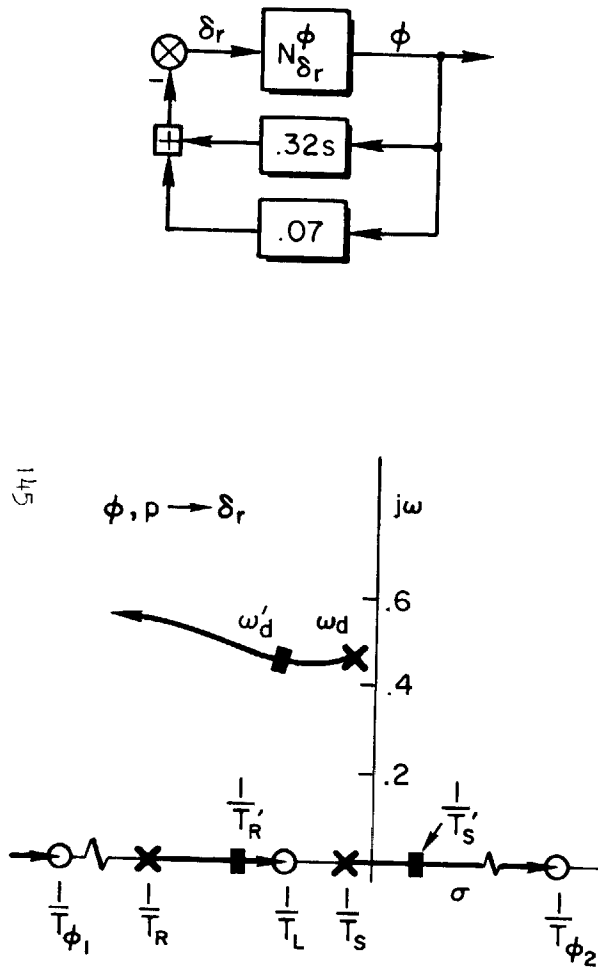
In order to restabilize the spiral mode, it is necessary to close the bank angle-to-aileron loop at all times. The block diagram is shown in Fig. 57 and a system survey plot of the resulting lateral-directional dynamics is shown in Fig. 58. It may be noted from the survey plot that a minimum gain is required to move the spiral back into the left half plane and that any further gain increase rapidly couples the spiral and roll subsidence into a quadratic "lateral phugoid" which can be objectionable from a handling quality standpoint.

Finally, it should be noted that closure of the roll to aileron loop modifies the yaw rate-to-rudder numerator quadratic ( $\omega_r$ ) in a beneficial manner similar to that of  $p - \delta_a$ . That is, the coupled numerator is

$$N_{\delta_r}^r + K_{\phi} N_{\delta_a}^{\phi} \frac{r}{\delta_r}$$

and the effective zeros follow the locus indicated in the following typical survey sketch. As  $\omega_r$  moves toward the real axis, separation of  $\omega_r/\omega_d$  increases and the effectiveness of yaw rate feedback to rudder in damping dutch roll is improved.





$$Y_{OL} = K_p \left( s + \frac{K\phi}{K_p} \right) \frac{A\phi (s+1/T_{\phi_1})(s+1/T_{\phi_2})}{(s+1/T_S)(s+1/T_R) [s^2 + 2\zeta_d \omega_d s + \omega_d^2]}$$

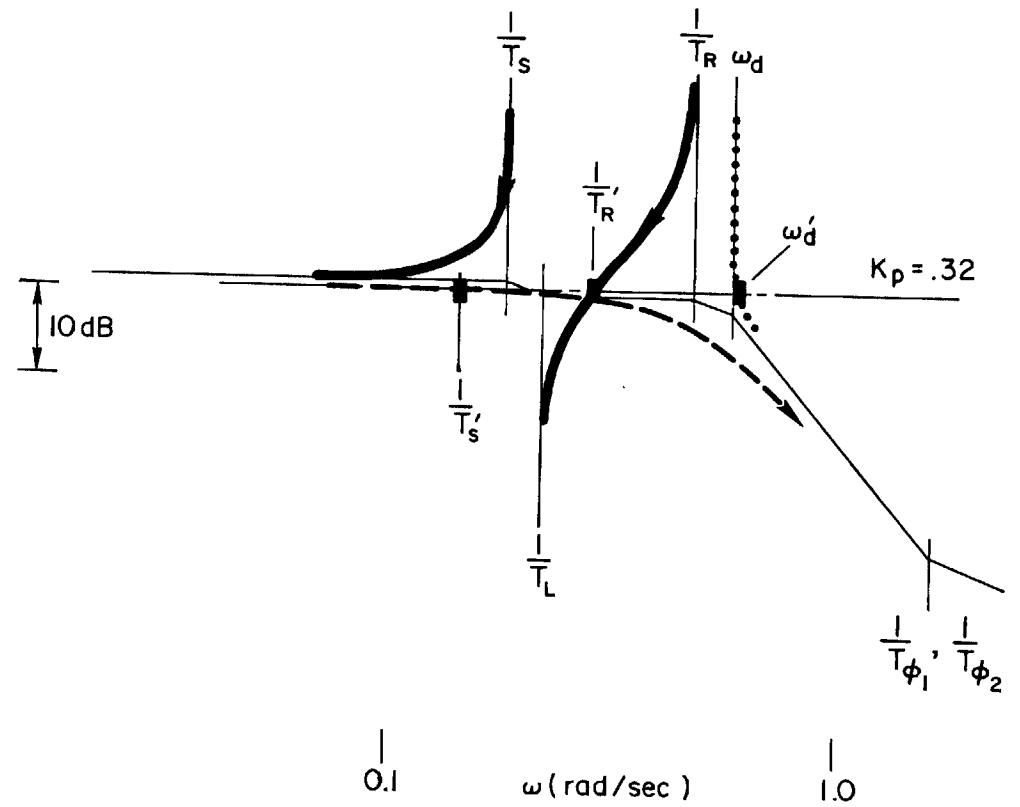


Figure 55. Survey Sketch for Bank Angle-to-Rudder

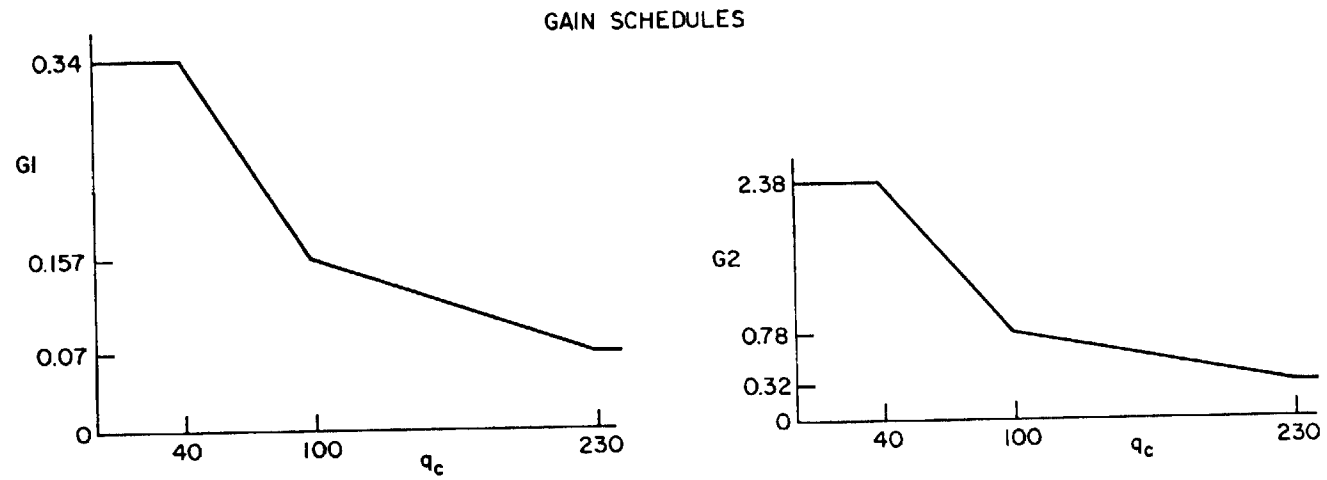
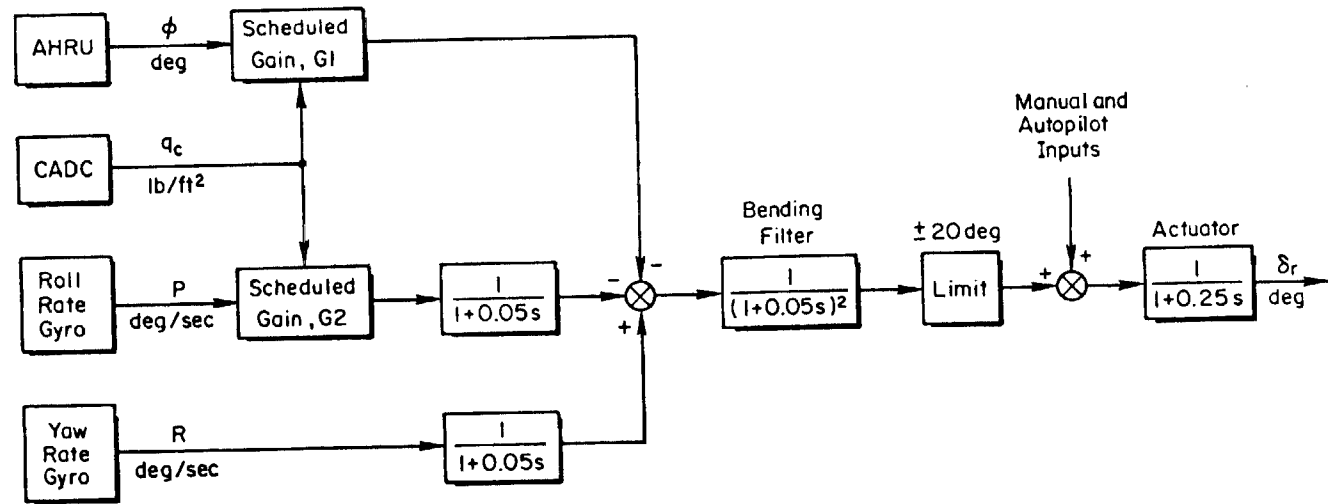
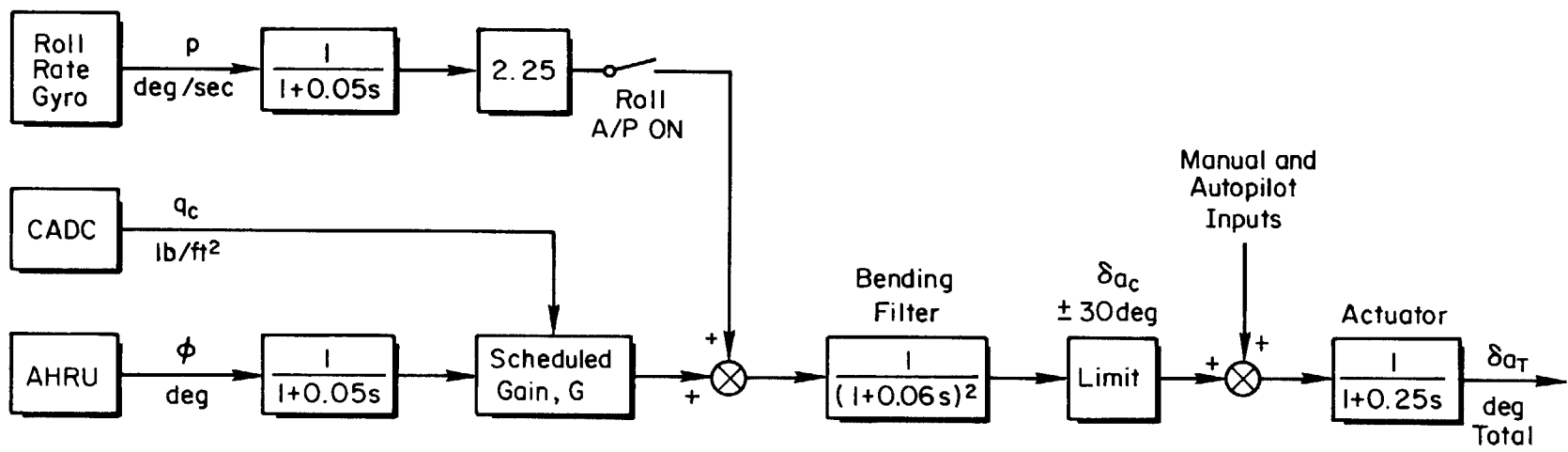


Figure 56. Yaw Stability Augmentation System (SAS)

147



### GAIN SCHEDULE

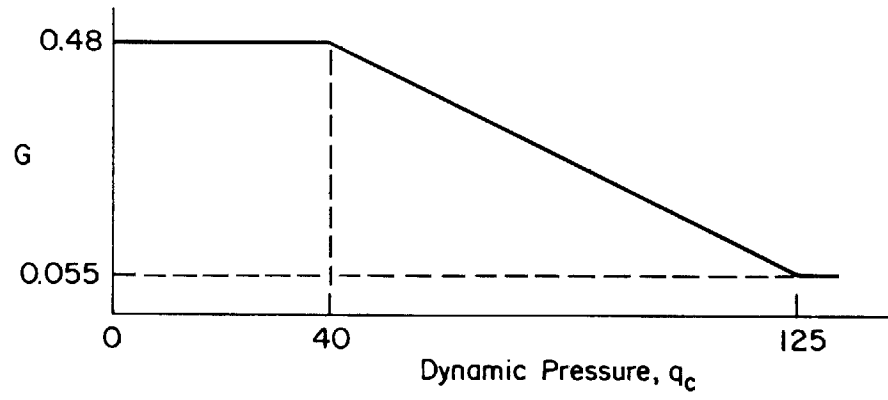


Figure 57. Roll Stability Augmentation System (SAS)

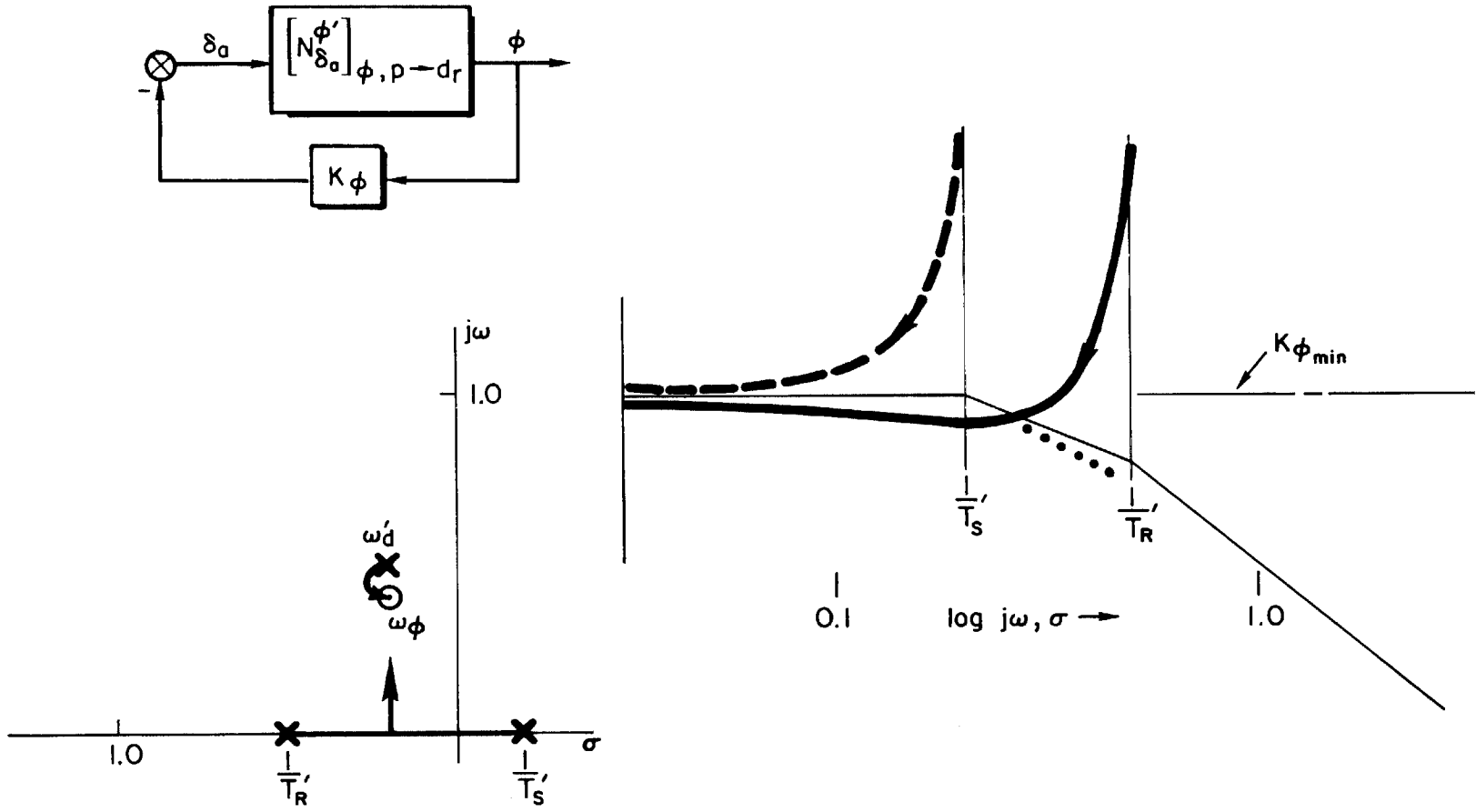


Figure 58. Survey Sketch of Bank Angle-to-Aileron

While the foregoing mechanization accomplishes the intended functions of dutch roll damping and turn coordination there are several associated problems. First, the mechanization is comparatively complex with all roll and roll rate gains scheduled with dynamic pressure. Second, stability of the spiral and/or presence of a "lateral phugoid" depends upon cancellation of effects and hence is sensitive to airframe parameter and system gain changes. Third, if any one feedback is lost the remaining system degrades the basic airframe flying characteristics and will necessitate turning off all feedbacks in both axes. This then leads to the use of massive redundancy to avoid the complete loss of any one signal.

## REFERENCES

1. McRuer, Duane, Irving Ashkenas, and Dunstan Graham, Aircraft Dynamics and Automatic Control, Princeton Univ. Press., New Jersey, 1974.
2. Stapleford, R. L., D. T. McRuer, L. G. Hofmann, and G. L. Teper, A Practical Optimization Design Procedure for Stability Augmentation Systems, AFFDL-TR-70-11, Oct. 1970.
3. Ashkenas, Irving L., and Duane T. McRuer, Approximate Airframe Transfer Functions and Application to Single Sensor Control Systems, WADC TR-58-82, June 1958.
4. Ashkenas, Irving L., Gordon E. Click, Dunstan Graham, James W. Hager, et al, Aircraft Hydraulic Servomechanisms, Richard A. Peters and Dunstan Graham, Ed., Systems Technology, Inc., TR 129-2, Mar. 1969.
5. Johnston, Donald E., Irving L. Ashkenas, and Jeffrey R. Hogge, Investigation of Flying Qualities of Military Aircraft at High Angles of Attack, AFFDL-TR-74-61, June 1974.
6. Graham, Dunstan, and Duane McRuer, Analysis of Nonlinear Control Systems, Dover Publications, Inc., New York, 1971.
7. Gelb, Arthur, and Wallace E. Vander Velde, Multiple-Input Describing Functions and Nonlinear System Design, McGraw-Hill Book Company, 1968.
8. Graham, Dunstan, and Lee Gregor Hofmann, Investigations of Describing Function Technique, AFFDL-TR-65-137, Feb. 1966.
9. Howell, G. D., "Advances in Aircraft Control Systems with Particular Reference to Combat Aircraft," AGARD Conference Proceeding No. 62, Preliminary Design Aspects of Military Aircraft, Sept. 1969.
10. Research and Development Automatic Flight Control System: Design, Installation and Flight Evaluation in Model F8U-1P, Chance Vought Aircraft Rept. E9R 12185, 30 June 1959.
11. Seventeenth Symposium Proceedings, 1973 Report to the Aerospace Profession, SETP, Tech. Review, Vol. 11, No. 4, 26-29 Sept. 1973.

## BIBLIOGRAPHY

- Abrams, C. R., A New Concept in Automatic Flight Control, Final Report, NADC AM 6904, 13 Feb. 1969.
- Abzug, Malcolm J., High-Speed Stability and Control Problems as They Affect Flight Testing, AGARD Rept. 120, May 1957.
- Allender, J. Reverdy, and Robert M. White, F-102A Phase IV Stability Test, AFFTC-TR-57-5, Apr. 1957.
- Archer, Donald D., and Charles L. Gandy, Jr., T-37A Phase IV Performance and Stability and Control, AFFTC-TR-56-37, Feb. 1957.
- Aston, P., Q-2C Pitch Axis Control System Analysis, Lear Siegler, Inc., Astronics Div., Inter-Office Correspondence SA69-239, 15 Oct. 1969.
- Bielka, R. P., A. P. Kavalok, W. L. Johnson, and R. E. Reel, Aircraft Flight Control Systems Field Safety Experience, Air Force Flight Dynamics Lab. TR-72-33, May 1972.
- Burrows, I. L., F-15 Progress Report: Part II, SETP 1973 Report to the Aerospace Profession, 17th Symposium Proceedings, Sept. 1973.
- Burtner, S. K., and Charles T. Garrington, Automatic Control and Stabilization System, Engineering Report, North American Aviation, Inc. Report NA59H-238, May 19, 1959.
- Carleton, David L., and Cecil W. Powell, Limited Air-to-Air Tracking and Qualitative Flying Qualities Evaluation of Selected Flight Control System Configurations in the F-4C/E Aircraft, AFFTC-TD-71-4, Aug. 1971.
- Carleton, David L., Richard E. Lawyer, and Cecil W. Powell, Development and Evaluation of the TWeAD II Flight Control Augmentation System, AFFTC-TD-72-1, Nov. 1972.
- Ciscel, B. H., A Description of the Honeywell E-10 Flight Control System, Minneapolis-Honeywell Regulator Co. Rept. R-ED 9048-2, 28 May 1954.
- Crawford, Charles C., and Jones P. Seigler, KC-135A Stability and Control Test, AFFTC-TR-58-13, May 1958.
- Darrieus, Bernard, Concorde Flight Control System, presented at the SAE A-18 Committee Meeting No. 20, Boston, Mass., Aug. 1967.
- Dempster, John B., and Kenneth L. Roger, Flight Test Evaluation of an Advanced Stability Augmentation System for the B-52 Aircraft, AIAA Paper No. 68-1068, Oct. 1968.
- Dempster, John B., and Kenneth L. Roger, Evaluation of B-52 Structural Response to Random Turbulence with Various Stability Augmentation Systems, AIAA Paper No. 66-998, Nov. 1966.

- Devlin, B. Terry, and Robert H. Parker, "The SP-77 Automatic Flight Control System for the 737," Sperry Rand Engineering Review, Vol. 20, No. 3, 1967, pp. 26-33.
- Eldridge, W. M., Lateral Control Augmentation for Transport Aircraft, presented at the Boeing Conference on Manned Vehicle Flying Qualities, Seattle, Wash., Mar. 1962.
- Ettinger, Robert C., Robert L. Majoros, and Cecil W. Powell, Air Force Evaluation of the Fly-By-Wire Portion of the Survivable Flight Control System Advanced Development Program, AFFTC-TR-73-32, Aug. 1973.
- Falkner, V. L., Functional Configuration of Pre-Production No. 3, AFCS, Honeywell, Inc., SEM No. 115.0090A, 6 Aug. 1970.
- Finch, Thomas W., and Gene J. Matranga, Launch, Low-Speed, and Landing Characteristics Determined from the First Flight of the North American X-15 Research Airplane, NASA TM X-195, Sept. 1959.
- Fling, G. K., XC-124A Control System, SAE Paper No. 670571, June 1967.
- Gaertner, R. V., R. C. McLane, and V. Baxter, Flare Out Program for Air Force Type E-10 Automatic Pilot, Minneapolis-Honeywell Regulator Co. Aero Rept. AD5501-TR1, 15 Aug. 1957.
- Gerrity, Robert J., Test and Evaluation of a Versatile Drone Automatic Flight Control System for the BQM-34A, Society of Flight Test Engineers Report No. 13, presented at the Symposium on Test and Evaluation of Automatic Control Systems, Aug. 31, Sept. 1-2, 1971.
- Guion, H. D., Regulus II Lot I Autopilot—Section IX, Chance Vought Aircraft Service Training Manual, Jan. 11, 1956.
- Hanke, C. Rodney, and Donald R. Nordwall, Simulation of a Jumbo Jet Transport Aircraft. Vol. II: Modeling Data, Boeing Co. Rept. D6-30643, Vol. II, Part 1, Sept. 1970.
- Hannegan, E. A., Evaluation and Flight Test of Self Adaptive Automatic Flight Control Systems, Report No. 1, General Electric System, NATC Proj. TED No. PTR-RAAV-43021, FT2121-39, 7 Feb. 1961.
- Harper, Robert P., Jr., In-Flight Simulation of the Lateral-Directional Handling Qualities of Entry Vehicles, WADD-TR-61-147, Feb. 1961.
- Harris, Pat, Some Aspects of the 727 Flight Control System, presented at the SAE A-18 Committee Meeting No. 14, New York, July 1964.
- Hart, John E., and Harold A. Valery, C-5A Flight Control Report (Aerospace Vehicle). Flight Control Subsystem. Volume I, Lockheed-Georgia Company Report No. IG1US42-2-1, 17 Dec. 1966.

- Hendrick, R. C., A. J. Bailey, L. D. Edinger, et al., Design Criteria for High Authority Closed Loop Primary Flight Control Systems, AFFDL-TR-71-78, Aug. 1972.
- Hilburger, E. A., Control Systems Design Report for A3J-1 Attack Airplane, North American Aviation, Inc. Report NA 59H-98, 10 Apr. 1959.
- Hillman, W. J., and W. Titchnell, Avionic Flight Control System (AFCS), (Preliminary), Lockheed-California Co. Document No. TB3002, 29 Mar. 1968.
- Hoey, Robert G., and Louis W. Schalk, Air Force Evaluation of the Automatic Pitch Control for the F-104A, AFFTC TN 57-11, Feb. 1957.
- Howell, G. C., Flight Experience of Rate Demand Control Using Electric Signaling in the Avro 707C Aircraft, AGARD Report No. 536, May 1966.
- Hurt, George J., Jr., and James B. Whitten, Flight Investigation of an Automatic Pitchup Control, NASA TN D-114, Aug. 1960.
- Jamison, Gene S., C-5A Flight Control System, SAE Paper No. 670574, presented at the Aerospace Systems Conference, Los Angeles, Calif., June 27-30, 1967.
- Jex, H. R., Summary of T-38A PIO Analyses, Systems Technology, Inc., TR-239-1 Jan. 1963.
- Johnston, D. E., and R. K. Heffley, Preliminary Assessment of the F-14A Longitudinal Handling Characteristics, Systems Technology, Inc., TR-193-1, Oct. 1970.
- Johnston, D. E., O. Imai, and D. D. Miles, F-89D Sideslip Stability Augmenter Operation and Maintenance, Airplanes N-2216 through N-4577, Northrop Aircraft, Inc., Rept. No. NAI-54-767, 15 Oct. 1953.
- Johnston, D. E., and D. H. Weir, An Assessment of Operational and Cost Trade-off Factors for a Typical High Performance AFCS, Systems Technology, Inc. TR-119-1, June 1962.
- Kastner, T. M., and R. H. Soderquist, Evaluation of a General Electric Self Adaptive Flight Control System in the F-4A Airplane, Final Report, NATC Tech. Rept. FT2123-49R-64, 8 July 1964.
- Kempel, Robert W., Analysis of a Coupled Roll-Spiral-Mode, Pilot-Induced Oscillation Experienced with the M2-F2 Lifting Body, NASA TN D-6496, Sept. 1971.
- Kisslinger, Robert L., and George J. Vetsch, Survivable Flight Control System, Interim Report No. 1, Studies, Analyses and Approach. Supplement for Control Law Development Studies, AFFDL-TR-71-20, Suppl. 2, May 1971.
- LaGue, T., F-106A Damper Systems, Convair Rept. DC-8B-135, Rev. A, 11 Mar. 1958.

- Lindhahl, J., W. McGuire, and M. Reed, Advanced Flight Vehicle Adaptive Flight Control System. Part VII: Final Report on Study, Development, and Test of the MH-96 System for the X-15, WADD-TR-60-651 (VII), Dec. 1963.
- Martin, C. E., Preliminary Flight Control Subsystem Engineering Report for the F-111A/B Aircraft, General Dynamics, Fort Worth, Rept. FZM-12-874, 21 Oct. 1964, (Rev. 26 Jan. 1965).
- McEntire, Kenneth G., and E. H. Underwood, Jr., Flight Test Evaluation of the A-7D/E Emergency ("Back-Up") Flight Control System, Society of Flight Test Engineers Report No. 14, Aug.-Sept. 1971.
- Miller, H., and R. H. Wagner, Flight Control System for Jet Transports, Sperry Gyroscope Co., no date.
- Mueller, Leo J., Some Experiences in VTOL Automatic Flight Control, presented at the SAE A-18 Committee Meeting No. 14, New York, July 1964.
- Naumann, Erwin A., and Herman Schmier, "Design and Development of the Stability Augmentation System for the Lockheed/Army XV-4A," Proc. of the 20th Annual National Forum of the American Helicopter Society, Washington, D. C., May 1964, pp. 140-151.
- Newberry, C. F., B-52 Autopilot Modification, Boeing Company Technical Paper D3-4525, presented to SAE Committee A-18 Aerospace Vehicle Flight Control Systems, 14 June 1962.
- Quinlivan, R. P., Multimode Flight Control Definition Study, AFFDL-TR-72-55, May 1972.
- Rabenberg, B. E., and J. J. Gondek, XB-70 Flight Control System Summary Test Report, North American Aviation, Inc. Report NA-66-360, 30 Sept. 1966.
- Rickard, Richard R., Stability and Control Evaluation of an F-4C Aircraft with a High-Gain Adaptive Control Augmentation System, AFFTC-TR-71-17, June 1971.
- Rickard, Richard R., and Jerauld R. Gentry, Development Testing of a High-Gain Adaptive Control Augmentation System Installed in an F-4C Aircraft, AFFTC-TD-70-4, Vols. I and II, Sept. 1970.
- Rickard, Richard R., Richard H. Kogler, and Cecil W. Powell, Stability and Control Evaluation of an F-4C Aircraft with a High-Gain Adaptive Control Augmentation System, AFFTC-SD-71-17, June 1971.
- Russell, Walter, R., and William L. Alford, Flight Investigation of a Centrally Located Rigid Force Control Stick Used with Electronic Control Systems in a Fighter Airplane, NASA TN-D-102, Sept. 1959.
- Russell, Walter R., Sigurd A. Sjoberg, and William L. Alford, A Flight Investigation of the Handling Characteristics of a Fighter Airplane Controlled Through a Rate Type of Automatic Control System, NACA RM L56FO6, Sept. 1956.

- Russell, Walter R., Sigurd A. Sjoberg, and William L. Alford, Flight Investigations of Automatic Stabilization of an Airplane Having Static Longitudinal Instability, NASA TN D-173, Dec. 1959.
- Sanctuary, G. E., and A. M. Roberto, Low Speed "Adverse" Yaw Flight Simulator, Evaluation, General Dynamics/Fort Worth Div., S/C TM No. 52, 28 Oct. 1966.
- Schuetz, A. J., R. L. Fortenbaugh, and W. E. Becker, An Aerodynamic Stability and Control Data Summary for Several Selected Military Aircraft, Volume I: Conventional Aircraft, Naval Air Development Center Report AM-7106, 28 Sept. 1971.
- Seacord, Charles L., The Honeywell AFCS (MH-157) for the Swedish Viggen (AJ-37) Aircraft, Honeywell, Inc., Report T-230, circa 1969.
- Seeman, William G., and Floyd H. Moody, Using the Man to Test Unmanned Aircraft, Society of Flight Test Engineers Report No. 16, presented at the Symposium on Test and Evaluation of Automatic Control Systems, Aug. 31, Sept. 1-2, 1971.
- Seth, W. A., A-7D Estimated Flying Qualities, LTV Vought Aeronautics Report No. 2-53320/8R-8089, 15 Jan. 1968.
- Sexton, H. A., Jr., Flight Testing the F-104 Automatic Flight Control System, AIAA Paper No. 64-328, July 1964.
- Shah, N. M., G. Gevaert, and L. O. Lykken, The Effect of Aircraft Environment on Category III Autoland Performance and Safety, AIAA Paper No. 72-811, Aug. 1972.
- Shields, M. E., Estimated Flying Qualities XC-142A V/STOL Assault Transport, LTV Vought Aeronautics Division Report No. 2-53310/4R 939, 22 May 1964.
- Simmons, Carl D., and Donald M. Sorlie, F-101B Air Force Stability and Control Evaluation, AFFTC-TR-58-11, May 1958.
- Sjoberg, Sigurd A., Walter R. Russell, and William L. Alford, A Flight Investigation of the Handling Characteristics of a Fighter Airplane Controlled through an Attitude Type of Automatic Pilot, NACA RM L56A12, April 1956.
- Sjoberg, Sigurd A., Walter R. Russell, and William L. Alford, Flight Investigation of a Normal-Acceleration Automatic Longitudinal Control System in a Fighter Airplane, NASA Memo 10-26-58L, Dec. 1958.
- Taylor, Lawrence W., Jr., Analysis of a Pilot-Airplane Lateral Instability Experienced with the X-15 Airplane, NASA TN D-1059, Nov. 1961.
- Teper, Gary L., and Richard H. Klein, Analysis for the MQM-74A Drone Control System, Systems Technology, Inc., TR-279-1, Feb. 1968.
- Terrill, W. H., L. R. Springer, and J. G. Wong, Investigation of Pilot-Induced Longitudinal Oscillation in the Douglas Model A4D-2 Airplane, Douglas Aircraft Company, Inc., Rept. LB-25452, May 15, 1957.

Tomlin, K. H., C-5 Flight Control Report (Aerospace Vehicle) Stability and Control, Lockheed-Georgia Company Report No. IGLUS42-1-1, 1 Oct. 1966.

Townsend, Marland W., and William B. Rhodes, Flight Evaluation of the Lear Advanced Automatic Flight Control System (AFCS) Installed in an F-8D Airplane, Final Report, NATC Tech. Rept. FT2121-63, 31 Dec. 1963.

Tremant, Robert A., Operational Experiences and Characteristics of the X-15 Flight Control System, NASA TN D-1402, Dec. 1962.

Wolowicz, C. H., and R. B. Yancey, Summary of Stability and Control Characteristics of the XB-70 Airplane, NASA TM X-2933, Oct. 1973.

Advanced Automatic Flight Control System for Attack/Fighter Aircraft, Lear Siegler, Inc., Rept. ADR-565, 15 Feb. 1964.

Automatic Flight Control System, Control Stick Steering, Evaluation of Report No. 1, Interim Report, NATC Proj. TED No. PTR AV-37009, ST312-190, 2 June 1959.

Automatic Flight Control System, Control Stick Steering, Evaluation of, Report No. 2, Final Report, NATC Proj. TED No. PTR AV-37009, ST312-283, 10 Aug. 1959.

B-52 Autopilot Modification, Boeing Company Document D3-4360, 15 March 1962, presented at the Boeing Conference on Manned Vehicle Flying Qualities, Mar. 15-16, 1962, Seattle, Washington.

B-58 Flight Control System Air Force Review Board, General Dynamics/Fort Worth FZE-4-049, 6 Nov. 1962.

Current Autopilot Block Diagrams, SAE A-18 Committee, Oct. 1959.

Experience with the X-15 Adaptive Flight Control System, NASA TN D-6208, Mar. 1971.

F-111 Category I Flight Test Progress Report, Preliminary Stability and Control/Flight Control Subsystem Flight Test Results, General Dynamics/Fort Worth Div., Rept. FZM-12988-13-2, 14 Feb. 1966. (Report Confidential, Title Unclassified)

Flight Control Systems for F-100F Airplane, North American Aviation, Inc., Rept. NA56-731, 1956.

Flight Manual, USAF Series F-100C, Air Force T.O. 1F-100C-1, 22 Dec. 1960.

Flight Manual, USAF Series F-101A and F-101C, Air Force T.O. 1F-101A-1, 15 May 1962.

Flight Manual, USAF Series F-102 and TF-102A, Air Force T.O. 1F-102A-1, 4 Oct. 1962.

Flight Manual, USAF Series F-104A and F-104B, Air Force T.O. 1F-104A-1, 15 Dec. 1961.

Flight Manual, USAF Series F-105B, Air Force T.O. 1F-105B-1, 15 July 1962.

Flight Manual, USAF Series C-130A Aircraft, Air Force T.O. 1C-130-1, 10 Jan. 1963.

Flight Manual, USAF Series C-133A and C-133B Aircraft, Air Force T.O. 1C-133A-1, 14 June 1962.

Flight Manual, USAF Series C-135A and B- , Air Force T.O. 1C-135A-1, 1 Mar. 1963.

Handbook Operation and Maintenance Instructions, MH-67 Automatic Flight Control System, Publication No. 95-4256B, May 1964.

The Honeywell Flight Boundary Control System, Honeywell, Inc., Government and Aeronautical Products Div., Brochure ADC 364, Jan. 1972.

Maintenance Instructions Manual, Navy Models F-4B and RF-4B Aircraft, Flight Control Group AN/ASA-32 Series and Related Systems, NAVWEPS 01-245FDB-2-6.3, 1 Dec. 1965.

Maintenance Manual, Flight Control Systems, USAF Series F-102A and TF-102A, Air Force T.O. 1F-102A-2-7, 5 Jan. 1962.

Maintenance Manual, Flight Control Systems, USAF Series F-106A and F-106B Aircraft, 20 Dec. 1962.

MH-96 Flight Control System for the X-15 Aircraft. Vol. V: System Description and Bench Test Procedure, Minneapolis-Honeywell Regulator Co. Aero Report 2373-TM1 (Vol. V), 31 Aug. 1962.

Organizational Maintenance Manual, Flight Control Systems, USAF Series T-38A, Air Force T.O. 1T-38A-2-3, 1 Sept. 1962.

Preliminary Flight Control Subsystem Analysis for the F-111A/B Airplanes, General Dynamics/Fort Worth Div., Report FZM-12-278, 16 Aug. 1963. (Report Confidential, Title Unclassified)

Preliminary Flight Manual DSN-3 Drone and Target Control System AN/SRW-4B, Bureau of Naval Weapons NAVWEPS 01-150DHB-1, 1 Jan. 1962.

Preliminary Report on Lateral Piloted Handling Quality Problems, Honeywell Aeronautical Division, CEL No. DS 567, 12 Nov. 1963.

Presentation to ASD Division Advisory Group, General Dynamics/Fort Worth Div., Report FZM-12-2357, June 1966.

Proposal for a Product Improvement Program for the BQM-34A Automatic Flight Control System (Versatile Drone Autopilot), Lear Siegler, Inc., Astronics Division, Report AD-975, 17 July 1970.

Report of the B-58 Flight Control System Review Board, Sect. VII-A, Aerodynamic Trade-Off Team Report, Aeronautical Systems Division, 5 Dec. 1962.

Research and Development, Automatic Flight Control System: Design, Installation and Flight Evaluation in Model F8U-1P, Chance Vought Aircraft, Inc., Report E9R 12185, 30 June 1959.

Round Up Review, Division Advisory Group-ASD, 21 and 22 June 1968, Flight Control System/Stability and Control, General Dynamics/Fort Worth Div., Report FZM-12-5964-2, 21 June 1968. (Report Confidential, Title Unclassified).

S-3A Automatic Thrust Control System, (Unpublished notes).

Simulator System Test Report for A2F-1 Airplane, Part a, Grumman Aircraft Engineering Corporation, Report No. AV-128R32.0, no date.

"TA-4F Accident Provides Some Costly Lessons," Approach, Vol. 15, No. 8, Feb. 1970, pp. 36-41.

Transfer Functions and Block Diagrams of the SP-30AL Automatic Pilot and Z-14 Flight Director as Applied to the Douglas Model DC-8-60 Series of Aircraft, material transmitted to STI in Sperry Flight Systems Division letter of 29 Sept. 1969.

USAF Type A/A37G-3 Flight Control Subsystem of the Type Q-2C Drone, Ryan Aeronautical Co. Spec. 12459-2A, no date.

## INDEX

- Acceleration
  - Lateral, 122
  - Normal, 108
- Adverse yaw
  - Aileron, 12, 39, 119, 122, 141
  - Reduction, 13
  - Rolling velocity, 12
  - Yaw damper, 15, 17, 134
- Aileron/rudder interconnect, 12, 137
  - Equalized crossfeed, 13, 137
  - Ideal crossfeed, 14
  - Gain variation, 137
  - Influence of SAS, 14
- Autotrim, 95, 108, 111, 112
  - C.g. shift, 100
  - Opposition to manual inputs, 96, 98, 102, 114, 137
  - Stick force lightening, 96
  - Trim rate effects, 96, 98
- Backside [of thrust required curve], 32, 38, 110, 113
- Bank angle control, 9
  - Body rate command, 120
  - Inertial platform sensing, 121
  - Roll back, 121
  - Roll coasting, 121
  - Vertical gyro sensing, 121
- Blended feedbacks, 113, 114, 135
- Bobweight, 50, 53, 99, 109
  - Effective moment arm, 74, 109
  - Effective numerator, 74
  - Influence on CAS sensing, 89, 92, 94
  - Influence on stick free dynamics, 76
  - Pilot's arm, 90, 119
  - Stick force, 71
- CAS command sensing, 86, 95, 97
  - Displacement, 93, 97
  - Force, 86, 97
  - Pseudo force, 91
- CAS electrical command, 103
  - Gain shaping, 106, 113, 119
  - Mechanical nonlinearities, 87, 91, 94
  - Phase lag, 106
  - Prefilter considerations, 105
  - Saturation (limiting), 112, 119
  - Threshold, 87, 93
- Jenter of percussion, 109, 122, 136
- Center of rotation, 109, 122
- Command augmentation, 69
  - Blended normal acceleration and pitch rate, 113
  - Command saturation, 112, 119
  - Derived attitude rate, 114
  - Feedback saturation, 112, 119
  - Normal acceleration, 108, 111
  - Pitch rate, 111
  - Roll attitude, 120
  - Roll rate, 117
  - Yaw rate, 122
- Complexity, 80, 116, 148
- Control reversal, 87
- Crossfeed
  - Aileron to rudder, 12, 137
  - Lateral stick to rudder, 140
  - Roll attitude to rudder, 142
  - Roll rate command to rudder, 141
  - Roll rate to rudder, 12, 134
  - Derived attitude rate, 114, 121
- Dissimilar parallel paths, 82, 117, 120
- Divergence
  - Nose slice, 4, 29, 39
  - Path, 108
  - Speed, 4, 32, 108, 110
- Dutch roll, 9, 11, 12, 124, 136, 143, 149
  - Aileron excitation, 12
  - Reduction, 13, 122
- Effective numerators, 14, 74
- Equivalent system, 48, 52
- Feel system, 50, 53, 86, 97, 98
  - Breakout, 85
  - Linear dynamic models, 56
    - Damper influence, 58
    - Feel spring influence, 59, 86
    - Lags introduced, 58, 78
    - System inertia, 59
  - Nonlinearities, 61
- Flight path divergence, 4, 29, 108, 110
- Fly-by-wire, 82
- Force sensing, 86, 99
  - Bobweight effects, 89

- Force sensing (continued)
  - Ground, 86
  - Kickback, 89
  - On/off transients, 90
  - Structural bending, 90
  - Transducer null, 90
  - Transducer vulnerability, 90
  - With parallel trim, 88
- Forward loop integration, 99, 108, 111, 112
- Frontside [of thrust required curve], 33
- Hardover failure, 84, 95
- High angle of attack, 109, 121, 131, 135
- Hydraulic actuator dynamics
  - Idealized, 24
  - Load contributions, 20, 22, 24
  - No load, 24
  - Phase lag, 70, 98
  - Rate limiting, 27
  - Support contributions, 20, 22
  - Valve forces, 85
- Inertial platform, 121
- Integral control, 35
- Inverse model feedback, 119
- Kickback, 69, 85, 89, 92, 94, 95, 99
- Lateral acceleration
  - At pilot, 142
  - Directional stiffening, 135
  - Feedback shaping, 123
  - Feedback to rudder, 15, 16, 122
  - Gain compensation, 123, 135
  - Integration, 137
  - Structural mode attenuation, 123
- Lateral-longitudinal coupling, 4, 11, 39, 109
- Limit cycle, 66, 70
- Low-frequency droop, 35
- Neutral speed stability, 100
- Nonlinearities
  - Backlash, 67
  - Describing function analysis, 64, 70
  - Detent, 87
  - Hydraulic valve friction, 69, 85
  - Hysteresis, 62
  - Mechanical friction, 61, 78, 87
  - Preload, 87
  - Stiction, 87
- Non-minimum phase zeros, 4, 29
  - Altitude control, 30
  - Lateral acceleration, 123
  - Normal acceleration, 109
  - Pitch attitude control, 33, 39
- Normal acceleration feedback
  - Feedback shaping, 109
  - Gain scheduling, 111
  - Gravity vector, 108
  - Sensor location, 109
  - Sensor orientation, 108
  - Washout, 108
- Nose slice divergence, 4, 29, 39
- Parallel actuation, 84, 97, 103
  - Authority, 98
  - On/off transients, 99
  - Overpower, 98
- Performance reversal, 4
  - Corrections of  $1/Th_1$ , 33
  - Pitch attitude, 39
  - Speed, path, 29
- Phase lag
  - Hydraulic actuator, 70, 98
- Pilot cues, 102, 109, 116
- PIO, 3, 66, 70, 106, 110, 119
- Pitch attitude control, 114
  - Attitude rate command, 114
  - Body rate command, 114
  - Pitch back, 114
- Power boost actuator, 85, 97
- Primary flight control system
  - Backlash, 67
  - Detent, 87
  - Hydraulic valve friction, 69
  - Hysteresis, 62
  - Mass imbalance influence, 89
  - Mechanical friction, 61, 78, 87
  - Preload, 61, 66, 87
  - Stick to surface gearing, 67
- Pseudo force sensing, 91
  - Bobweight interaction, 92
  - Feel system interaction, 91
  - Kickback, 92
  - On/off transients, 93
  - Structural bending, 92
  - Transducer null, 92
  - Transducer vulnerability, 93
  - Trim system interaction, 92
- Quadratic dipole problems
  - Hydraulic actuator, 24
  - $\omega_B/\omega_{sp}$ , 76
  - $\omega_r/\omega_d$ , 4, 17, 132
  - Roll damper influence, 17
  - Yaw rate gyro tilt, 132

Quadratic dipole problems (continued)  
    $\omega_p/\omega_d$ , 3, 9, 120  
   ARI influence, 13  
   Yaw damper influence, 16  
 Rate gyros, 111  
   Pitch rate, 111  
   Roll rate, 117  
   Yaw rate, 131  
 Response feedback, 107  
   Lateral acceleration, 122, 137  
   Lateral acceleration and yaw rate, 136  
   Normal acceleration, 108  
   Normal acceleration and pitch rate, 113  
   Pitch attitude, 113  
   Pitch rate, 111  
   Roll attitude, 120, 143  
   Roll rate, 117, 135  
   Yaw rate, 131  
 Right half plane zeros, 4, 29, 39, 109, 123  
 Rudder maneuvering, 119, 122  
 Saturation (limiting)  
   Actuator position, 85  
   Actuator rate, 69, 85, 98  
   CAS command, 112, 119  
   CAS feedback, 110, 112, 119  
 Sensor location effects  
   Lateral accelerometer, 122  
   Normal accelerometer, 109  
 Sensor orientation, 46, 108  
   Body vs. Euler axis, 113, 121, 131  
   Lateral acceleration, 131  
   Normal acceleration, 108  
   Roll rate gyro, 117  
   Yaw rate gyro, 131  
 Series actuation, 84  
   Full authority, 84, 85  
   Limited authority, 84, 95, 97  
   Washed-out feedback, 99, 100  
 Series servo  
   Backup, 67, 85  
   Ground, 85  
   Kickback, 69, 85, 89, 92, 94, 95  
   Support, 22  
 Sideslip  
   Intentional, 119, 122, 138  
   Lateral-longitudinal coupling, 39  
   Roll control induced, 13  
   Sensing, 122, 136  
   Turn coordination, 136  
   Speed divergence, 4, 32, 108, 110  
   Spin recovery, 110, 113  
   Stall, 32, 39, 96, 108, 110, 113, 116, 119  
   Stick displacement sensing, 93, 102  
     Bobweight interaction, 94  
     Feel system interaction, 93  
     Kickback, 94  
     On/off transients, 94  
     Structural bending, 94  
     Transducer null, 94  
     Transducer vulnerability, 94  
     Trim system interaction, 94  
   Stick force per g, 86, 92, 108, 111, 113  
   Augmentation, 108, 111  
   Lightning, 89, 96, 110, 112, 114, 119  
   Variation with gravity vector, 108  
   Stick nibble, 114  
 Trim  
   Automatic  
     Parallel, 95, 119  
     Series, 99, 109  
   Electrical, 110  
   Opposition of manual and automatic, 96  
   Parallel, 88, 92, 94, 99  
   Series, 88, 94  
   Turn coordination, 122, 136  
   Valve forces  
     Bernoulli, 85  
     Centering, 85  
     Friction, 69, 85  
   Vertical gyro, 113, 121  
   Washout  
     Aileron/rudder crossfeed, 138  
     Normal acceleration, 108  
     Servo feedback, 99, 111  
     Yaw rate damper, 17, 122, 134, 142  
   Yaw rate gyro  
     Feedback to rudder, 14, 16, 122, 131  
     Inclination effects, 131  
   Zeros  
     Intentionally introduced, 4, 29  
     Inverse model, 46, 119  
     Non-minimum phase (right half plane), 4, 29, 39, 109, 123

